Department of Physics and Astronomy

University of Heidelberg

Master thesis

in Physics

submitted by

Florian Dinger

born in Aalen

2014

Characterisation of a Cavity Ring-Down Spectrometer for measuring CO_2, CH_4, $\delta^{13}CO_2$, and $\delta^{13}CH_4$ in ambient air

(Revised version from August 2014)

This Master thesis has been carried out by Florian Dinger

at the

Institute of Environmental Physics

under the supervision of

Dr. Martina Schmidt and Dr. Ingeborg Levin

Abstract

Continuous measurements of the greenhouse gases CO_2 and CH_4, along with their isotopologues $^{13}CO_2$ and $^{13}CH_4$, are the basis for estimating the atmospheric CO_2 and CH_4 fluxes on high temporal resolution and for identifying their sources and sinks. The Cavity Ring-Down Spectrometer (CRDS) G2201-i measures $^{12}CO_2$, $^{13}CO_2$, $^{12}CH_4$, $^{13}CH_4$, and H_2O continuously and simultaneously in a gas sample. In this thesis, the CRDS G2201-i has been installed in Heidelberg for routine ambient air analysis and for measurements of highly concentrated CH_4 samples. It has been characterised and thoroughly tested in terms of accuracy, precision, and compatibility. It was found, that for accurate results, the internal water vapour correction is insufficient, which makes a preceding drying necessary. Furthermore, an instrumental non-linearity in the CO_2 and CH_4 concentrations was observed. Nevertheless, a single-point calibration yields CO_2 and CH_4 concentrations which are compatible to other routine instruments (i.e. Fourier Transform InfraRed spectrometer (FTIR) and gas chromatograph) in Heidelberg within the World Meteorological Organization recommendations. The $\delta^{13}CO_2$ results of CRDS, FTIR, and the mass spectrometer in Heidelberg are compatible for cylinder measurements. For continuous ambient air measurements a systematic offset of $\Delta(\delta^{13}CO_2)_{\mathrm{CRDS-FTIR}} = (0.07 \pm 0.11)\,‰$ was observed.

Kurzfassung

Kontinuierliche Messungen der Treibhausgase CO_2 und CH_4, sowie deren Isotopologe $^{13}CO_2$ und $^{13}CH_4$, erlauben zeitlich hochaufgelöste Abschätzungen der atmosphärischen CO_2- und CH_4-Flüsse sowie eine Analyse ihrer Quellen und Senken. Das Cavity Ring-Down Spektrometer (CRDS) G2201-i misst kontinuierlich und simultan $^{12}CO_2$, $^{13}CO_2$, $^{12}CH_4$, $^{13}CH_4$ und H_2O in einer Gasprobe. In dieser Arbeit wurde das CRDS G2201-i in Heidelberg für routinemäßige atmosphärische Messungen und zur Vermessung von hochkonzentrierten CH_4-Proben installiert. Das Instrument wurde charakterisiert und sorgfältig bezüglich Genauigkeit, Präzision und Kompatibilität getestet. Es wurde festgestellt, dass die interne Wasserdampfkorrektur zu ungenauen Ergebnissen führt und somit eine vorhergehende Trocknung notwendig ist. Außerdem wurde eine instrumentelle Nichtlinearität in den CO_2- und CH_4-Konzentrationen beobachtet. Dennoch führt bereits eine Ein-Punkt-Kalibrierung zu CO_2- und CH_4-Konzentration, die mit den anderen routinemäßigen Heidelberger Instrumenten (d.h. Fourier Transform InfraRed Spektrometer (FTIR) und Gas-Chromatograph) innerhalb der Empfehlungen der World Meteorological Organization vereinbar sind. Die $\delta^{13}CO_2$-Ergebnisse von CRDS, FTIR und dem Massenspektrometer in Heidelberg sind für Tankmessungen miteinander vereinbar. Bei kontinuierlichen Außenluftmessungen wird hingegen eine systematische Abweichung von $\Delta(\delta^{13}CO_2)_{\mathrm{CRDS-FTIR}} = (0.07 \pm 0.11)\,‰$ beobachtet.

Contents

1 Introduction

Life on Earth is determined by its climate system. This is shown most prominently by the glacials, the extinction of the dinosaurs or simply by the inhospitality of deserts. But already less startling climate changes had a great impact on mankind. For example, the rise and fall of the Roman empire might be supported by climate changes [*Huntington*, 1917]. A major aim of climate science is to understand the climate system of the Earth and thereby to forecast the impact of a climatic change on the environment we are living in.

The functioning of the Earth's climate system is based on the incoming solar radiation which alone would heat up the Earth's surface, in radiative equilibrium, to 255 K. However, the current global mean surface temperature is 288 K. The discrepancy is understood since *Arrhenius* [1896] introduced the concept of the atmosphere as a heating element of the climate system. As a black body, the Earth's surface is permanently emitting infra-red radiation to space. Several atmospheric trace gases, the so-called greenhouse gases, partially absorb this infra-red radiation and emit a fraction back to Earth, leading to a 33 K higher surface temperature than without atmosphere. Consequently, an increase in the greenhouse gas concentrations leads to an increased surface temperature. The most important greenhouse gases are water vapour (H_2O), carbon dioxide (CO_2), methane (CH_4), and nitrous oxide (N_2O). In paleo-records, a correlation between increasing greenhouse gas concentrations and increasing surface temperature has been observed. Especially the extreme changes in CO_2 match with the extreme changes in the surface temperature [*IPCC*, 2013].

Today, such a parallel increase in greenhouse gas concentrations and surface temperature is also observed. But contrary to the changes in the past, the atmospheric CO_2 concentration is extremely fast increasing. During the Holocene the global mean surface temperature and the greenhouse gas concentrations were more or less constant. Since the beginning of the industrialisation in 1850, the temperature increased by more than 1 °C and the CO_2 concentration increased from 285 ppm to 400 ppm (see Figure 1.1) [*IPCC*, 2013]. From Antarctic ice cores, it is reconstructed that the global mean of the atmospheric CO_2 concentration varied within the last 800 kilo-years between 200 ppm and 285 ppm [*IPCC*, 2013]. Thus, the increase in atmospheric CO_2 since the industrialisation is larger than the maximum natural variation within the last 800 kilo-years. Because all natural parameters of the climate system did not change significantly in the last millenniums most of this increase in concentration is caused by the exponentially increasing anthropogenic activity since the industrialisation, i.e. primarily due to the burning of fossil fuels.

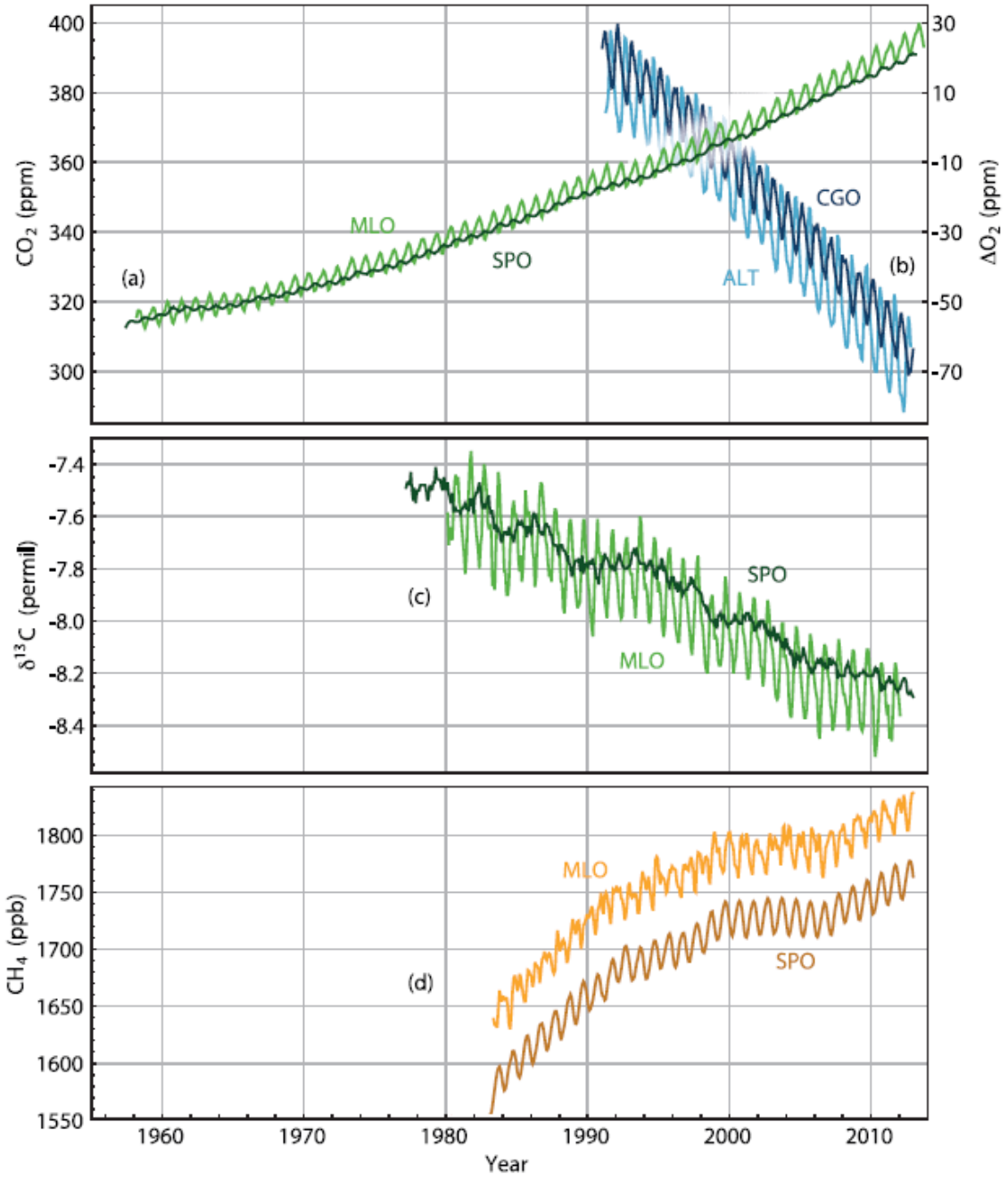

Figure 1.1: *Upper and middle panel: Together with the modern increase in CO_2 (a), the atmospheric concentration of oxygen (b) and the isotopic $\delta^{13}C$ signature of the atmospheric CO_2 (c) are decreasing. Lower panel: The concentration in atmospheric CH_4 is continuously increasing (d). The data are from the stations at Mauna Loa (MLO), South Pole (SPO), Alert (ALT), and Cape Grim (CGO). Modified version of Figure 6.3 in [IPCC, 2013].*

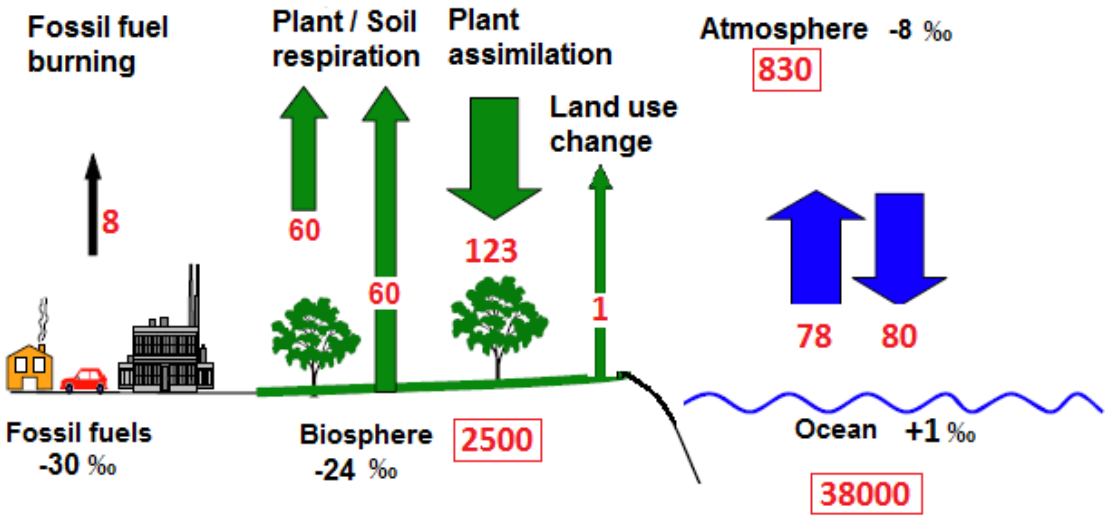

Figure 1.2: *The global atmospheric CO_2 cycle consists of the interacting reservoirs ocean, biosphere, and atmosphere. Without disturbance, the natural reservoirs are in dynamic equilibrium, i.e. there is no net flux between two reservoirs in the global and annual mean. Since the beginning of the industrialisation the burning of fossil fuel has continuously added CO_2 to this balanced system. By the emissions, initially the atmospheric CO_2 concentration has increased. But the disturbed system reaches for a new equilibrium, wherefore the exchange fluxes between atmosphere and the biosphere respectively the ocean increased and furthermore net fluxes occurred. The red numbers give, for the current disturbed system, the estimated carbon inventory of the reservoir (in PgC) and the carbon fluxes (in PgC/year) between two reservoirs. The black numbers give its mean isotopic $\delta^{13}CO_2$ signature. The sketch is drawn by Ingeborg Levin, the data are from [IPCC, 2013] and [Mook, 2000].*

In the undisturbed climate system, the CO_2 concentration in the atmosphere, the biosphere, and the ocean were in a dynamic equilibrium. The biosphere absorbed by photosynthesis 109 PgC per year from the atmosphere and emitted 107 PgC per year by respiration of plants, fauna, and soils. Due to the inhomogeneity of the ocean surface with respect to temperature and salinity some ocean regions permanently absorbed CO_2 from the atmosphere while other regions permanently released CO_2 to the atmosphere. In the dynamical equilibrium an amount of 60 PgC was exchanged per year [*IPCC*, 2013]. In the current disturbed system (see Figure 1.2), additional 9 PgC per year are emitted to the atmosphere by burning fossil fuels or land use change. But only 4 PgC of this additional input stay in the atmosphere while 3 PgC get stored in the biosphere and 2 PgC in the ocean, respectively. Furthermore, the total CO_2 exchange fluxes increased to about 120 PgC per year between atmosphere and biosphere, and about 80 PgC per year between atmosphere and ocean. By these

exchange processes, it is more difficult to detect the source of the additional CO_2 by atmospheric observations. Thus, while the increase in the atmospheric CO_2 concentration is not deniable, it is not obvious which amount is directly contributed by anthropogenic activity and which amount is the result of feedback effects, i.e. released from natural reservoirs.
Fortunately, each CO_2 source has its own *isotopic signature* (see Figure 1.2). When the isotopic signatures of all relevant sources are known, it is possible to reconstruct from the measured isotopic signature of the atmosphere in which fractions the different sources have contributed to the additional CO_2 in the atmosphere. However, the isotopic $\delta^{13}CO_2$ signature of CO_2 from the biosphere and fossil fuel burning are practical indistinguishable. But measuring also the atmospheric $\Delta^{14}CO_2$, the absolute contribution from fossil fuels can be determined [*Levin et al.*, 2003].

Already alarming, the increasing mean global surface temperature is just a globally averaged value. The climate change has a much bigger and less understood impact on continental and regional scale. But to understand the highly complex climate system in a sufficient degree of details, also highly complex physical models are required which are then simulated via computer power. For a satisfying simulation output it is crucial to enter most accurate data for the numerous climate parameters like the atmospheric greenhouse gas concentrations. Most accurate data, that means small measurement errors but also sufficient local and temporal resolution. A good temporal resolution is managed by continuous monitoring and a good local resolution by a worldwide measurement network.

The first optical technique which measured the atmospheric CO_2 concentration in-situ was by Non-Dispersive Infra-Red (NDIR) Absorption which was most prominently installed at Mauna Loa by Charles Keeling in 1958 [*Keeling*, 1960]. Since the 1980s, atmospheric CH_4 is measured by Gas Chromatography (GC) [*Valentin et al.*, 1985], while NDIR is not able to measure the atmospheric CH_4 concentration with high precision. But GC is maintenance-intensive and the typical measurement frequency is a measurement all 5 min [*Hammer et al.*, 2008]. Thus, GC is not well suited for automatic measurement stations and the temporal resolution appears to be unsatisfactory for high resolution simulations. In the last two decades, the quality of tunable lasers has improved significantly and new cavity-enhanced techniques like Fourier Transform Infra-Red (FTIR) Spectrometry and Cavity Ring-Down Spectrometry (CRDS) became practicable for atmospheric gas concentration measurements [*Paldus and Kachanov*, 2005]. Today, these techniques are robust and require only little maintenance wherefore such optical spectrometer are already commercially available and better suited for automatic measurements than GC. While measurement frequencies down to a data point each second are realised, at least the 1-min averages are comparable with the quality of GC analysis. By this, high-resolution in-situ monitoring of the atmospheric greenhouse gas concentrations became reality. Furthermore, optical spectrometer are relatively small and thus suited for field campaigns or can even operate while driving.

Nevertheless, these new optical instruments are also able to measure the concentration of rare isotopologues and thus, isotopic signatures. The only non-optical technique to measure isotopic signatures is the mass spectrometry (MS). But MS requires 30-60 min per measurement and permanent maintenance. Thus, MS instruments are generally not suited for continuous monitoring. However, now in 2014 the MS still gives the most accurate values for the isotopic signature of CO_2 and CH_4. On the other hand, optical instruments treat each isotopologue the same way, in principle. Consequently, also $^{13}CO_2$ and even $^{13}CH_4$ can be measured virtually continuously by CRDS.

The Institute of Environmental Physics at Heidelberg University is monitoring several greenhouse gases since decades and is contributing to the European measurement networks ICOS and InGOS. Besides the atmospheric concentrations of CO_2, CH_4, N_2O, CO, SF_6, and H_2, also the isotopic signature of CO_2 with respect to ^{13}C, ^{14}C, or ^{18}O is monitored. A new compact CRDS, the G2201-i from Picarro, was purchased in order to use this spectrometer in Heidelberg and possibly as mobile instrument at other stations or close to emitters like landfills and power plants. The G2201-i measures continuously (with a temporal resolution of 3.6 sec) and simultaneously the concentrations of $^{12}CO_2$, $^{13}CO_2$, $^{12}CH_4$, $^{13}CH_4$, and H_2O within a gas sample. The aim of this master thesis was to install, characterise, and test this new instrument.

2 Theoretical background

2.1 Basics of carbon isotopes

This section follows [*Mook*, 2000].

2.1.1 Physical origin and properties

Atoms with the same proton number but differing neutron numbers are called *isotopes*. Molecules which differ in one or more isotopes are called *isotopologues*. Isotopologues have the same chemical behaviour but differ slightly in physical properties. A higher neutron number implies a higher mass. The number in the left upper edge of the element's letter gives its atomic mass, e.g. the masses of ^{12}C and ^{13}C differ by one atomic mass unit. Due to its increased mass the heavier isotopologue differs also in all mass-depending physical quantities. At a given temperature, it has normally a higher binding energy, a smaller velocity and a smaller molecular diffusion coefficient. Together these quantities lead to a smaller collision frequency with other molecules and a smaller reaction velocity.

For most elements one *common isotope* is much more abundant than the other *rare isotope(s)*. For example, 98.9 % of all carbon on Earth consists of ^{12}C but only 1.1 % consists of ^{13}C. Therefore, the measurement of the common isotope gives, in principle, already all relevant information about how e.g. a carbonic gas acts in the climate system. A separate concentration measurement of a rare isotope provides no additional information concerning the *state* of the climate system. But because of fractionation, the isotopic ratio R of the abundance of a particular rare isotope relative to the common isotope gives insight in the *processes* which run the climate system and also in the sources of the gas:

$$R = \frac{\text{abundance of rare isotope}}{\text{abundance of common isotope}}. \tag{2.1}$$

However, it is not suitable to report the actual value of the isotope ratio R_{sample}. More convenient is the comparison with the isotopic ratio $R_{standard}$ of a standard. Because the relative deviation usually differs only by several per mill, it appears to be useful to report this comparison in the *δ-notation* just by subtracting 1:

$$\delta = \frac{R_{sample}}{R_{standard}} - 1. \tag{2.2}$$

Due to better reading, δ-values are usually given in per mill. In the case of ^{13}C, the associated δ-value is noted as δ^{13}C.

2.1.2 Isotope fractionation

Whenever a chemical substance coexists in two interacting physical phases (e.g. as a gas or bound in a solid) an equilibrium in concentration occurs between these phases. This equilibrium depends on the thermodynamic conditions and the properties of the substance. Due to its slightly different physical properties the heavier isotopologue is normally more abundant in the denser phase, i.e. ${}^{13}R_{solid} > {}^{13}R_{gas}$.
A very important exception are plants. Because ${}^{12}C$ diffuses and reacts faster, the metabolism of plants leads to a depletion of $\delta^{13}CO_2$ in the plant compounds, in general holds ${}^{13}R_{plant} < {}^{13}R_{air}$ [*Park and Epstein*, 1961].

2.1.3 Isotopes in carbon

Carbon is realised in nature in two stable isotopes and one radioactive isotope. The common isotope is ${}^{12}C$ with an abundance of 98.9 %, the rare isotope ${}^{13}C$ has an abundance of 1.1 %. The radioactive isotope ${}^{14}C$ has an abundance of less than 10^{-10} % and a half-life of 5700 years. The ${}^{14}C$ measurement is well developed for dating purposes. Furthermore, it can be used to determine the amount of fossil fuel CO_2 in an air sample [*Levin et al.*, 2003], [*Vogel et al.*, 2010], [*Levin et al.*, 2011]. In this thesis only ${}^{12}C$ and ${}^{13}C$ are measured and discussed.

By convention, the international standard for the ratio ${}^{13}C/{}^{12}C$ is given by the Vienna Pee Dee Belemnite (VPDB) scale ${}^{13}R_{VPDB} = 0.0112372$ [*IAEA*, 1993]. It is the, artificially constant, isotopic ratio ${}^{13}R$ in the marine fossil *Belemnitella americana* found in the Pee-Dee formation in South Carolina. By definition, it is associated with $\delta^{13}C = 0$ ‰. Furthermore, this fossil belongs to the most enriched natural substances with respect to ${}^{13}R$. As a consequence, most other carbonic compounds have a negative $\delta^{13}C$ signature (see Figure 2.1). The annual mean isotopic signature of atmospheric CO_2 at the marine station in Mace Head (Ireland), a good estimation for the atmospheric background in Heidelberg, was in 2012 $\delta^{13}CO_2 = -8.4$ ‰ [*NOAA*, 2014]. The isotopic signature of CO_2 respired by plants is lower due to fractionation during photosynthesis, ranging for C_3 plants from $\delta^{13}CO_2 = -20$ ‰ to -30 ‰. From measurements of ${}^{14}CO_2$ in Heidelberg ambient air, in winter the source strength of biosphere and anthropogenic activities are split in half and in summer the biosphere is contributing even more [*Levin et al.*, 2003]. Thus, for estimating how much and which kind of fossil fuel is burned it is mandatory to have a sufficient knowledge of the biosperic carbon flux. The biospheric signal in Heidelberg comes primary from C_3 plants, the only relevant C_4 plant is corn, which is cultivated on 16 % of the surrounding cropland [*Statistisches Landesamt Baden-Württemberg*, 2014a] and emissions from the fauna are presumable contributing less than 10 %. The mayor anthropogenic CO_2 sources in Baden-Württemberg are the energy sector (26 % of anthropogenic source strength), industry (16 %), heating (26 %), and traffic (32 %) [*Schmidt*, 2014]. The isotopic signature of the major CO_2 sources in Heidelberg are listed in Table 2.1.

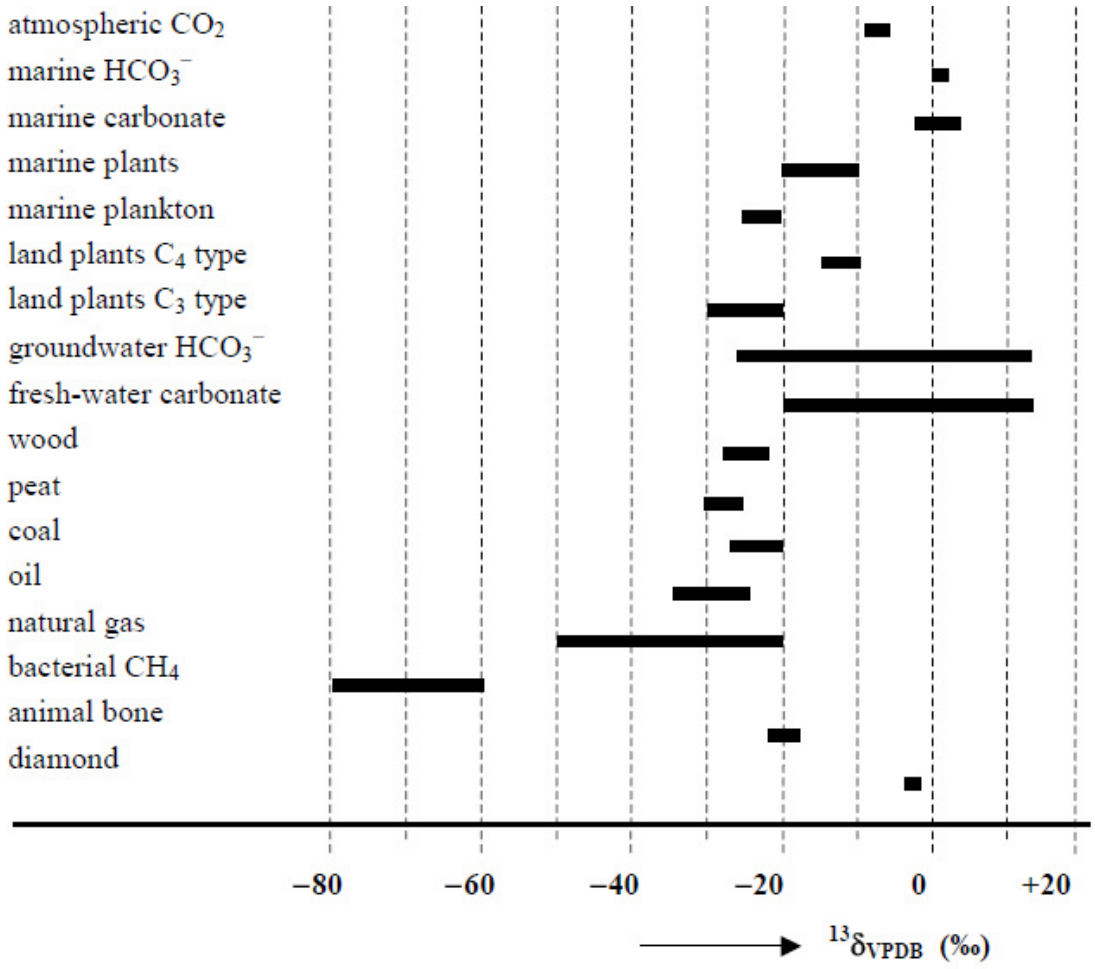

Figure 2.1: *$\delta^{13}C$ signature in carbonic compounds [Mook, 2000]*

In 2010 in Baden-Württemberg 54 % of the methane emissions are from the agriculture (cattle breeding), 31 % from waste management, and 11 % from mining and gas supply [*Statistisches Landesamt Baden-Württemberg*, 2014b].
Furthermore, all regional data might be influenced by large industrial emitters like Heidelberg Zement (Leimen) and BASF (Ludwigshafen).

Table 2.1: *Isotopic signatures of the major sources of CO_2 and CH_4 in Heidelberg.*

Name	$\delta^{13}CO_2$ in ‰	$\delta^{13}CH_4$ in ‰	Reference
Mace Head (clean air)	-8.40 (2011-12)	-47.47 (2010-11)	[*NOAA*, 2014]
C_3 Plants	-25 ± 5	(negligible)	[*Mook*, 2000]
Exhaust emissions	-28.4 ± 0.1	-28.0 ± 2.4	[*Bönisch*, 1997]
Coal power plant MA	-25	(negligible?)[1]	[*Vardag*, 2012]
Domestic heating	-38.5	-40.3 ± 0.7[2]	[*Vardag*, 2012]
BASF (industry)	-49	?	[*Vardag*, 2012]
Cattle breeding	(negligible)	-61.8 ± 2.0	[*Glatzel-Mattheier*, 1997]
Landfill sites	(negligible?)	-55.4 ± 1.4	[*Bergamaschi et al.*, 1998]

[1] The isotopic signature of coal gas is -27.2 ± 2 ‰, ranging from -70 to -13 ‰ [*Glatzel-Mattheier*, 1997]. However, the methane emissions from a coal power plant are either not existing or at least negligible.

[2] Isotopic signature of the natural gas provided by the municipal utilities in Heidelberg. However, it seasonally varies from -50 to -34 ‰ [*Glatzel-Mattheier*, 1997], see also Chapter 6.

2.2 Cavity Ring-Down Spectrometry (CRDS)

Due to quantum mechanics each molecule has its unique absorption spectrum. From the physical point of view, isotopologues are just different molecules. When a gas sample is irradiated by a laser beam with a suitable wavelength, only one of the isotopologues is significantly absorbing some light while the others are not. Thus, different isotopologues can be differentiated by irradiating the gas sample with a laser beam of a matching wavelength [*Demtröder*, 2010].

In Cavity Ring-Down Spectrometry (CRDS), the beam from a single-frequency laser enters a cavity defined by two or more high reflectivity mirrors. The mirrors are not perfectly reflecting but have a reflectivity of 99.999 % [*Van Pelt*, 2008]. So a small fraction of the light is continuously leaking out. A photodetector is counting the photons which leak through one of the mirrors. When the photodetector measures a certain threshold (reached after a few tens of microseconds) the laser is immediately turned off. Afterwards, the light intensity $I(t)$ in the cavity continuously decreases due to leakage. The leaking rate is proportional to the remaining intensity and therefore, the decay, respectively the *ring-down*, of the intensity is governed by an exponential decay law:

$$I(t) = I_0 \cdot e^{-\lambda_0 \cdot t} \tag{2.3}$$

with the initial intensity I_0 and the ring-down time $\tau_0 = \frac{1}{\lambda_0}$ of the "empty" cavity. In this context, an empty cavity is not evacuated but filled with a gas which is not absorbing at the current wavelength of the laser. Practically, an empty cavity is realised by shifting the wavelength of the temperature-tunable laser in a range where no absorber exists. When an absorbing gas enters the cavity (respectively the laser wavelength is tuned for matching the absorption line of this gas), a second loss mechanism occurs. Again the laser is turned off when the photodetector reaches the threshold, so the initial intensity I_0 is the same. But the light beam experiences two exponential loss mechanisms, the leakage and the absorption:

$$I(t) = I_0 \cdot e^{-(\lambda_0 + \lambda_a) \cdot t} \tag{2.4}$$

where the absorption coefficient λ_a depends according to the Beer-Lambert law, more or less linearly, on the concentration of the absorbing molecules. The ring-down time of the "filled" cavity is $\tau_a = \frac{1}{\lambda_0 + \lambda_a}$. By comparing the ring-down time of the empty cavity and of the filled cavity, the absorption coefficient λ_a and thus the concentration of the absorbing gas can be derived.

The absorption lines of molecules are no perfectly discrete peaks but Lorentz-shaped due to the natural line width, Doppler broadening, and pressure broadening. By fitting a Lorentz-peak in the data of a scanned absorption line, the absorption coefficient can be determined with high accuracy.

A detailed overview of CRDS can be found in [*Paldus and Kachanov*, 2005].

3 Experimental set-up of the Heidelberg system

3.1 Cavity ring-down spectrometer

The cavity ring-down spectrometer (G2201-i from Picarro) is able to measure the gas concentrations of $^{12}CO_2$, $^{13}CO_2$, $^{12}CH_4$, $^{13}CH_4$, and H_2O continuously and simultaneously with a temporal resolution of 3.6 sec. It is not measuring isotopologues which contain other isotopes than ^{16}O and ^{1}H and is therefore explicitly not able to measure the total concentrations of CO_2 and CH_4 without assumptions concerning the not detected isotopologues. On the other hand, the measurement output enables to calculate $\delta^{13}CO_2$ and $\delta^{13}CH_4$ directly.

3.1.1 Cavity and Lasers

The G2201-i cavity has a volume of 35 ml and a length of 25 cm. The measurement conditions are controlled by multiple sensors and hold constant. The cavity temperature is regulated at $(45 \pm 0.0003)\,°C$ and the cavity pressure at (148 ± 0.02) Torr. The laser beam is hold in the cavity by a three-mirror-systems which may lead to an effective path length of more than 20 km. Two mirrors would lead to a standing wave, three mirrors lead to a guided travelling wave which offers much higher accuracy [*Van Pelt*, 2008].

The spectrum is scanned by three temperature-tunable lasers with wavelength ranges around 1600 nm, 1651 nm, and 1659 nm, respectively (see Figure 3.2, and 3.3 or A.8). The laser at 6252 $\frac{1}{cm}$ matches with the absorption lines of $^{12}CO_2$ and $^{13}CO_2$ (see Figure 3.2), the second laser at 6057 $\frac{1}{cm}$ matches with the absorption lines of HP-$^{12}CH_4$, and the third laser at 6229 $\frac{1}{cm}$ scans HR-$^{12}CH_4$, $^{13}CH_4$ (same peak in HP- and HR-mode, see next section about these modes), and H_2O (see Figure 3.3 for the second and third laser). The exact wavelength of the absorption lines are listed in Table 3.1. Altogether the lasers scan at 68 different wavelengths.

For the scans, the wavelength steps are realised by a laser targeting control loop and a wavemeter which feedback the laser control electronics until the laser is tuned to a suitable wavelength which is then saved at the wavemeter. Within the cavity, the laser beam is guided in cycle by three mirrors and a photodetector is continuously measuring the intensity, which is transmitted through one of the mirrors. From the detected intensity evolution, the analysis electronics calculate for every

isotopologue the ring-down time and finally the gas concentration by comparing the ring-down time with the actual wavelengths saved at the wavemeter (see Figure 3.1).

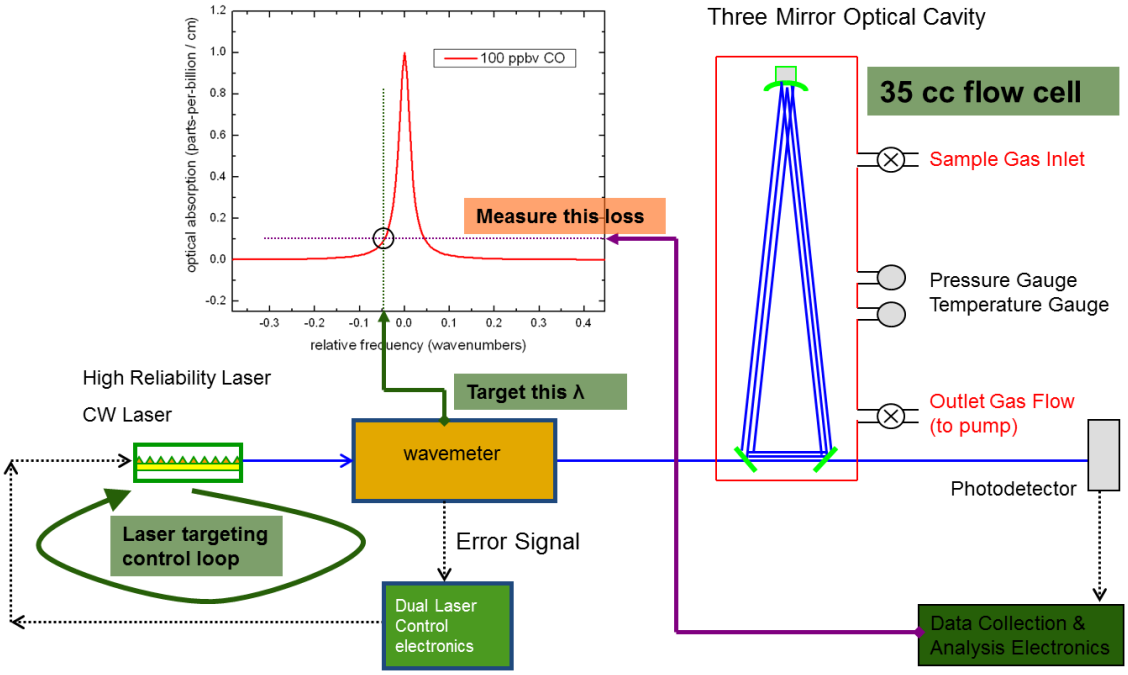

Figure 3.1: *Measurement principle of the G2132-i [Internal presentation of Picarro provided by Chris Rella, 2014] which is similar to the G2201-i. The scans are performed by three lasers with temperature-tunable wavelength. The laser is tuned to the desired wavelength by the laser targeting control loop and a wavemeter, which temporarily saves the wavelength. The laser beam enters the cavity where the beam is guided in cycle by three mirrors. The cavity has a volume of 35 ml and is pressure and temperature controlled. The light intensity, which is leaking through one of the mirrors, is detected by a photodetector. The analysis electronics calculate the ring-down times from the measured intensity evolution. Finally, the ring-down times are compared with the actual wavelengths saved by the wavemeter to determine the gas concentration.*

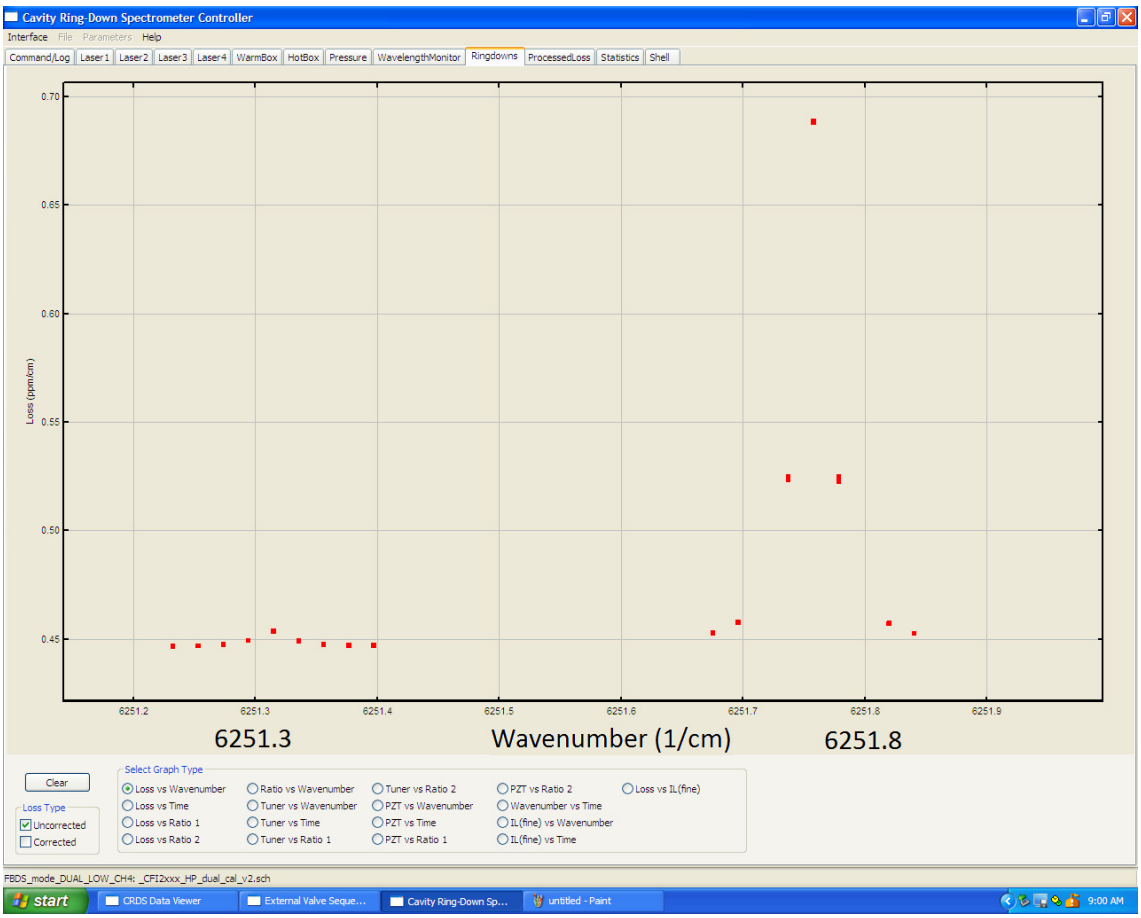

Figure 3.2: *The scanned CO_2 lines as displayed in the CRDS Controller: Both peaks, $^{12}CO_2$ at 6251.8 $\frac{1}{cm}$ and $^{13}CO_2$ at 6251.3 $\frac{1}{cm}$, are scanned by the same laser. For the other two lasers similar spectra can be displayed in the controller, see Figure A.8.*

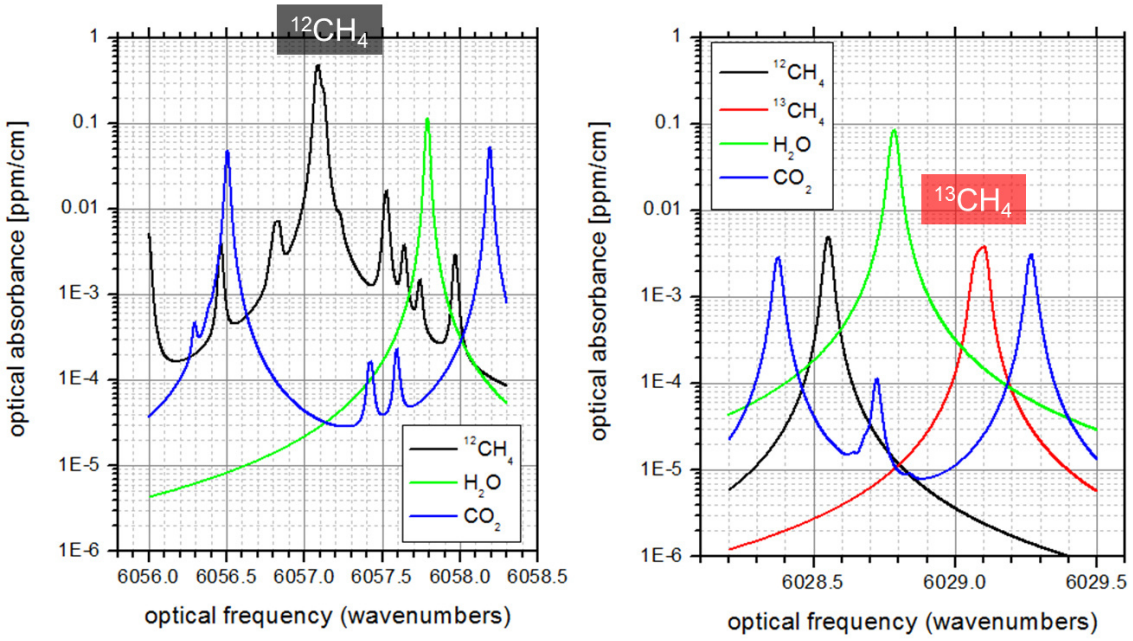

Figure 3.3: *Environment of the absorption lines of CH_4 and H_2O which are scanned by two of the lasers. Left: HP-$^{12}CH_4$ peak. Right: HR-$^{12}CH_4$ peak, $^{13}CH_4$ peak, and H_2O peak. Modified figure from [Internal presentation of Picarro provided by Chris Rella, 2014].*

Table 3.1: *Wavenumber and wavelength of absorption lines scanned by the lasers*

Peak	$^{12}CO_2$	$^{13}CO_2$	HP-$^{12}CH_4$	HR-$^{12}CH_4$	$^{13}CH_4$	H_2O
Wavenumber in $\frac{1}{cm}$	6251.76	6251.32	6057.08	6028.55	6029.09	6028.78
Wavelength in nm	1599.5	1599.7	1650.9	1658.8	1658.6	1658.7

3.1.2 Two measurement-modes in methane

For ambient air conditions, $^{12}CH_4$ and $^{13}CH_4$ have suitable absorption lines at 1650.9 nm and 1658.6 nm, respectively. These lines are scanned in every measurement and are the data basis for the *High Precision* HP-mode. Unfortunately, the $^{12}CH_4$ peak at 1650.9 nm saturates when the CH_4 concentration exceeds 12 ppm (see Figure A.8, where this peak is already sharp formed at only 2 ppm). For a larger operating range, the instrument is also scanning another $^{12}CH_4$ line at 1658.8 nm. This line is much broader than the line at 1650.8 nm, meaning a higher saturation level but also less precision for a CH_4 concentration below 12 ppm. The data of this line are the basis of the *High Range* HR-mode. For the measurement of ambient air with the typical $^{12}CH_4$ mole fraction of 2 ppm, the HP-mode is more precise. For samples with a mole fraction around 10 ppm the precision of both modes is comparable. For concentrations higher than 12 ppm the HP-mode is not working.

3.2 Sample inlet system

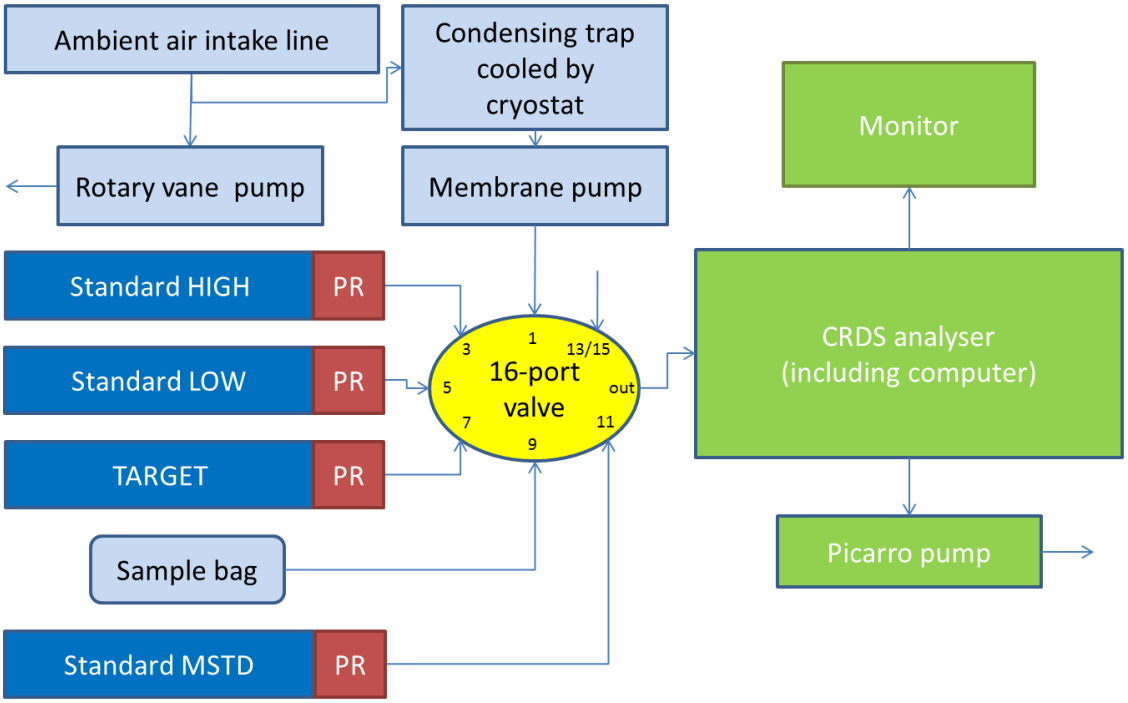

Figure 3.4: *Set-up of the measurement system. Green: Devices from Picarro. Dark blue: Calibration and quality control cylinders. Red: Pressure Regulators PR. Light blue: Ambient air sampling system and natural gas sample bag. All samples are connected to an inlet port of the 16-port valve. The 16-port valve is controlled by the software of the CRDS analyser.*

For automatic measurement, we have built an inlet system containing a 16-port rotary-valve (Valco Valve from VICI®, model: EMT2CSD16UWE). Its outlet is connected to the inlet of the CRDS analyser. At up to 16 inlet ports different gas samples (e.g. cylinders, bags, ambient air line) can be connected. The computer can control the 16-port valve via a serial port. The pre-installed Picarro Scheduler allows to perform automatic and cyclic measurement sequences.
For security, every second port of the valve is closed by a blind plug. So effectively only eight ports are in use at the moment. Three ports (3,5,7) are reserved for calibration and quality control cylinders. Two ports (9,11) are usually in use for measuring and calibrating samples which are highly concentrated CH_4. Ambient air is permanently connected to port 1 and two ports are available for additional samples. The whole inlet system is built with stainless steel tubes from Dockweiler® (size: 1/16", 1/8", 1/4", TCC-quality) and fittings from Swagelok®.

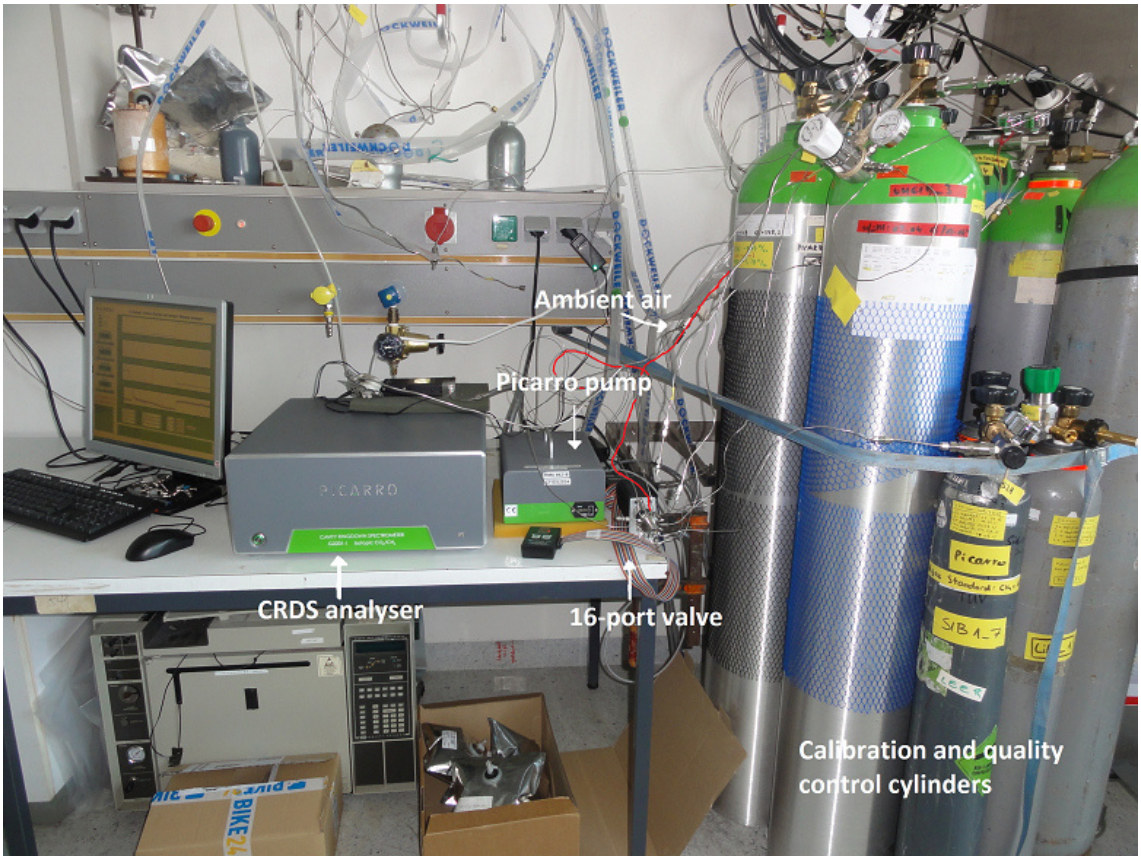

Figure 3.5: *Photography of the experimental set-up. The core components do not require more than a desk. Aiming for a mobile instrument, smaller calibration cylinders are required. Because every 5 hours only about 800 ml of calibration gas are required, also smaller calibration cylinders appear to be possible. All in all, the G2201-i set-up is suitable as mobile instrument.*

3.3 Ambient air measurement

At the Institute of Environmental Physics, two suction pipes supply the laboratory with ambient air from the roof of the building (sampling height: ca. 30 m). One pipe is sampling air from South-East, where the city lays, the other line is sampling air from South-West, where the campus of the university is located. The CRDS is measuring South-East air only. This air intake is also continuously sampled by the *Fourier Transform Infra-red Spectrometer* [*Hammer et al.*, 2013] and, via a buffer volume, by the *Gas Chromatograph* [*Hammer et al.*, 2008]. The comparison with these instruments is presented in Section 5.

The South-East air intake line is flushed by a rotary vane pump. From this intake line, a supply line, which is flushed by a membrane pump (KNF Neuberger GmbH) and an overpressure valve, branches off to the CRDS. Before measurement, the ambient air is dried by a water condensing trap connected in series between the suction pipe and the membrane pump. The trap (volume: 230 ml) is located in a well-isolated reservoir of ethanol which is kept at a temperature of -40 °C by a cryostat (Lauda ETK50). The condensing trap has to be replaced twice a week.

Despite the instrument is able to measure without preload pressure due to the Picarro pump at the outlet of the instrument, the recommended preload pressure is 0.2-0.5 bar. A preload pressure of more than 0.5 bar might damage the internal overpressure valve (personal correspondence with Picarro). To be on the save side, we supply the spectrometer with an ambient air flow of 40 $\frac{\text{ml}}{\text{min}}$, which roughly matches with an preload pressure of 0.5 bar. This value can be realised by the matching setting of the overpressure valve. In this setting, the membrane pump supplies a flux of roughly 1.38 $\frac{\text{L}}{\text{min}}$ to the overpressure valve when the condensing trap does not contain any ice. In summer, when a lot of water is condensing, only a flow of down to 0.36 $\frac{\text{L}}{\text{min}}$ is supplied before the condensing trap is replaced.
For consistency, all measured cylinders should also supply a flow of 40 $\frac{\text{ml}}{\text{min}}$ which we carefully controlled since April 2014. Before that date, we measured with somewhat arbitrary flows between 30 and 70 $\frac{\text{ml}}{\text{min}}$ (preload pressure of 1.5 bar).[1]

3.4 Calibration and quality control

For the calibration (Section 4.5) of the ambient air data and samples at ambient air conditions, we used the calibration cylinders which are called in Figure 3.4 LOW and HIGH. For the calibration of samples which are highly concentrated in CH_4, we used the calibration cylinder MSTD. Furthermore, for quality control the cylinder TARGET is measured with a fixed frequency in between ambient air (or other) measurements. All cylinders were filled with a diving compressor (model: P3W, Bauer, Germany) in Heidelberg. The nominal concentrations of these cylinders are

[1] Information about the supplied flow is logged as the parameter *Outlet Valve* in the output file.

taken from GC analysis of the pressurised cylinders, the δ-values are results from mass spectrometry (see Table 4.7).
We used by default pressure regulators from Scotty™ (model: 14A, Scott Specialty Gases, USA). For comparison we tested a pressure regulator from Tescom which finally was connected at HIGH since April 2014.

4 Characterisation and calibration

It is quite easy to install the G2201-i and after switching on it starts automatically to measure and record whatever is connected to its gas inlet. But aiming for accurate and precise measurements, potential instrumental cross-sensitivities need to be characterised and a suitable calibration and measurement strategy has to be developed. After the installation of the instrument in April 2013, we performed the first series of tests. In June 2013, we detected a correlation between the measured $\delta^{13}C$ values and the barometric pressure, which exceeded the instrument specifications (see Figure 4.8). Consequently, the instrument was in repair at Picarro (U.S.A.) from August to October 2013. As long as not otherwise stated, all data shown in this thesis are measured with the repaired instrument.

4.1 Data output and analysis

4.1.1 Data output of the instrument

The basic data output is saved in one ASCII file per hour. The output is already translated from raw electric signals to physical quantities by the software of the analyser. Per default, 50 parameters are saved in the basic files[1]. Within each 3.6 s, four data rows are added to a file. The most important parameters are:

- The mole fraction of $^{12}CO_2$, $^{13}CO_2$, $^{12}CH_4$, $^{13}CH_4$, and H_2O. For CH_4, all data are provided separately in HP- and HR-mode.

- The internal computer automatically applies a water vapour correction for $^{12}CO_2$ and $^{12}CH_4$. The output contains the actual measured (wet) and the water vapour corrected (dry) data.

- Furthermore, the computer automatically calculates $\delta^{13}CO_2$ and $\delta^{13}CH_4$ by using the dry ^{12}C mole fraction and the wet ^{13}C mole fraction. The δ-values are provided as raw data but also averaged as running means with respect to 30-sec, 2-min, and 5-min intervals.

- Several time stamps like date, clock time, and Lotus-time are provided.

[1] This is the default number of parameters. With the pre-installed Set-up Tool also other parameters can be added to the basic output file. Anyway, all measured parameters are saved in the additional log-files.

- The instrument can communicate with the 16-port-valve. The current port is documented for every measurement point. This information is required for the external data analysis.

- Already in the basic files, but more prominent in the additional log-files, a lot of sensor data are documented, which helps in trouble-shooting. First of all, the thermodynamic process quantities, the temperature and the pressure in the cavity and the gas flow through the internal overpressure valve, are monitored.

4.1.2 Data analysis with GNU R

Picarro is not providing a program for external data analysis. I wrote the analysis routine by myself with the programming language *GNU R*. This language is well suited for treating large amounts of data and is able to plot the results in a wide variation of user modified ways. The core routine consists of more than 3000 lines of code. With its help, we can automatically import all relevant data in GNU R, flag bad data, apply corrections, and calibrate the corrected data. For external treatment, the routine gives out several csv-files containing intermediate results: 1) all raw data of the measurement bond in one file, 2) the flagged raw data, 3) the corrected data, and 4)+5) the calibrated data. The calibrated data are produced in two files depending on the desired physical quantities (see Section 4.5.4). Furthermore, a bundle of modules is available which will be listed in a supplementary manual.

All data are evaluated in UTC to be consistent throughout the year and the globe.

4.1.3 Specifications of the instrument

By default, the instrument simultaneously measures $^{13}CO_2$ and $^{13}CH_4$ but it is also able to focus on one of them. In these modes, the other one is not measured but the focussed one is measured more precisely. The mode selection is previous to the measurement and thereby obligatory during an automatic measurement. Primarily aiming for atmospheric monitoring, we are now only discussing the "Simultaneous mode". In Section 4.2, we will also introduce the "$\delta^{13}CH_4$-only mode".

The temporal resolution of the CRDS is 3.6 sec[1]. On the one hand, this is much higher than required and on the other hand the 3.6-sec data are influenced by noise. Therefore and due to limited computing capacity, we decided to average the output data to 1-min values. In the following, we treat these 1-min values as our actual *raw data* where we ignore the statistical error of the 1-min averages and therefore regard these raw data points as error free and Gaussian distributed. Later, we will

[1]The instrument output is containing 4 lines all 3.6 s, one line per spectrum. A complete measurement cycle contains 4 spectra.

primarily use 15-min averages as lowest temporal resolution.
The manufacturer gives specifications for the performance of the instrument, which give the worst-case benchmarks for the expectable precision and drifts. To check the specifications, we measured an ambient air cylinder for three days. The raw, internally water-corrected results averaged over 1, 5, and 60 min are shown in Figure 4.1.

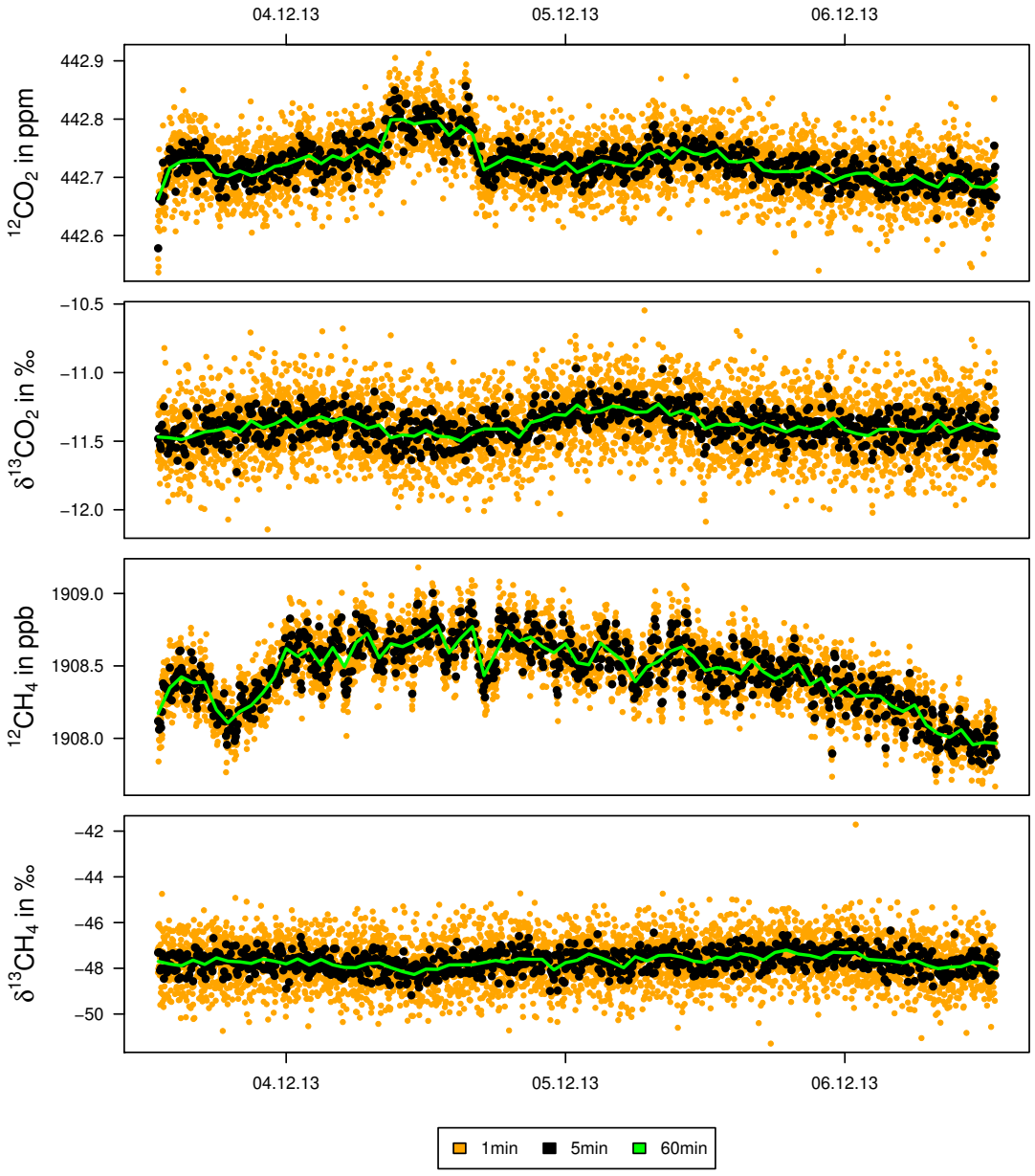

Figure 4.1: *Raw, internally water-corrected data of a dry gas cylinder measurement averaged over 1, 5, or 60 min. No calibration or drift correction was applied.*

The definition of the specifications were made by the manufacturer [*Picarro*, 2014], the specifications of the manufacturer are marked as grey lines in Figure 4.2 and 4.3.

^{12}C Concentration Precision Based on the raw 1-sec data, the specification is defined as the standard deviation within an interval of 30 sec. For CH_4 was specified $\sigma_{30\,s} = 5\,\text{ppb} + 0.05\,\%$ of reading while we measured $\sigma_{30\,s} = 3.5\,\text{ppb}$. For CO_2 a relative error of up to 2.2 % was specified. With an overall CO_2-concentration of roughly 450 ppm, we measured with a precision of $\frac{\sigma_{30\,s}}{[CO_2]} \approx \frac{0.74}{450} = 0.16\,\%$. The ^{12}C-specification is matched for both gases.

δ^{13}C Precision Based on 5-minute averages, the specification is defined as the standard deviation of these 5-min values during 1 hour. The mean standard deviations are $\sigma_{1\text{hour@5min}}(\delta^{13}CO_2) = 0.095\,‰$ and $\sigma_{1\text{hour@5min}}(\delta^{13}CH_4) = 0.4\,‰$, see Figure 4.2. The δ^{13}C precision-specification is matched for both gases.

δ^{13}C Drift Based on 1-hour averages, the specification is defined by the peak-to-peak difference within an interval of 24 hours. For both gases, the mean drift is only half as large as specified, the δ^{13}C drift-specifications are matched, see Figure 4.3. **Remark:** The data shown in Figure 4.1 are from December 2013. When checking the specifications in April until June 2013, the drift in $\delta^{13}CH_4$ was sometimes more than twice the specification. Therefore, we sent the instrument back for repair (see Section 4.4.1).

Table 4.1: *Specifications of the repaired instrument given by the manufacturer and measured in December 2013. The exact definitions are given in [Picarro, 2014].*

Specification	Definition	Manufacturer	Measured
$^{12}CO_2$ precision	$\sigma_{30\,s}$	<2.2 % of reading	0.16 % o. r.
$^{12}CH_4$ precision	$\sigma_{30\,s}$	5 ppb+0.05 % o. r.	3.5 ppb
$\delta^{13}CO_2$ precision	$\sigma_{1\text{hour@5min}}$	0.16 ‰	0.095 ‰
$\delta^{13}CH_4$ precision	$\sigma_{1\text{hour@5min}}$	1.15 ‰	0.4 ‰
$\delta^{13}CO_2$ drift	Δ_{max} in 24 h @1 h	0.6 ‰	0.3 ‰
$\delta^{13}CH_4$ drift	Δ_{max} in 24 h @1 h	1.5 ‰	0.8 ‰

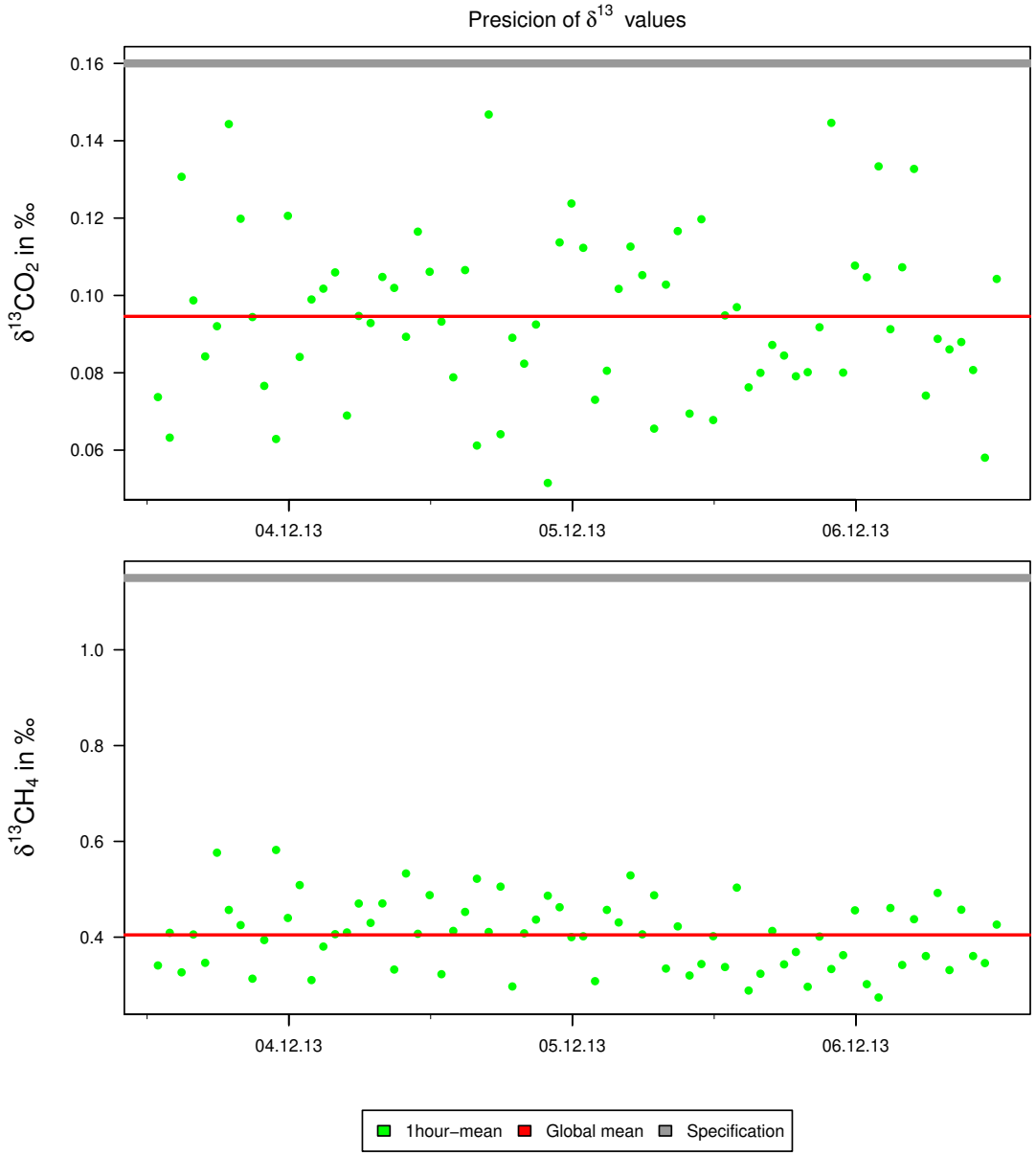

Figure 4.2: *Checking the precision-specification of $\delta^{13}CO_2$ and $\delta^{13}CH_4$ (in simultaneous mode). The precision is here defined as standard deviation of 5-min values averaged over 1 hour. Grey lines: specifications given by the manufacturer. Red lines: mean precision over 3 days.*

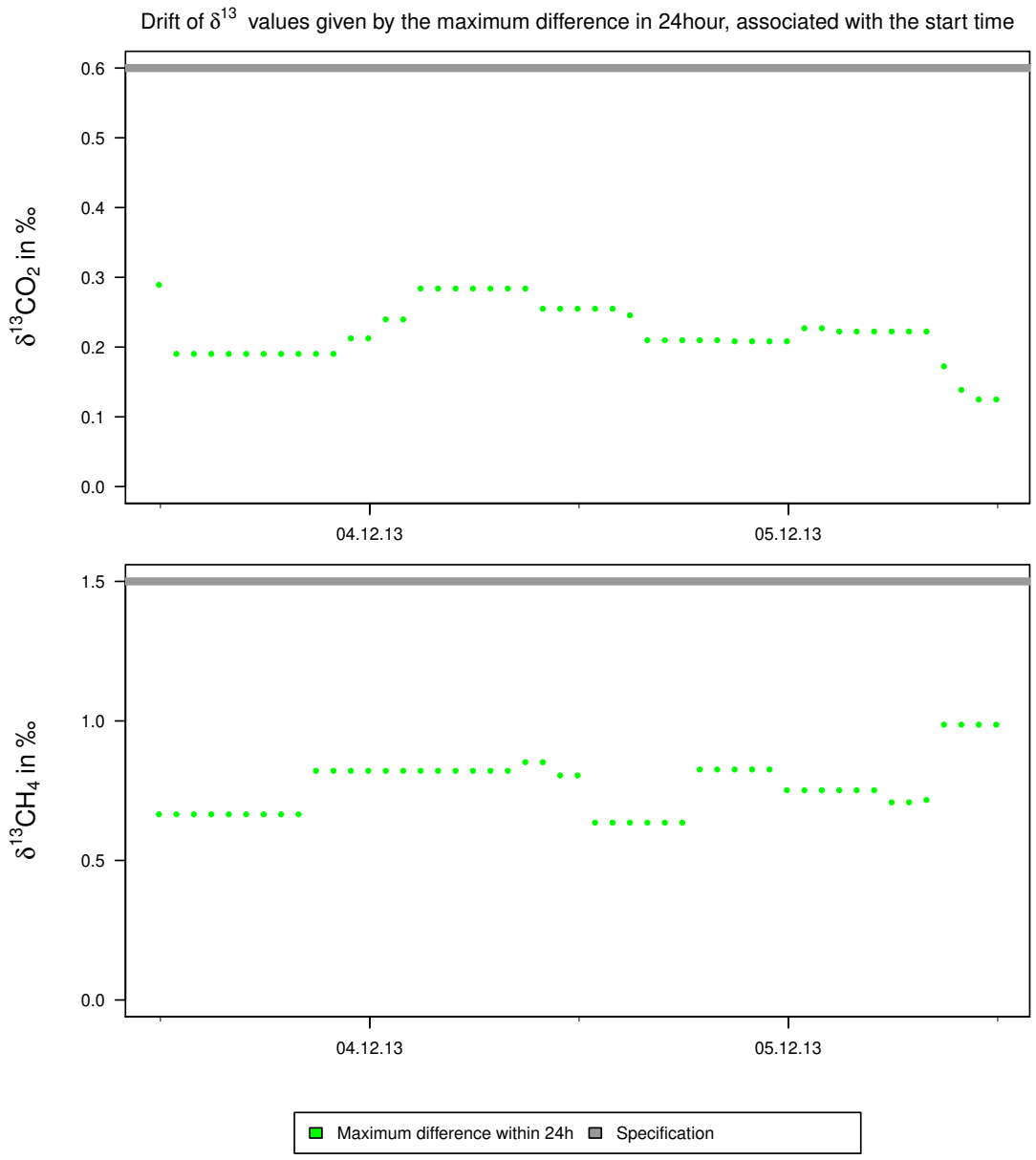

Figure 4.3: *Checking the drift-specification of $\delta^{13}CO_2$ and $\delta^{13}CH_4$ (in simultaneous mode). The drift is defined as peak-to-peak difference of 1-hour averages within 24 hours. Grey lines: specifications given by the manufacturer.*

4.2 Allan variance analysis of the output data

From Figure 4.1, we can see that 1-min and even 5-min averages have still an unsatisfactory precision and measurement error for the δ^{13}C values. With a larger averaging period, the precision can be increased, at least for a drift-free instrument. However, a larger averaging period means less temporal resolution. Thus, a compromise between precision and temporal resolution has to be found. Moreover, in a non-drifting instrument the standard deviation has a constant value which indicates the intrinsic noise of the instrument. But in reality, the standard deviation is not constant due to the time-dependent instrumental drift. Therefore, an upper limit for sensitive averaging periods exists. For longer periods not only the resolution but also the precision gets worse. For a well-grounded choice of the optimal averaging period, we have to derive the standard error of the global mean value of a measurement as a function of the temporal resolution of the data (i.e. after the initial averaging of the raw data). This is done by the *Allan variance analysis* which is explained in *Werle et al.* [1993].

In the Allan variance analysis, the un-calibrated data of a long-term non-stop measurement with N equidistant data points is split in m sub intervals with each containing n measurement points ($N = m \cdot n$). First, at a fixed n for every sub interval the mean value is calculated and the averaging error is omitted. Then, the standard deviation of this set of mean values is calculated. This final value is called *Allan deviation* and gives the standard error $\bar{\sigma}$ of the global mean value of the overall measurement for this choice of n. By repeating this procedure for all possible n, we get the function $\bar{\sigma}(n)$.

To derive the Allan deviations of our instrument, we used the same data as for the specification check (see Figure 4.1). The Allan deviations as function of n are plotted in Figure 4.4 and the numeric values of several averaging periods are listed in Table 4.2. The plots show the typical decline for averaging periods up to 30-60 min followed by a more or less sharp rise. What happens after the rise does not matter because the instrumental drift is significantly contributing to the results, further minima are just random. The following conclusions can be read off:

1. There is no optimal averaging period for all parameters, at once. While $\bar{\sigma}([^{12}CO_2])$ reaches the minimum within 30 min and $\bar{\sigma}([^{12}CH_4])$ is more or less constant for all periods between 4 and 30 min, the Allan deviations $\bar{\sigma}(\delta^{13}CO_2)$ and $\bar{\sigma}(\delta^{13}CH_4)$ are optimal for 60 min. The choice of the optimal averaging period depends on the aim of the measurement.

2. Within the first 60 min no slope is rising. Concerning the concentrations, we might waste temporal resolution when averaging up to 60 min but at least do not degrade the Allan deviation.

3. The Allan deviation for 1 min gives the actual standard deviation of measurements which are not drift-corrected, i.e. the instrumental repeatability.

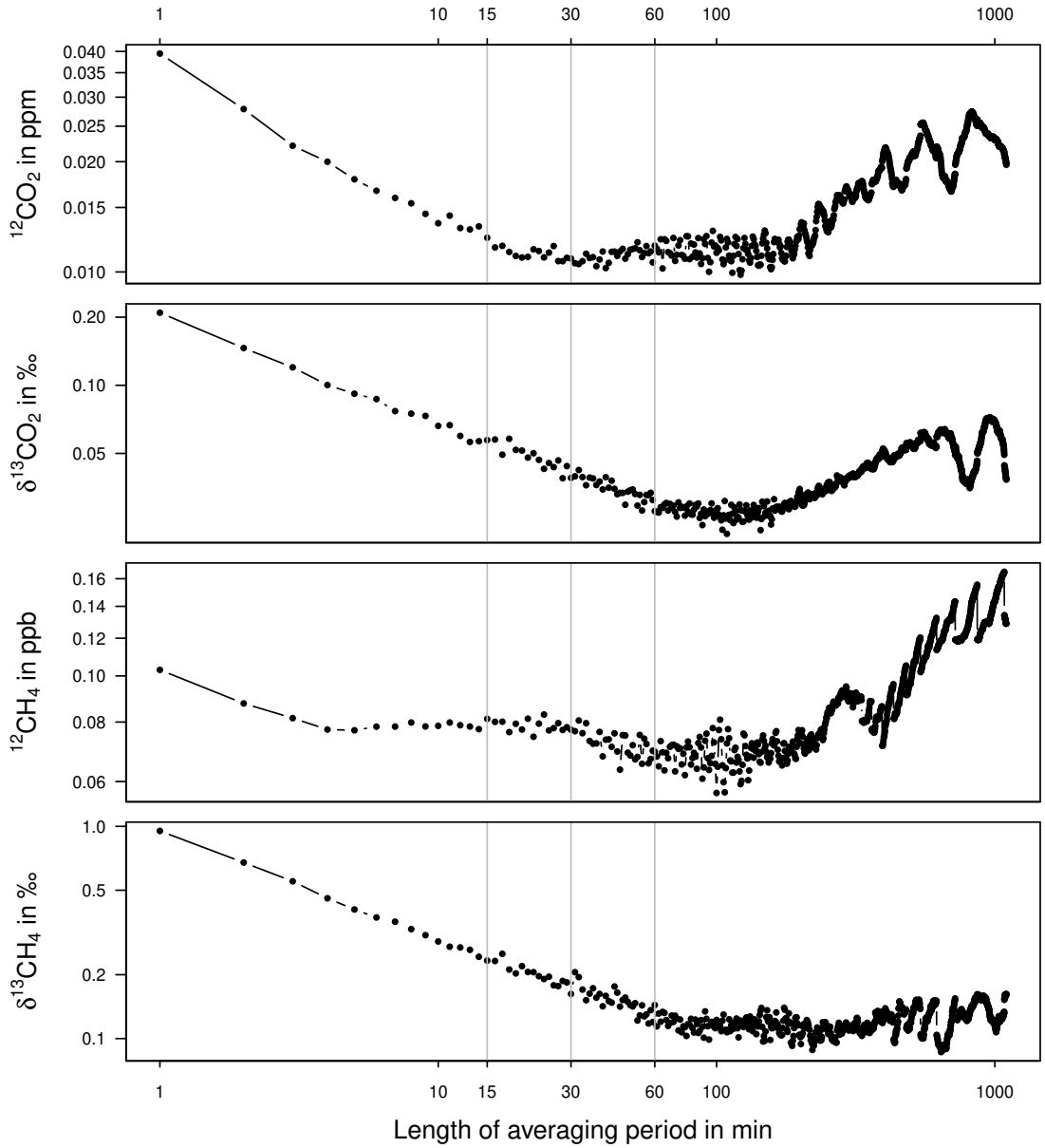

Figure 4.4: *Allan deviation of different measured quantities, calculated on the basis of 1-min values. Starting from the 1-sec data the Allan deviations are virtually the same. For concentration measurements, already 15-min averages give most satisfying precision. For the measurements of isotopic signatures, 60-min averages give the best precision.*

Table 4.2: *Allan deviations of selected averaging periods. For $\delta^{13}CH_4$, the second value gives the Allan deviation of data measured in the $\delta^{13}CH_4$-only mode (not shown in Figure 4.4). The Allan deviation for 1 min is the intrinsic error of our averaged raw data and furthermore the standard deviation of data which is not drift-corrected by calibration.*

Average	$[CO_2]$ in ppm	$\delta^{13}CO_2$ in ‰	$[CH_4]$ in ppb	$\delta^{13}CH_4$ in ‰
1 min	0.039	0.209	0.103	0.949 resp. 0.690
5 min	0.018	0.091	0.078	0.406 resp. 0.286
15 min	0.013	0.056	0.081	0.232 resp. 0.157
25 min	0.011	0.045	0.077	0.197 resp. 0.114
30 min	0.011	0.038	0.077	0.164 resp. 0.112
60 min	0.012	0.027	0.069	0.144 resp. 0.098

From Table 4.2 we can read off that for the concentration of CO_2 and CH_4 virtually optimal precision is already reached with 15-min averages. However, for $\delta^{13}CO_2$ and $\delta^{13}CH_4$ 30-min or even 60-min averages give more precise results.
For $\delta^{13}CH_4$, we evaluated a measurement which was similar to the one shown in Figure 4.1 (first of all, the CH_4-concentration was also about 2 ppm) but measured in $\delta^{13}CH_4$-only mode. The Allan deviations of this measurement are significantly smaller than for the simultaneous mode. They are given in the last column of Table 4.2 at second position.

4.3 The challenge of a small flow

4.3.1 Flushing time

When a new measurement is started, i.e. the particular sample is connected via the inlet system to the analyser, the cavity is still filled by the gas of the former measurement. But these remains would lead to wrong observations of the new sample. The required *flushing time* is depending on the cavity volume and the incoming and outgoing flow. The cavity has a volume of 35 ml and is pressure-controlled by the internal overpressure valve which is supplied by approximately 40 $\frac{\text{ml}}{\text{min}}$. To determine the flushing time, we evaluated the temporal evolution within the measurement intervals of a calibration cylinder which was routinely measured every 4 hours for 20 min. (In this case the pressure regulator effect is negligible, see below.) A respective measurement interval is shown in Figure 4.5. The 16-port valve switched within the minute (exactly: at the 38$^{\text{th}}$ second) of the first red dot, i.e. since then the cavity was flushed by gas from the cylinder. In the last 22 sec of the first red dot apparently only the former sample was measured. Also during the next minute, the influence of the former sample is obvious. By zooming in towards the blue dots, we receive that the cavity has to be flushed for 4 min with the new sample before the actual measurement can start. To be on the save side, we add another minute and get a flushing time of 5 min. Therefore, the first 5 min of every measurement interval have to be omitted.

4.3.2 Pressure regulator effect, equilibration time

Besides the flushing time also the *pressure regulator effect* may influence the actual measurement. Each pressure regulator is reacting with the gas flow (flowing from the cylinder, passing the pressure regulator, to the analyser). When the pressure regulator was not flushed for some time, the gas in the pressure regulator is in a static equilibrium with the pressure regulator surfaces. When the pressure regulator is flushed, this static equilibrium becomes disturbed and after some time a dynamical equilibrium is reached. Then the pressure regulator is *conditioned* with respect to the particular gas and there is no more net reaction between pressure regulator and flowing gas. The magnitude of the pressure regulator effect depends on the used pressure regulator, but also on the time between two measurements (i.e. flushings) of the cylinder, the size of the flow, and the time since first flushing. Facing a large flow of several 100 $\frac{\text{ml}}{\text{min}}$, the pressure regulator equilibrates quite fast with the flowing gas why the new equilibrium is reached in a short time. However, being able to measure with a flow of only 40 $\frac{\text{ml}}{\text{min}}$, we are facing a long equilibration time.

The upper panel in Figure 4.6 shows the calibrated CO_2 concentration[1] of a cylinder with a Scotty pressure regulator which was not flushed for half a year, i.e. the reg-

[1] For CH_4, the pressure regulator effect is much lower and the equilibrium is already reached within the flushing time of 5 min.

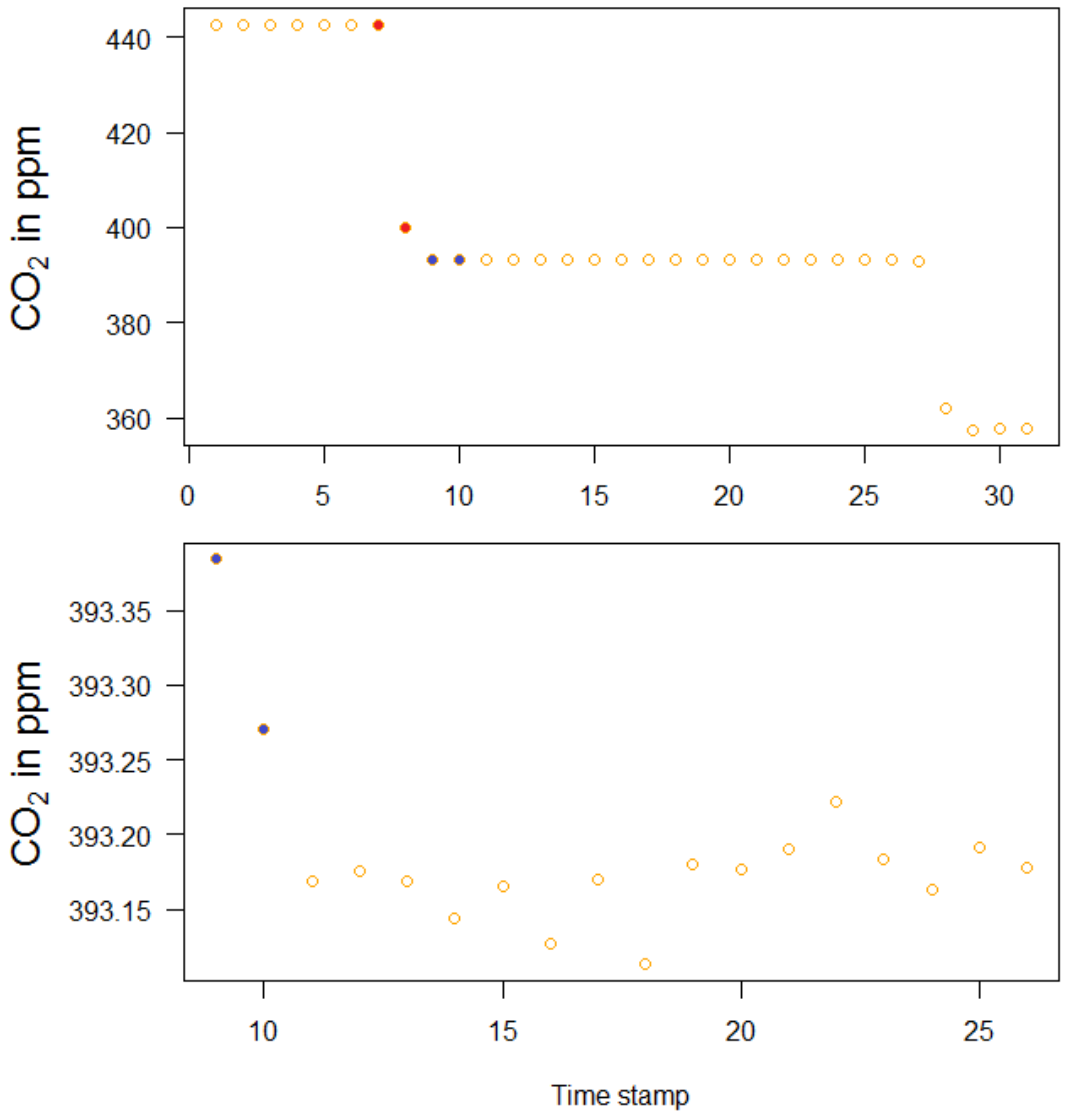

Figure 4.5: *A measurement interval of a calibration cylinder and the embracing measurements are shown. The regarded interval started in minute 7, the lower panel is a zoom of minute 9 to 26. After switching the port of the 16-port valve, the cavity has to be flushed for at least 4 min before the actual measurement can start (see red and blue dots). For safety, we estimate a flushing time of 5 min.*

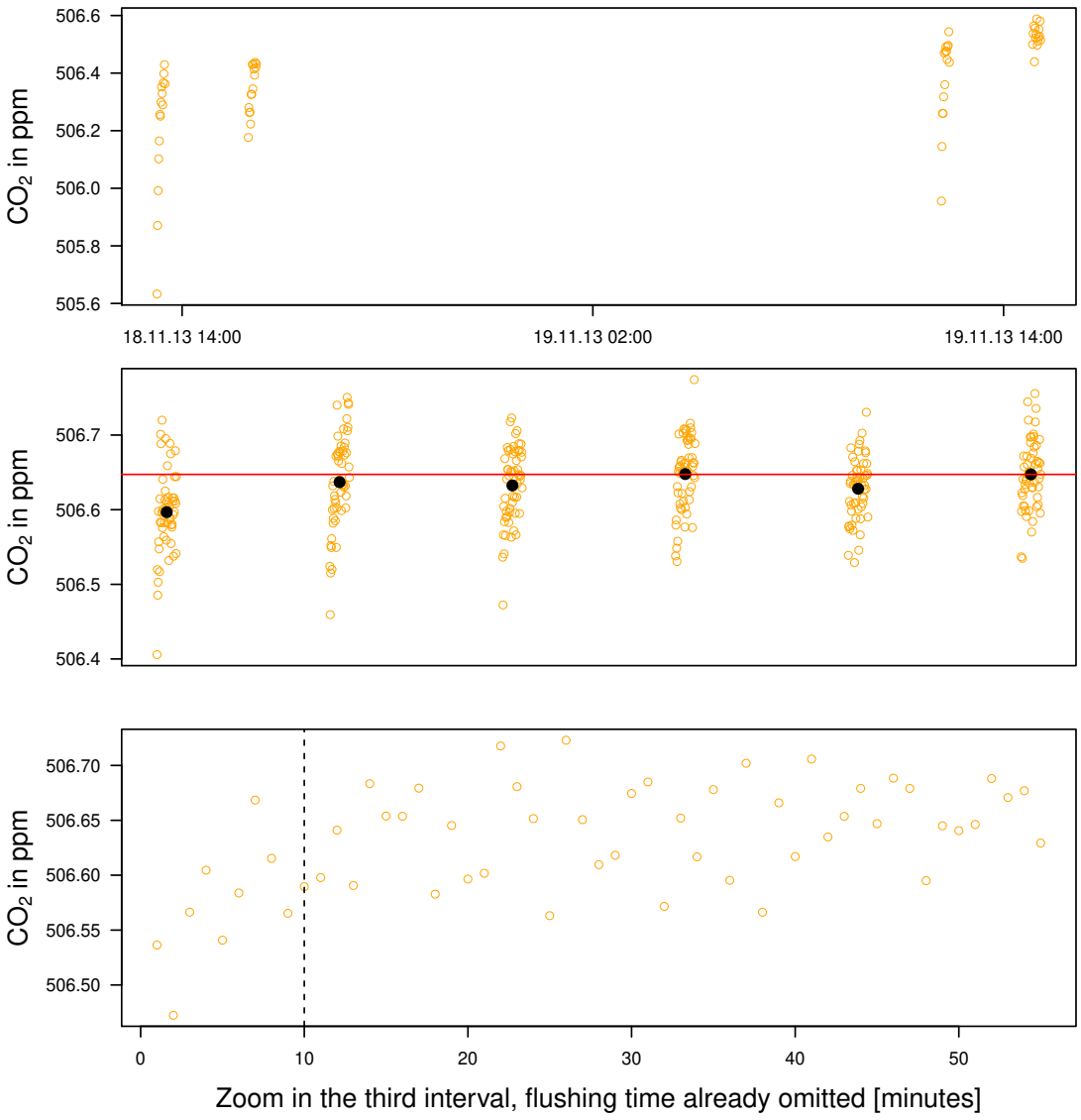

Figure 4.6: *Upper panel: Measurement results with a badly conditioned pressure regulator, each time measured for 20 min. Middle panel: Results of the same cylinder but well pretreated and measured each time for 1 hour. Lower panel: For the third measurement in the middle panel, a equilibration time of 10 min (plus 5 min flushing time) can be read off.*

ulator was in "absolute static equilibrium". Before the measurement, the pressure regulator was flushed for half a minute. However, this flushing was not sufficient for reaching a stable concentration with the measurement interval of 20 min.
Eight days later, we repeated the measurement. This time, we manually flushed the pressure regulator several times before starting the measurement and measured the cylinder every 6 hours for 1 hour (see middle panel of Figure 4.6). Here, already the second interval gave the same results as the last interval. Hence at a gas flow of 40 $\frac{\text{ml}}{\text{min}}$, we observed an equilibration time of 2 hours (first measurement, i.e. upper panel, plus the first measurement interval of the second measurement) which is required to "re-activate" the pressure regulator from "absolute static equilibrium" to "operation". Without wasting measurement time, this re-activation can also be reached when flushing without connection to the instrument. However, this might waste sampled gas.
Nevertheless, the cylinder was again not completely equilibrated at the beginning of the third interval because the equilibrium within the pressure regulator drifted back towards the static equilibrium during the measurement break. For a fluently measured (e.g. every 5 hours for months) calibration cylinder, the equilibration is already reached within the flushing time of 5 min. For newly measured cylinders like in this measurement, we determined that additional to the flushing time of 5 min the next 10 min of each measurement interval have to be omitted. (See the zoom in the third interval of the middle panel shown in the lower panel of Figure 4.6.)
We actually measured six sample cylinders, or rather pressure regulators, in this experiment. The discussed regulator showed the most prominent effect. Other regulators had smaller or even negligible equilibration times. Within this small statistics we regard the shown results as an estimation for the "worst case".

When we later measured six of our valuable NOAA standards (see Section 4.6), we did not dare measuring and flushing over night. Because the NOAA standards are routinely measured all 4 month by the gas chromatograph and furthermore connected to Tescom pressure regulators (which lead to a smaller pressure regulator effect than a Scotty pressure regulator), the equilibration time was assumed to be less than 2 hours. For safety, we measured each cylinder for 4 hours at once, only disrupted by 20 min of calibration measurement after 2 hours. For most NOAA standards this strategy worked. In Figure 4.7 the calibrated results of NOAA 7 are shown. For calculating the red linear fit, only the first twenty minutes have been omitted. The fit is virtually horizontal and therefore the equilibration time was about 20 min. This measurement strategy worked for most NOAA standards, however NOAA 10 was still slightly drifting after the total 4 hours.

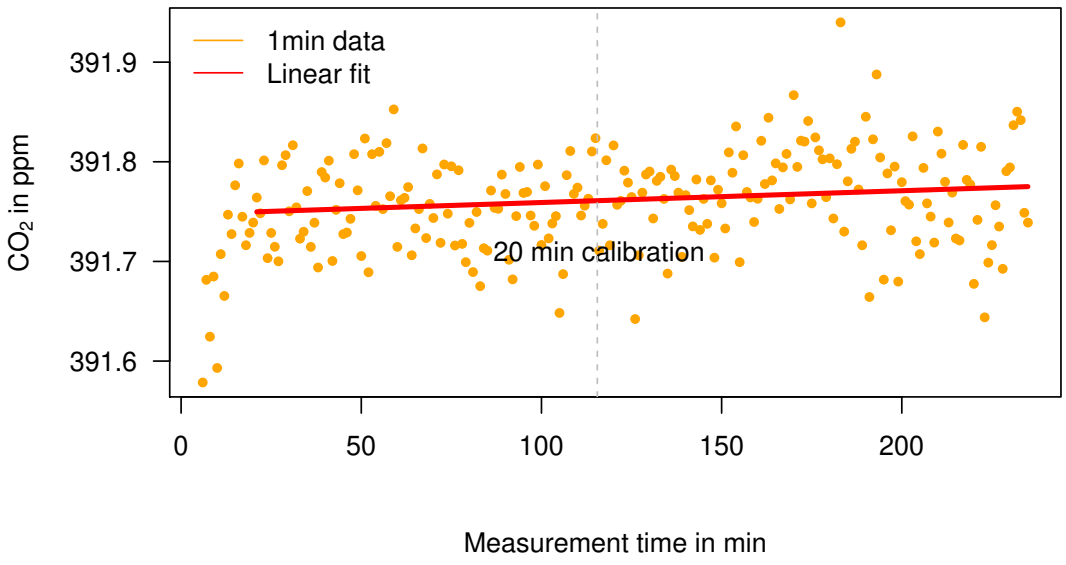

Figure 4.7: *Single-point calibrated CO_2 results of NOAA 7. For calculating the linear fit, only the first 20 min have been omitted due to the pressure regulator effect.*

Guideline for the measurement of a cylinder sample

1. Before measuring a new cylinder sample, the pressure regulator has to be flushed, at a gas flow of 40 $\frac{\text{ml}}{\text{min}}$, for about 2 hours. Alternatively, this flushing might be accelerated by manually flushing at a larger flow.

2. During an automatic measurement the time period between the measurements of the cylinder sample should be as small as possible to avoid long equilibration times. For fluently measured cylinders like the calibration cylinders, which are measured every 5 hours, the dynamic equilibrium is already reached within the flushing time of 5 min.

3. Anyway, we recommend to measure the cylinder sample at once. After the cylinder sample is prepared as explained in statement 1, the residual equilibration will only require 15-20 min. The choice of the total measurement time depends on the precision goals.

4.4 Cross-sensitivities and correlations

4.4.1 Correlation in δ^{13}C data and the barometric pressure

The instrument was installed in April 2013. We started to check the specifications guaranteed by the manufacturer. The results were mostly the same as in December 2013 (see Figure 4.1). However, sometimes we measured unsystematic peaks in $\delta^{13}CO_2$ and $\delta^{13}CH_4$ which moreover anti-correlated. After several months of testing, we finally determined a correlation between the barometric pressure and the δ^{13}C values. An example of those unsystematic peaks is shown in Figure 4.8. The cylinder gas was measured for 3 days and the un-calibrated data are shown. The decrease in the barometric pressure of roughly 10 mbar was accompanied by an increase of +0.5 ‰ in $\delta^{13}CO_2$ and -3 ‰ in $\delta^{13}CH_4$.
The reason of this correlation was the non-encapsulated light path between the laser source and the wavemeter. Thus, in spite of the perfectly controlled conditions in the cavity, the measurement was still depending on the ambient conditions. Due to this highly problematic systematic error we sent the instrument back to Picarro. They solved the problem by installing a "Quarter Wave Plate" in the optical alignment to correct for the non-encapsulated light path (personal correspondence with Picarro). The repair and testing process at Picarro required more than 3 months. The instrument arrived in Heidelberg at 31.10.2013.

When we performed the same test as shown in Figure 4.8 in November 2013[1], the ambient conditions were stronger varying and the barometric pressure was increasing by 17 mbar within 36 hours. Despite the repair, we still observed a significant increase in $\delta^{13}CO_2$ by +0.2 ‰ and decrease in $\delta^{13}CH_4$ by -2 ‰ (see Figure 4.9). However, while the drift in barometric pressure was three times larger than in July 2013, the drift in $\delta^{13}CH_4$ was smaller as before the repair. Furthermore, the sign of the correlation changed. The effect seems to be slightly over-corrected. Moreover, since the repair we also performed measurements where no correlation in the barometric pressure and the δ^{13}Cvalues could be observed. Thus, this phenomena is still neither perfectly corrected nor fully understood. Nevertheless, the results are significantly improved since the repair.

[1] Unfortunately, the measurement in December 2013, which is shown in Figure 4.1, is not suitable for comparison because there was no variation in barometric pressure.

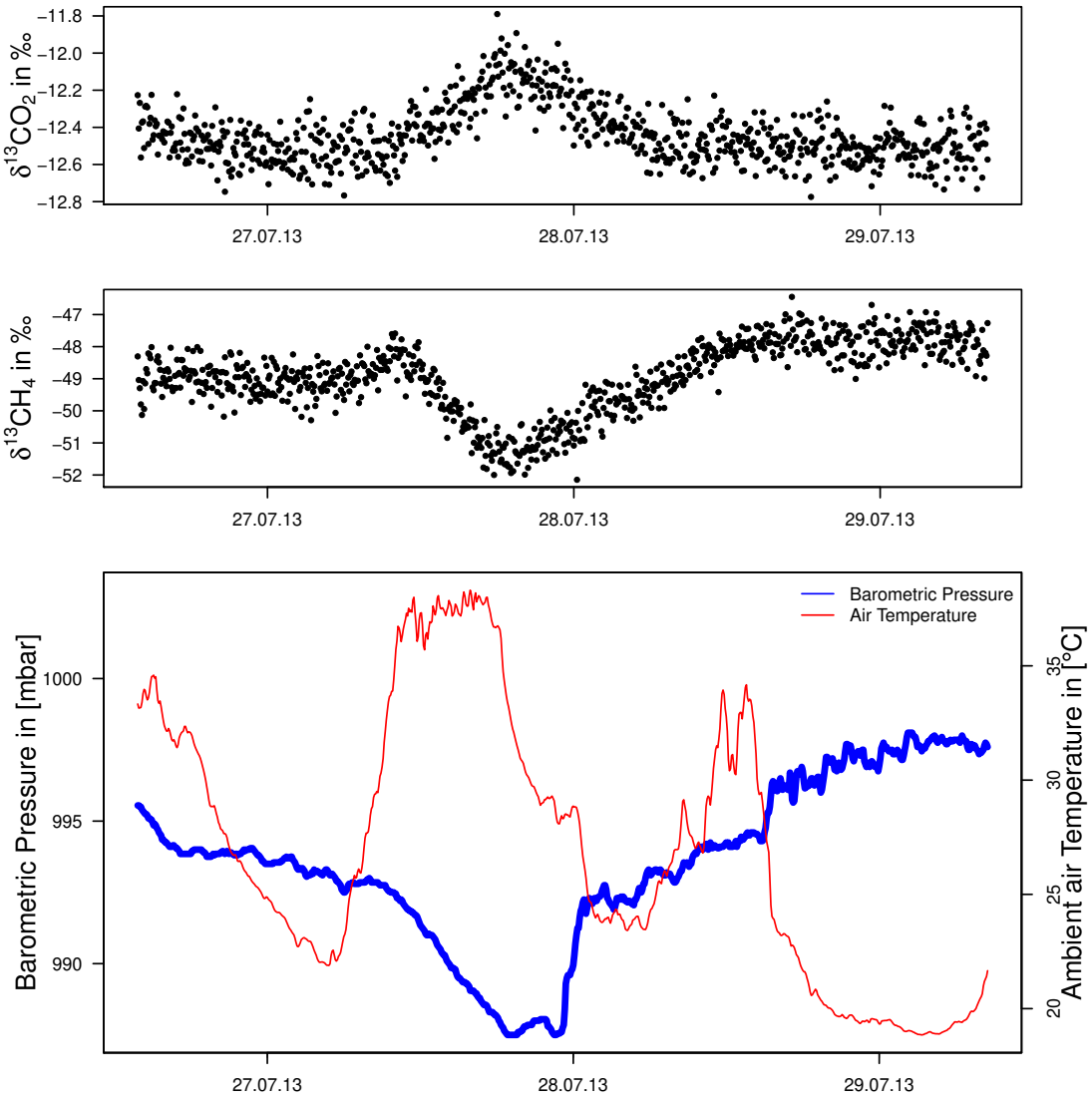

Figure 4.8: *Cylinder gas test before repair, in July 2013: The upper panels show the un-calibrated $\delta^{13}C$ data of a cylinder gas measurement. The peaks in $\delta^{13}CO_2$ and $\delta^{13}CH_4$ are highly anti-correlated. The lower panel shows the variation of the barometric pressure and the ambient air temperature during the measurement. The $\delta^{13}C$ values and the barometric pressure are highly (anti-)correlated.*

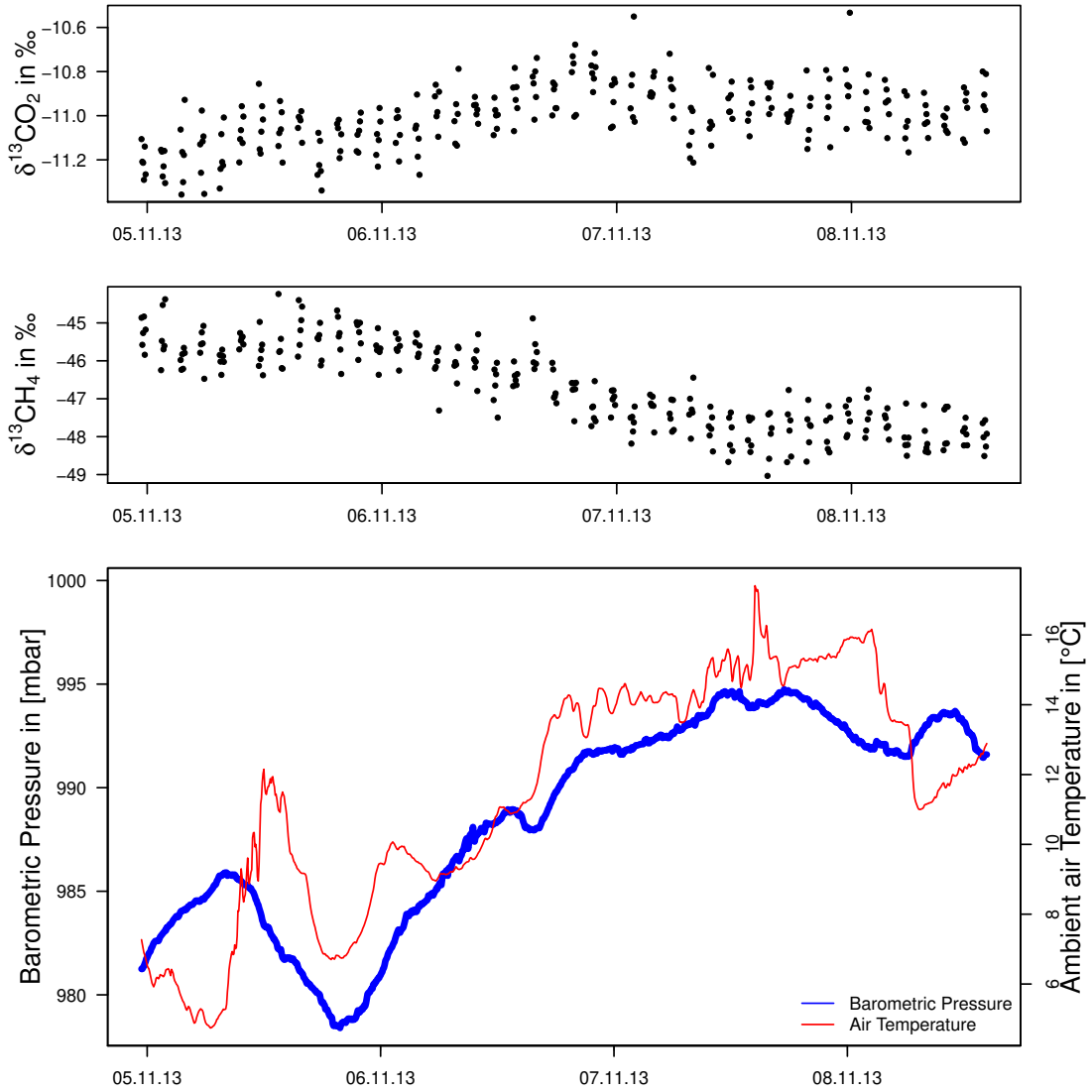

Figure 4.9: *Cylinder gas test after repair, in November 2013: The upper panels show the un-calibrated $\delta^{13}C$ data of a cylinder gas measurement. The lower panel shows the variation of the barometric pressure and the ambient air temperature during the measurement. There is still a correlation between the $\delta^{13}C$ values and the barometric pressure. However, the effect is much smaller than before the repair. Furthermore, the sign of the correlation changed, possibly due to a slight over-correction.*

4.4.2 Water vapour cross-sensitivity

The atmospheric water vapour is varying in time and location between almost 0 % and about 5 % [*Rödel and Wagner*, 2011]. A meaningful comparison of atmospheric greenhouse gas concentrations is only possible for dry air. Dry air data can be received either by a previous drying of the gas sample before the measurement or by a subsequent water vapour correction. The systematic offset of the wet measurement is dominated by the dilution effect which is proportional to the water vapour concentration. Thus, a simple linear correction is already correcting most of the offset. However, for most accurate measurement also the non-linear broadening effects or spectral overlaps should be corrected [*Rella*, 2010].

According to Picarro, i.e. especially *Rella* [2010], with the G2201-i it is possible to measure wet air, with a water range up to 4 %, with high accuracy. Because the instrument is also measuring the current water vapour concentration, an internal algorithm automatically performs the water vapour correction. As we will see in this section, one has to be careful with this algorithm for at least two reasons:
1) The algorithm is only correcting the ^{12}C concentrations. The ^{13}C concentrations and $\delta^{13}C$ values are not water vapour corrected.
2) The internal water vapour correction is using an empirically derived linear or quadratic cross-sensitivity between the water vapour concentration and the ^{12}C concentrations, following [*Rella*, 2010]. But these global coefficients for the water vapour correction are only best estimates. As *Rella* [2010] already stated, each instrument has its own cross-sensitivities and thus it appears to be more reasonable to determine and apply the correction by oneself.

On the other hand, previous drying requires a more complex set-up which is not to underestimate, especially during a field campaign. To determine the quality of the internal water vapour correction, we installed the two-path set-up shown in Figure 4.10. The flow from a dry cylinder was split up in two flows. The flow rates were controlled by mass flow controllers (MFC) which were automatically operated by a computer program. One of the paths contained a condensing trap filled with distilled water which acted as a simple humidifier[1]. Both flows mixed within a tube of about 1 m length before the mixture was measured in the spectrometer. By varying the ratio between the flows, we were able to measure with different water vapour concentrations. For all settings of the MFCs, the total flow was 35 $\frac{\text{ml}}{\text{min}}$. In earlier measurements, we observed that several hours are required until a constant water vapour concentration was provided by our set-up. Hence, we measured every setting of the water vapour concentration for 3 hours, separated from each other

[1] We did not required a more complex humidifier because we did not want to exactly set the water vapour concentration of the measured flow. However, with this simple set-up, we only received a water vapour mole fraction up to 1.5 %. To avoid potential absorption of CO_2 by the water during the measurement, we flushed the condensing trap before the measurement for several days with the later measured cylinder gas.

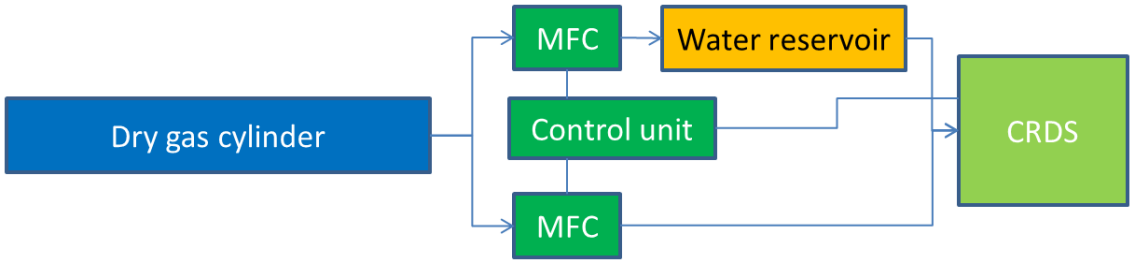

Figure 4.10: *Two-path set-up of the humidifier experiment. The gas flow from the dry sample cylinder is split in two flows. The flow rates were controlled by mass flow controllers (MFC). In the upper path, the flow becomes wet due to a humidifier. Both flows mix within a line of about 1 m and the mixture is measured with the spectrometer.*

by calibration measurements. The measured correlations between the water vapour concentration as directly measured with CRDS and the calibrated, wet respectively internally water vapour corrected data are shown in Figure 4.11 and 4.12. Each data point represents the average over the last 30 min of the measurement, i.e. after omitting 2.5 hours due to equilibration. The measurement errors are the standard errors of this average. However, the data point at around 0.2 % is omitted because it was still far away from equilibrium. Also for some other water vapour concentrations, we did not reached the equilibrium within 3 hours, but the drift was already sufficiently low. The parameter of the shown fits and the fit errors are given in Table 4.3 and Table 4.4. The fits are error weighted.

Table 4.3: *Parameters and errors of the linear fit through the wet data shown in Figure 4.11.*

	$[CO_2]$ in ppm	$\delta^{13}CO_2$ in ‰	$[CH_4]$ in ppb	$\delta^{13}CH_4$ in ‰
Slope per 1% H_2O	-7.53 ± 0.04	17.80 ± 0.08	-25.3 ± 0.2	11.85 ± 0.11
Intercept	434.31 ± 0.03	-10.37 ± 0.08	1983.3 ± 0.2	-48.16 ± 0.12

Table 4.4: *Parameters and errors of the linear fit through the internally water vapour corrected data shown in Figure 4.12.*

	$[CO_2]$ in ppm	$\delta^{13}CO_2$ in ‰	$[CH_4]$ in ppb	$\delta^{13}CH_4$ in ‰
Slope per 1% H_2O	0.03 ± 0.03	-0.10 ± 0.04	-1.4 ± 0.2	-0.17 ± 0.15
Intercept	438.24 ± 0.02	-10.19 ± 0.03	1983.3 ± 0.1	-47.97 ± 0.12

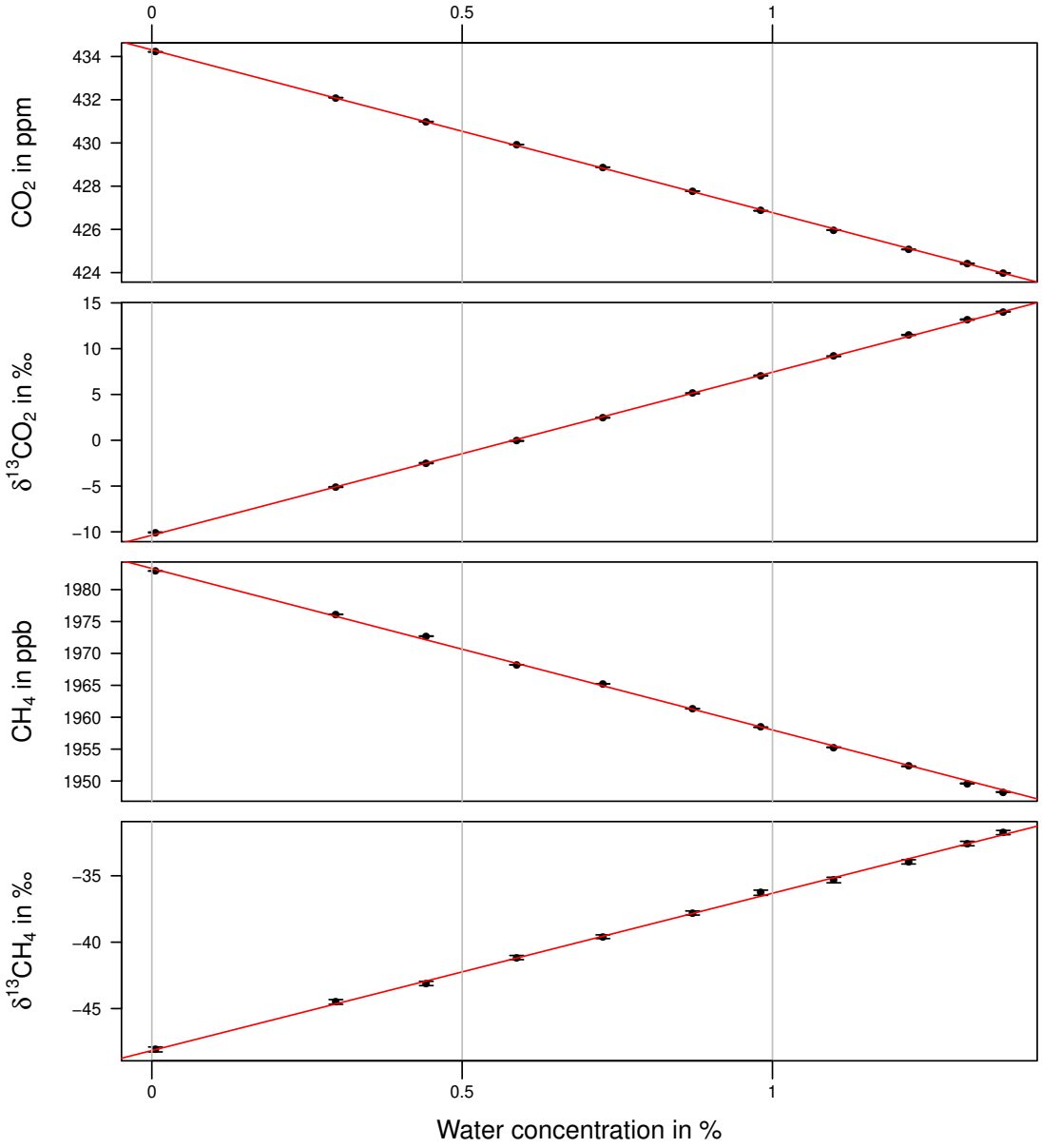

Figure 4.11: *For the shown range of the water vapour concentration, the virtually linear correlation between the wet CO_2 or CH_4 concentrations and the water vapour concentration, which is also expected due to the dilution effect, is observed. Surprisingly, also the $\delta^{13}C$ values are linearly dependent on the water vapour concentration although isotopic signatures are not affected by the dilution effect. The fit parameters are shown in Table 4.3.*

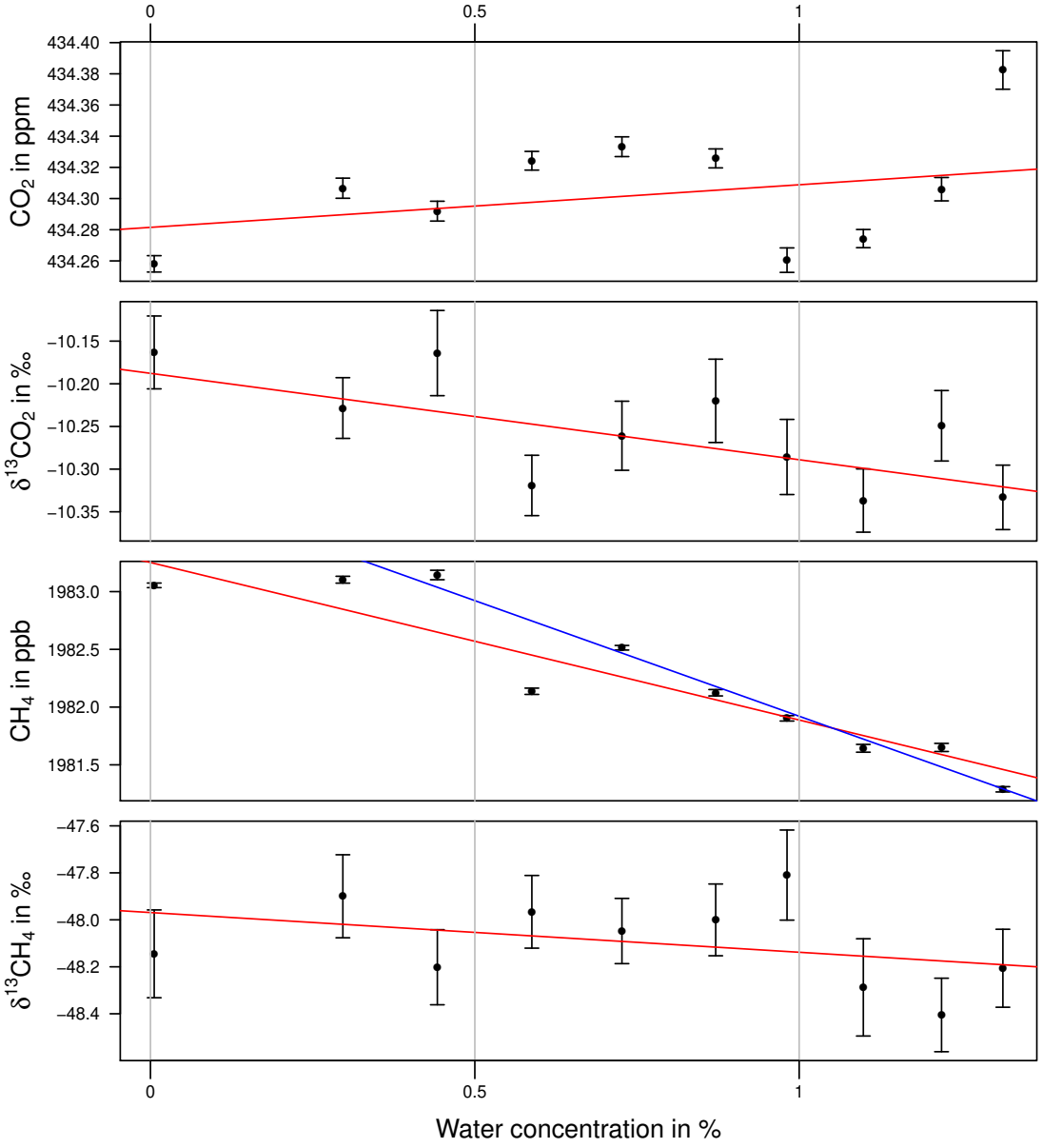

Figure 4.12: *Correlation of the internally water vapour corrected data and the water concentration. For all parameters, there is still a residual slope. However, for the CO_2 concentration and $\delta^{13}CH_4$ the fit error is in the order of the slope. For CH_4, there is apparently no water cross-sensitivity until 0.5 % H_2O (blue fit). For $\delta^{13}CO_2$, we observed a quite problematic residual slope of -0.1 ‰ per 1 % H_2O. A further evaluation shows that $^{13}CO_2$ does not depend on the water vapour concentration thus the slope in $\delta^{13}CO_2$ is due to a positive slope in $^{12}CO_2$. The fit parameters are shown in Table 4.4.*
Furthermore, especially for CO_2, the linear fit is not really matching the data. Apparently, there is a concentration-dependent structure, possibly caused by overlapping water absorption lines.

On the basis of our data (see Table 4.4), we do not recommend the internal water vapour correction. All water vapour corrected quantities (Figure 4.12) still show a significant water-dependency. In context of a field campaign, the residual errors are acceptable for a concentration measurement but for isotopic measurements, and especially for $\delta^{13}CO_2$, the systematic errors are unacceptable. Furthermore, especially the CO_2 data show no linear cross-sensitivity but apparently a substructure, possibly due to overlapping water absorption lines.

We also evaluated the direct cross-sensitivity between the water vapour concentration and the ^{12}C and ^{13}C isotopologues, the fit results are listed in Table 4.5. Surprisingly, the fit slopes through the wet ^{13}C data are negligible, $^{13}CO_2 = (-0.0002 \pm 0.0003)$ ppm and $^{13}CH_4 = (-0.019 \pm 0.003)$ ppb, per 1 % H_2O. Apparently, the dilution effect is neutralised by non-linear effects. No water vapour correction is required for the ^{13}C concentrations.

Table 4.5: *Parameters and errors of the linear fit through the wet ^{12}C and ^{13}C concentrations. These are treated similar to the total concentration and $\delta^{13}C$, but are not shown in a figure. The slopes give the empirical water cross-sensitivity of the un-manipulated measurement results.*

	$^{12}CO_2$ in ppm	$^{13}CO_2$ in ppm	$^{12}CH_4$ in ppb	$^{13}CH_4$ in ppb
Slope per 1% H_2O	-7.49 ± 0.03	-0.0002 ± 0.0003	-25.3 ± 0.2	-0.019 ± 0.003
Intercept	427.16 ± 0.02	4.7510 ± 0.0003	1961.2 ± 0.2	20.982 ± 0.003

In principle, we are able to correct the wet output data by using the empirical cross-sensitivities, i.e. slopes listed in Table 4.3 or 4.5. But because the fit errors are relatively large, we decided that manual drying is compulsory for most accurate concentration and isotopic measurements. However, even the condensing trap is not absorbing all the water vapour. Therefore, we nevertheless used the dry values, comfortably calculated by the internal water vapour correction for analysis.
Furthermore, we recommend to use a condensing trap due to another issue. In summer, when we tested the set-up without water trap some water condensed inside the ambient air line. Fortunately, there is a filter in front of the cavity which holds liquid water away from the cavity and therefore protects the instrument (personal correspondence with Picarro). But our peripheral flow meter was damaged.

4.4.3 CO_2 cross-sensitivity

Vogel et al. [2013] has shown that there is no CO_2 cross-sensitivity for $\delta^{13}CO_2$ for the earlier Picarro-instrument G1101+. To test the CO_2 cross-sensitivity of our instrument, we used a similar set-up as in the humidifier experiment (see Figure 4.13). Only the humidifier was replaced by a cartridge with Ascarite® (from

Sigma-Aldrich®) and another one with magnesium-perchlorate. Ascarite is absorbing CO_2 from a gas flow and is not fractionating between $^{12}CO_2$ and $^{13}CO_2$, at least after some saturation time *Hammer et al.* [2013]. Ascarite is, however, releasing water when absorbing CO_2. The water is absorbed by the magnesium-perchlorate.

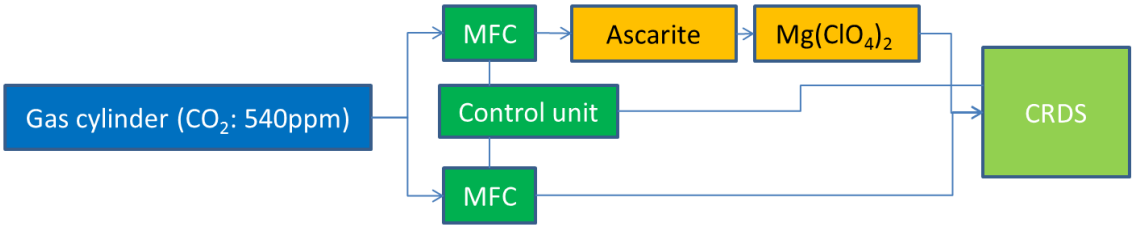

Figure 4.13: *Set-up of the Ascarite experiment. The gas flow from a cylinder with a CO_2 concentration of 540 ppm is split in two flows. The flow rates were controlled by mass flow controllers (MFC). In the upper path, all CO_2 is removed from the flow by the Ascarite. The water produced by the Ascarite is absorbed by the magnesium-perchlorate. Both flows mix within a line of about 1 m and the mixture is measured with the spectrometer.*

By varying the setting of the mass flow controllers, we measured at 9 different CO_2 mole fractions between 320 ppm and 540 ppm for at least 30 min. From the last 20 min, we calculated the mean values and standard errors (see Figure 4.14). The range of ambient conditions are spanned by the seven inner data points (blue fit). The two embracing data points are just measured for a linearity control (red fit). The parameters of the shown blue fits and their fit errors are given in Table 4.6. The fits are error weighted. In the following, we only discuss the ambient range.

For $\delta^{13}CO_2$ we observed a slope of 0.05 ‰ per 100 ppm CO_2, and for $\delta^{13}CH_4$ a slope of 0.2 ‰ per 100 ppm CO_2. However, the large fit errors and the embracing data points suggest that there is no cross-sensitivity. The CH_4 data are quite indifferent. For the ambient range, no cross-sensitivity is observed, but for the overall range from 320 ppm to 540 ppm a highly significant cross-sensitivity is detected. Nevertheless, for the ambient range the measurement errors are in the order of the slope of the cross-sensitivity fits. With these errors, we are not able to recommend a cross-sensitivity correction. If ever, this correction would be only small.

Table 4.6: *Parameters and errors of the blue linear fit shown in Figure 4.14.*

Measured quantity	$\delta^{13}CO_2$ in ‰	$[CH_4]$ in ppb	$\delta^{13}CH_4$ in ‰
Slope per 100 ppm CO_2	0.05 ± 0.06	-0.3 ± 0.2	0.2 ± 0.1
Intercept	-12.47 ± 0.25	1985 ± 1	-48.56 ± 0.56

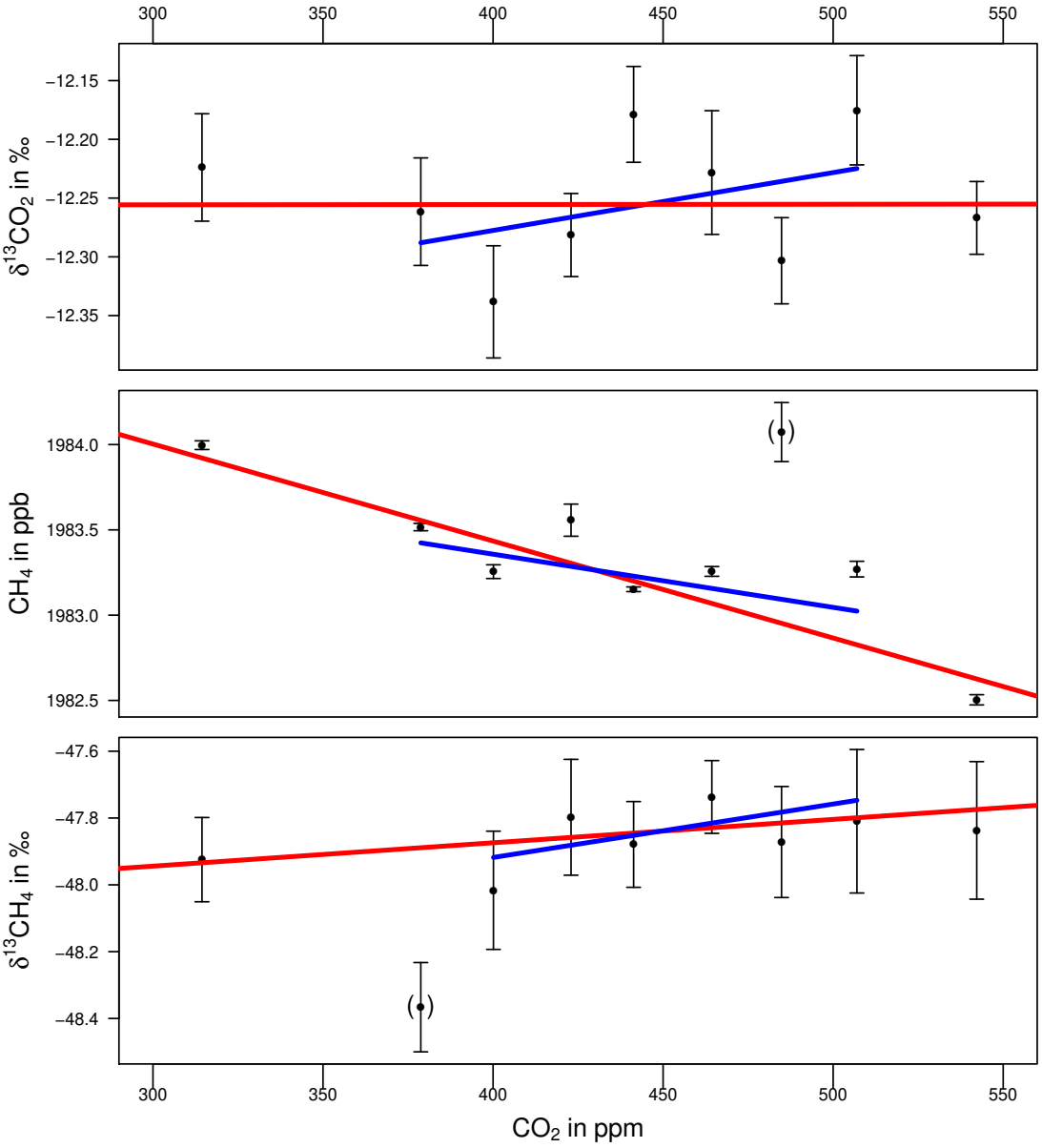

Figure 4.14: *CO_2 cross-sensitivity of the internally water vapour corrected data. The red lines indicate linear fits with respect to the whole range in CO_2-concentration. The blue lines indicate linear fits concerning the atmospheric range only. The data points in brackets are not used for the fits because they seem to be affected by external errors.*

4.5 Calibration

4.5.1 Response function of the instrument

The gas concentrations measured by the instrument are in general not matching with the "true" gas concentrations within the sample. This has to be corrected by using the *response function* of the instrument. It gives the response of the instrument, i.e. measured concentration, as a function of the input, i.e. true, or at least nominal, concentration. To determine the current response function of the instrument, we measured a set of cylinders with well-known concentrations which we call *calibration standards*. For each calibration standard, we measured a mean value of, e.g., CO_2. The response function is then the fit through the scatter plot of the pairs (measured concentration, nominal concentration).

By measuring the calibration standards several times, we do not only get information about the response function at several points in time but we are also able to calculate, by interpolation, the temporal evolution of the response function[1]. Finally, the response function is a function in time which allows to correct every data point of a sample measurement in such a way that the measured concentration matches, by best estimate, with the true concentration. This correction is called *calibration*. By a calibration, we solve at least three problems: First of all we anchor the arbitrary concentration scale of the instrument to the concentration scale defined by the calibration standards and increase thereby the accuracy. Furthermore, we correct for the drifting response function of the instrument which leads to an better reproducibility. Such a time-dependent drift can be seen in the raw data shown in Figure 4.1, most prominent for CH_4. For a non-drifting instrument the green line in Figure 4.1 would be a straight horizontal line with statistic variations only. By the calibration, the line becomes more horizontal. Finally, using at least two calibration standards, the calibration corrects for a non-linear response of the instrument.

In general, the response function $c_m(c_s)$ is a function of the nominal concentration c_s and is given by the polynomial $c_m(c_s) = \sum_{k=0}^{\infty} a_k \cdot (c_s)^k$. For a well designed instrument, it should be sufficient to neglect at least all orders higher than the square. The minimum number of required calibration standards is given by the number of free parameters in the approximated response function $c_m(c_s)$. A single-point calibration is sufficient in the case of $c_m(c_s) = a_1 \cdot c_s$. A two-point calibration allows an additional bias correction, $c_m(c_s) = a_1 \cdot c_s + a_0$.

4.5.2 NOAA-scale and JRAS-scale

As said before, by a calibration the internal scale of the instrument can be rescaled using the nominal concentrations of the calibration standards. However, this is still floating as long as the "true" concentration of the standards are not sufficiently

[1] If the response function changes linearly with time between these calibration points.

well known. For this reason, so-called *international mole fraction scales* are established. Commissioned by the World Meteorological Organization (WMO), the National Oceanic and Atmospheric Administration (NOAA) maintains the Central Calibration Laboratories (CCL) for CO_2, CH_4, N_2O, SF_6, and CO at ambient conditions. For these gases, the CCLs carefully created sets of large cylinder samples by using a gravimetric method respectively, in case of CO_2, a manometric method. By these methods, very accurate knowledge about the gas concentrations within the cylinders can be reached. These cylinders are called *primary standards*.

For CO_2, the set of primary standards contains 15 cylinders which span the atmospheric range. The response function of this set is the so-called NOAA-scale or WMO-scale. Thus, when any calibration corrects the raw data of a sample measurement exactly like the primary standards, then the instrument is *linked to the WMO-scale*. Other way round, an instrument is only linked to the WMO-Scale if its calibration standards are traceable back to the primary standards. NOAA uses its primary standards to calibrate *secondary standards* (Cylinders which are filled in a sensible way with ambient air or the like and measured by an instrument which is calibrated with the primary standards.) which are sold to national laboratories which therefore are able to specify tertiary calibration standards for the day to day instrumental calibration. Our working group owns 11 secondary NOAA-standards. All of them are specified for CO_2 and three are specified for CH_4. The gas chromatograph (GC) in Heidelberg is measuring every 4 months the whole set of secondary standards. If there is a deviation in the measured and the nominal concentration, all GC-data are corrected accordingly. By interpolating between two NOAA-standard measurements the GC is virtually non-stop linked to the WMO-Scale. By this, the GC is able to assign nominal concentrations to tertiary calibration standards which are used to calibrate the instruments in the Heidelberg laboratory.

The WMO-scale for ambient $\delta^{13}CO_2$ measurements is maintained by the Max-Planck-Institute (MPI) for Biogeochemistry in Jena. The associated primary standards are called the *Jena Reference Air Set 06 (JRAS(06))*. Furthermore, the MPI is also working at an ambient $\delta^{13}CH_4$ scale. For inter-laboratory comparison (at least with the MPI), we usually request the nominal $\delta^{13}CO_2$ and $\delta^{13}CH_4$ values for our calibration standards. Therefore, we send flask samples of the standards to Jena for analysis. Our mass spectrometer (MS) is also linked to the JRAS-scale and therefore able to assign nominal $\delta^{13}CO_2$ to tertiary calibration standards.

Remark: When specifying a secondary or tertiary standard, measurement and calibration errors occur. While in theory all calibration standards of all instruments should be by definition linked to the WMO-Scale, in practise no set of standards is perfectly linked to the WMO-Scale. To minimise the deviation, we occasionally double-check the assigned values of our calibration standards by GC and MS analysis. Additionally, NOAA is continuously updating the values of all secondary standards if improved measurement corrections are subsequently applied.

4.5.3 Mathematical description of single- and two-point calibration

For the single-point calibration the response function $c_{cal}(c_m)$ of the sample is a line through the origin. Its slope is given by the ratio of the nominal c_{nom} and the measured (or interpolated) c_{std} value of the only calibration standard:

$$c_{cal} = \frac{c_{nom}}{c_{std}} \cdot c_m. \tag{4.1}$$

This most simple calibration was applied per default during the whole measurement period, from November 2013 until May 2014. It applies a drift-correction but is not able to correct for a non-linear response function.

For the two-point calibration the response function $c_{cal}(c_m)$ of the sample is a line with a free intercept. The line is spanned by the measurements of two calibration standards:

$$c_{cal} = \frac{c_{nom1} - c_{nom2}}{c_{std1} - c_{std2}} \cdot c_m + \left[c_{nom1} - \frac{c_{nom1} - c_{nom2}}{c_{std1} - c_{std2}} \cdot c_{std1} \right] \tag{4.2}$$

$$= \frac{c_{nom1} - c_{nom2}}{c_{std1} - c_{std2}} \cdot (c_m - c_{std1}) + c_{nom1}. \tag{4.3}$$

This calibration is principally a better approximation of the response function. On the other hand, at the same calibration frequency twice as much time (and gas) is required for the calibration. Furthermore, both calibration standards have to span a wide range of concentrations. Otherwise the slope will be largely varying due to the measurement errors of the calibration points.

4.5.4 Converting $[CO_2]$ and $\delta^{13}CO_2$ to $[^{12}CO_2]$ and $[^{13}CO_2]$

Established measuring methods like gas chromatography and mass spectrometry can only measure total concentrations or δ^{13}C-values, respectively. Conventionally, the calibration laboratories give only assigned values for the total concentrations and δ^{13}C values. Optical techniques like CRDS are measuring $[^{12}CO_2]$ and $[^{13}CO_2]$. To overcome the problem of different physical quantities, either the assigned values of the calibration standards or the raw output data have to be converted to the particular quantities. For a straight-forward calibration of the CRDS data, we converted the assigned values of the calibration standards from $[CO_2]$ and $\delta^{13}CO_2$ to $[^{12}CO_2]$ and $[^{13}CO_2]$. This is also recommended in [*Wen et al.*, 2013], at least for two-point calibration. Chris Rella (personal communication, 2014) and *Vogel et al.* [2013] (plus personal communication, 2014) rather recommend a calibration based on total concentrations and isotopic signatures, because several cross-sensitivities

might cancel each other when calculating δ^{13}C prior to calibration.

For the total concentration $[CO_2]$ holds in general (where O = ^{16}O):

$$[CO_2] = [^{12}CO_2] + [^{13}CO_2] + [CO^{17}O] + [CO^{18}O] + \text{mixed} \tag{4.4}$$

With our CRDS, we are only able to measure $[^{12}CO_2]$ and $[^{13}CO_2]$. We have to estimate the relative mole fraction of isotopologues containing ^{17}O or ^{18}O:

$$R(^xO) = \frac{[CO^{17}O] + [CO^{18}O] + \text{mixed}}{[^{12}CO_2]} \approx 0.56\,\%^1. \tag{4.5}$$

Using this definition and Eq. 2.2 we can rewrite Eq. 4.4 as:

$$[CO_2] = [^{12}CO_2] \cdot \left(1 + R_{VPDB} \cdot (\delta^{13}CO_2 + 1) + R(^xO)\right) \tag{4.6}$$

Now holds for a **single-point calibration**

$$[^{12}CO_2]_{cal} = [^{12}CO_2]_m \cdot \frac{[^{12}CO_2]_{nom}}{[^{12}CO_2]_{std}} =: A_{12} \cdot [^{12}CO_2]_{nom} \tag{4.7}$$

where A_{12} is a measured quantity and $[^{12}CO_2]_{nom}$ is not directly available at the time being and has to be calculated by Eq.4.6. We get:

$$[^{12}CO_2]_{cal} = A_{12} \cdot \frac{[CO_2]_{nom}}{1 + R_{VPDB} \cdot (\delta^{13}CO_2 + 1)_{nom} + R(^xO)_{nom}}. \tag{4.8}$$

For $[^{13}CO_2]_{cal}$ holds analogue using Eq. 2.2:

$$[^{13}CO_2]_{cal} = A_{13} \cdot \frac{[CO_2]_{nom} \cdot R_{VPDB} \cdot (\delta^{13}CO_2 + 1)_{nom}}{1 + R_{VPDB} \cdot (\delta^{13}CO_2 + 1)_{nom} + R(^xO)_{nom}}. \tag{4.9}$$

So far, we calibrated the output of our instrument. For comparing with other instruments, we have to convert it to $[CO_2]_{cal}$ and $(\delta^{13}CO_2)_{cal}$. For $[CO_2]_{cal}$ holds:

$$[CO_2]_{cal} = [^{12}CO_2]_{cal} \cdot (1 + R(^xO))_{cal} + [^{13}CO_2]_{cal}. \tag{4.10}$$

Again we are blind for oxygen isotopes, i.e. $R(^xO)_{cal}$. A good approximation is to assume it to be constant and use the value which we plugged in above. Because the $R(^xO)$ is only of the order of 6 ‰ (and varying less), this estimation will not harm much. For $(\delta^{13}CO_2)_{cal}$ holds:

$$(\delta^{13}CO_2 + 1)_{cal} = \frac{[^{13}CO_2]_{cal}}{[^{12}CO_2]_{cal}} \cdot \frac{1}{R_{VPDB}} \tag{4.11}$$

$$= (\delta^{13}CO_2 + 1)_m \cdot \frac{(\delta^{13}CO_2 + 1)_{nom}}{(\delta^{13}CO_2 + 1)_{std}} \tag{4.12}$$

[1] Assuming $\delta^{18}O_{VSMOW} = -2$‰ and using the mole fraction and fractionation of ^{17}O given in [*Mook*, 2000].

An analogue derivation is possible for a **two-point calibration** by changing Eq. 4.7. The quantities $[^{12}CO_2]_{nom1}$ and $[^{12}CO_2]_{nom2}$ can be derived by using Eq. 4.6.

For CH_4 we used the identical conversion with $R(^xO)$ replaced by $R(^2H) = 0.57\,‰$[1].

Remark: The shown derivation differs from the single-point calibration which is used in literature. There, the $\delta^{13}C$ values are used like quantities which can be calibrated as in Eq. 4.7, e.g. [*Wen et al.*, 2013]. But omitting the "+1" holds only true for measured $\delta^{13}C$ values very near to the assigned value. Otherwise the errors become large. On the other hand, for the two-point calibration the error associated with this approximation is much lower and therefore this approximation is justified.

4.5.5 Applied calibration strategy

Besides the numbers of calibration standards and the range they span, also the calibration frequency and the calibration interval have to be chosen is a suitable way. Aiming for as much sample measurement time as possible, both, the frequency and the measurement interval of the calibration, should be as low as possible. On the other hand, the calibration point has to be highly precise. Otherwise, the calibration error would significantly contribute to the overall measurement error.

With the help of the Allan deviation analysis, we choose an averaging interval of 15 min which results in a calibration interval of 20 min, if we allow for a flushing time of 5 min. For this setting, the CO_2 and CH_4 concentrations have reached a decent precision and the precision of the isotopic signatures are also satisfying. If aiming for high precision isotope measurement, a longer calibration interval should be chosen.

Furthermore, the linear interpolation between calibration points is only valid for a sufficiently high calibration frequency. Additionally, the calibration frequency should not match with a "natural frequency" like twice per day because in this case ambient air is systematically not monitored for the same time intervals each day. We decided that calibrating every 5 hours is a sensible choice by which we still can correct for medium-term variations, like a changing barometric pressure, but which requires only 20 % of the total measurement time when measuring two calibration cylinders and one quality control cylinder. At last, one has to assure that the choice of a low calibration frequency does not lead to pressure regulator effects. For a frequency of every 5 hours, we observed no such effect.

Summarised, our calibration implement the following steps:

1. In between sample measurements, each calibration cylinder is measured in a fixed frequency for a fixed time interval. In our case every 5 hours for 20 min.

[1] Assuming $\delta^2H_{VSMOW} = -85\,‰$

2. After omitting the flushing time, we calculate the calibration points, i.e. from each calibration interval we extract the mean time of the interval and for every parameter the mean value.

3. For each calibration cylinder, we interpolate linearly between the calibration points and a thereby calculating the virtual temporal evolution of the particular calibration point.

4. From the temporal evolution of the calibration standards, we calculate the temporal evolution of the response function.

5. The raw sample data are calibrated by applying the response function.

4.5.6 Calibration and quality control cylinders

During the whole measurement period from November 2013 until May 2014, we measured two calibration cylinder s and one quality control cylinder. For calibration, we used most of the time the randomly filled cylinders HIGH and LOW listed in Table 4.7. For $[CO_2]$ and $\delta^{13}CO_2$, these calibration cylinders span a sufficiently wide range such that most ambient air measurements are embraced by the calibration cylinders. But for CH_4, this set of calibration cylinders is not suited for a two-point calibration, because they span only 1935-1962 ppb and their $\delta^{13}CH_4$ are virtually identical. Furthermore, the CO_2 concentration of HIGH drifted and even jumped during the 6 month. This problematic behaviour is most probable not caused by the cylinder but rather by the installed Scotty pressure regulator which we therefore replaced by a Tescom pressure regulator. All in all, the CO_2 data from HIGH are not suitable for calibration before 18.04.14. Facing these problems, we only applied a single-point calibration, using the LOW calibration cylinder. Due to consistency even for May 2014. Furthermore, we controlled the calibration with the TARGET cylinder until 09.05.2014 when it has been replaced.

For a suitable future two-point calibration, we filled and spiked a new calibration cylinder HIGH2, which has high concentrations in CO_2 and CH_4. Therefore, LOW and HIGH2 provide a set of calibration standards suitable for a two-point calibration. Since 09.05.2014, HIGH2 replaced the target, i.e. is connected to Port 7 of the 16-port valve. Because HIGH2, or rather its pressure regulator, has to equilibrate perfectly with the flow of 40 $\frac{\text{min}}{\text{ml}}$ and there are no nominal values available for $\delta^{13}CO_2$ and $\delta^{13}CH_4$, we are not able to use this cylinder for calibration within this thesis. In the future, the calibration should be done by LOW and HIGH2. HIGH might act as a target, however, HIGH is even a bad target because its CH_4-concentration is not within the calibration range.

Furthermore, measurements of highly concentrated CH_4 samples are calibrated by a single-point calibration using the MSTD cylinder which contains 10 ppm of CH_4.

Table 4.7: *Nominal values of the calibration and quality control cylinders. The CO_2 and CH_4 concentrations are taken from GC measurements (which are linked to the NOAA-scale) from May 2014, $\delta^{13}CO_2$ is taken from flask measurements at the mass spectrometry in Heidelberg (which is linked to the JRAS-scale) from April 2014, and $\delta^{13}CH_4$ was measured in a flask measurement at the mass spectrometer by MPI in Jena in April 2014. For MSTD, the concentrations are just self-measured by the CRDS and might therefore be inaccurate, especially for CH_4. For TARGET, the concentrations are only measured (in February 2014) with the FTIR and not with the GC.*

Name	Cylinder	[CO_2] in ppm	$\delta^{13}CO_2$ in ‰	[CH_4] in ppb	$\delta^{13}CH_4$ in ‰
HIGH	UHEI4_3	448.59	-11.052	1935.6	-47.74
LOW	UHEI8_2	398.43	-9.565	1962.6	-47.96
HIGH2	PIC2_2	484.21	(not yet available)	2350.6	(n. y. a.)
TARGET	B4704_2	408.25	-10.120	1887.0	-47.90
MSTD	Sib1_7	420.25	-11.000	10.1191 ppm	-43.32

4.6 Linearity of CO_2 and CH_4 concentration measurement

In general, the response function is a polynomial but for a well designed instrument a response function of the linear form $c_m(c_{spe}) = a_1 \cdot c_{spe} + a_0$ or even $c_m(c_{spe}) = a_1 \cdot c_{spe}$ should be a sufficient approximation. To determine the response function very precisely, we measured our set of secondary NOAA-standards. Due to the pressure regulator effect, we measured every cylinder for 4 hours where the measurement is disrupted after the first 2 hours by a calibration interval of 20 min. For the evaluation, we averaged the data of the last 30 min. We measured six NOAA-standards, the five which match the range of the current ambient CO_2 concentration in Heidelberg plus the NOAA-standard with the lowest CO_2 concentration for measuring over a large concentration. Three of these standards are also assigned for CH_4 concentration. To determine the non-linearity of the instrument, we calibrated the data with a single-point calibration using the LOW calibration cylinder. By this, the measurement output is anchored to the nominal value of the LOW cylinder and thus theoretically linked to the NOAA-scale. Furthermore, the instrumental drift is corrected. For the CO_2 and CH_4 concentration, we observed a linearly concentration-dependent non-linearity of the drift-corrected data (see Figure 4.15). When using a single-point calibration, better accuracy can be reach when applying the following non-linearity corrections:

$$(CO_2)_{corr} = (CO_2)_{uncorr} + [415\,\text{ppm} - (CO_2)_{uncorr}] \cdot 0.00199 \tag{4.13}$$

$$(CH_4)_{corr} = (CH_4)_{uncorr} + [2000\,\text{ppb} - (CH_4)_{uncorr}] \cdot 0.00611 \tag{4.14}$$

for data within the CO_2 range of 350-430 ppm and the CH_4 range of 1760-1960 ppb. However, one has to be careful with an extrapolation over these concentration ranges. Especially for CO_2 the last data point signals that for higher concentrations possibly a quadratic correction is required. Because we do not want to extrapolate, we will not apply this correction but keep it in mind when evaluating data within these ranges. For $\delta^{13}CO_2$, we observed no significant non-linearity when evaluating the data discussed in Section 5.4.1. For $\delta^{13}CH_4$, we did not evaluate the non-linearity.

In Figure 4.16, the results of a two-point calibration using LOW and HIGH are shown. As remarked earlier, this set of standards is not suitable for CH_4 calibration what can be seen in the lower panel. For CO_2, the two-point calibrated data within the calibration range from 398 ppm to 448 ppm match with the NOAA-scale within the WMO recommendation of ± 0.1 ppm.

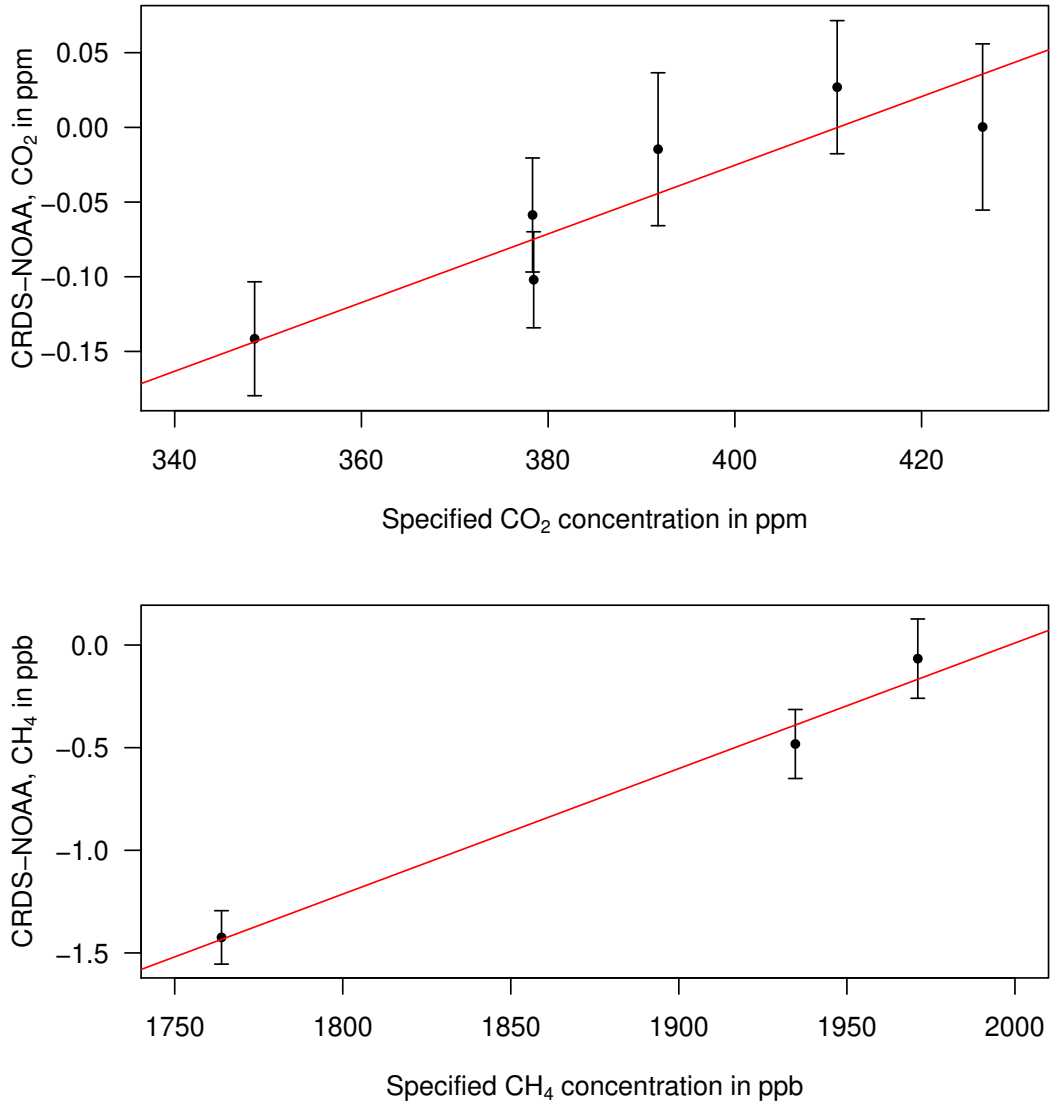

Figure 4.15: *Non-linearity of the CRDS: The measurement results of six NOAA standards are shown. The data are drift-corrected and single-point calibrated using LOW. Shown are the calibrated concentrations minus the assigned concentrations as a function of the assigned concentration. Measured cylinders: NOAA1, NOAA6, NOAA10, NOAA7, NOAA8, NOAA12*

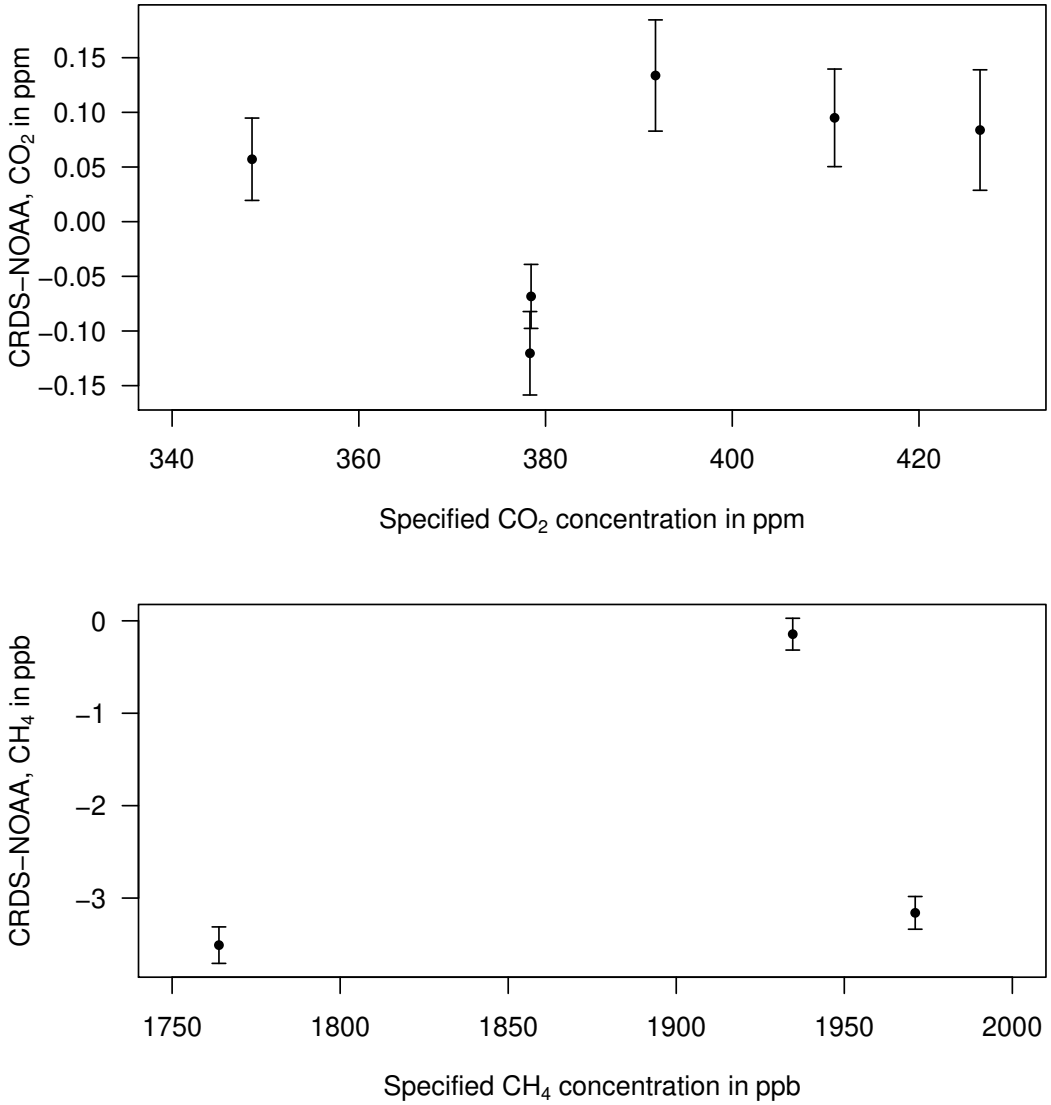

Figure 4.16: *NOAA standards measured with a two-point calibration of the CRDS: For CO_2, we observe a mean offset of the calibrated data of 0.09 ppm if omitting the two data points at 378 ppm. For CH_4 the two-point calibration is not working as explained in Section 4.5. Measured cylinders: NOAA1, NOOAA6, NOAA10, NOAA7, NOAA8, NOAA12*

4.7 Reproducibility of the target cylinder

For quality control, we measured the TARGET cylinder every 5 hours for 20 min (to be consistent with the calibration measurement). Only when the target is sufficiently reproduced, the measurement data around the particular target interval is correctly calibrated, respectively at least the drift-correction worked. In Figure 4.17 and 4.18, the single-point calibrated target data of 6 months are shown. The red and the grey lines give the mean value and the standard deviation of the 15-min averages, the blue line gives the nominal value measured by the FTIR. We observed a non-understood jump in the CO_2 concentration from December 2013 to January 2014 which results in a difference between the long-term mean value and the nominal value of 0.06 ppm. However, this difference is not significant because of the non-linearity of the instrument (see Figure 4.15) and the measurement error of the nominal value of about 0.05 ppm. For CH_4, we observed a general offset of 1 ppb between the nominal and the measured value. This offset is due to the non-linearity of the instrumental response for CH_4 (see Figure 4.15). On the other hand, the standard deviation of 0.17 ppb means a good reproducibility. For $\delta^{13}CO_2$ and $\delta^{13}CH_4$, the long-term mean value seems to be quite accurate, i.e. differing for both gases only by +0.01‰ and +0.05 ‰ from the nominal value, respectively. But the standard deviation of 0.10 ‰, respectively 0.34 ‰, is not good enough for most atmospheric applications.

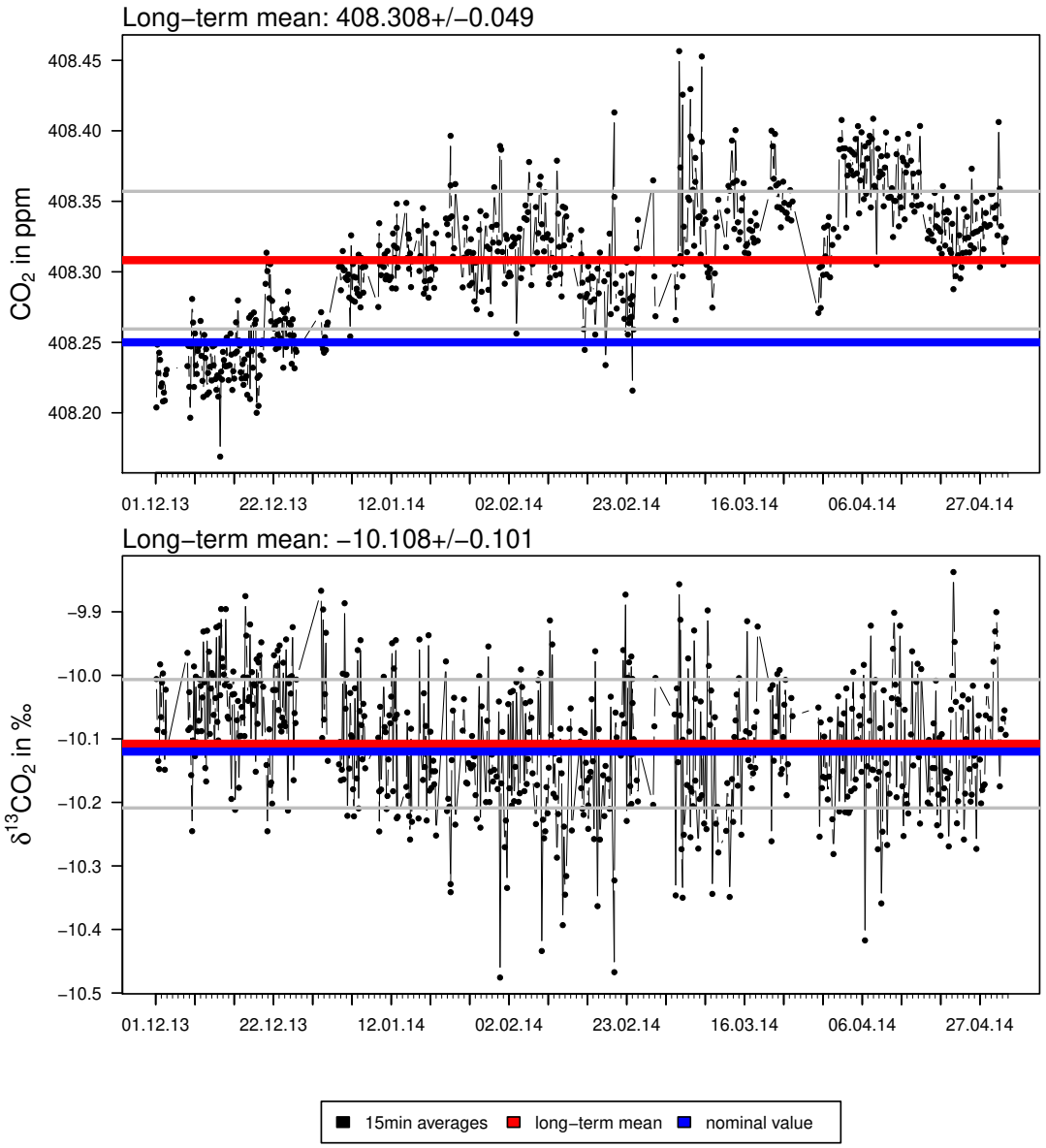

Figure 4.17: *Single-point calibrated target gas data of CO_2 and $\delta^{13}CO_2$ over 6 months. The red and the grey lines give the mean value and the standard deviation of the 15-min averages, the blue line gives the nominal value measured by the FTIR. The difference between the mean CO_2 concentration from January to April 2014 and the nominal value is not significant because on the hand of the non-linearity of the instrument (see Figure 4.15) and on the other hand the measurement error of the nominal value is about 0.05 ppm.*

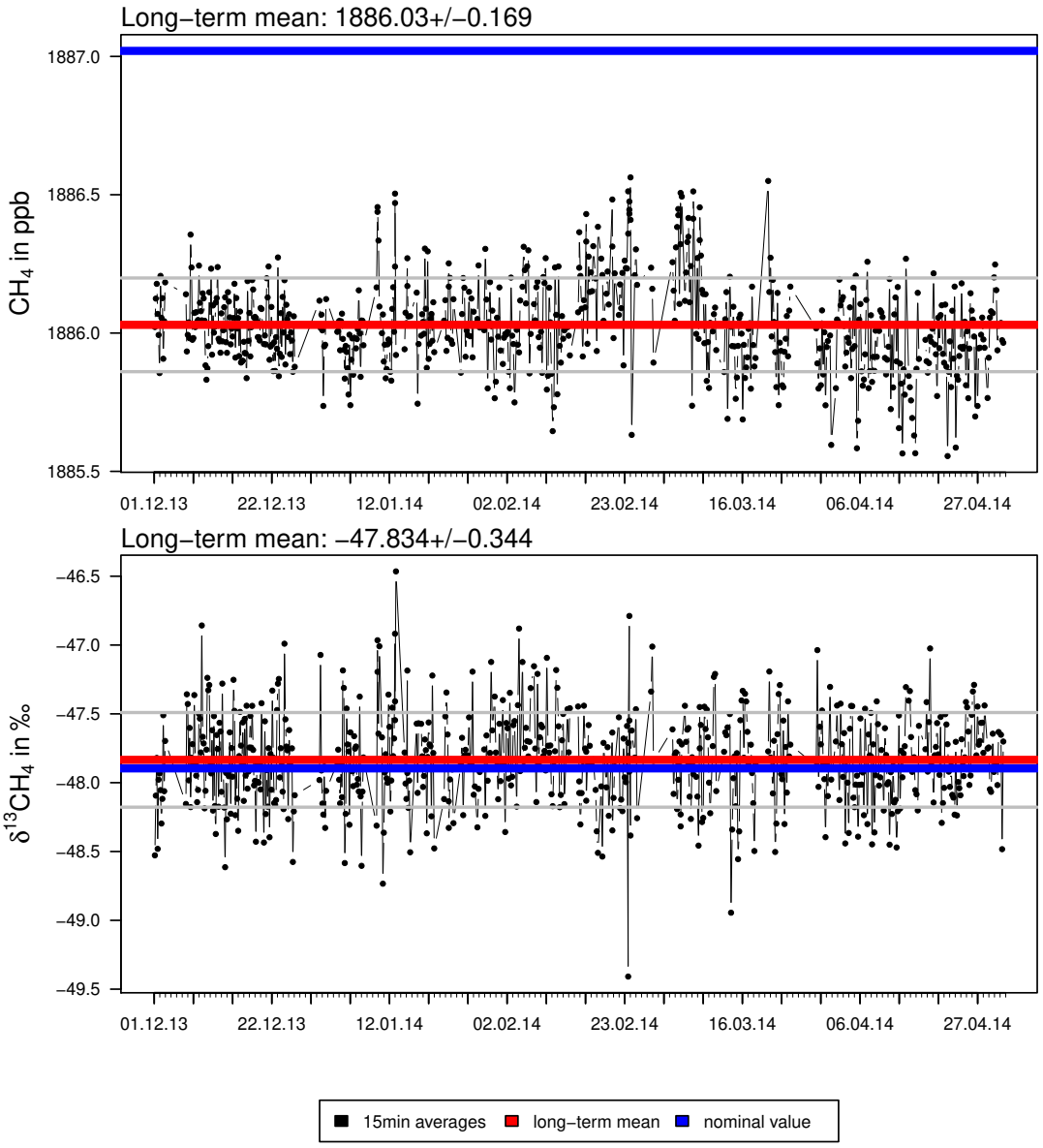

Figure 4.18: *Single-point calibrated target gas data of CH_4 and $\delta^{13}CH_4$ over 6 months. The red and the grey lines give the mean value and the standard deviation of the 15-min averages, the blue line gives the nominal value measured by the FTIR. The offset of 1 ppb in CH_4 is due to the non-linearity of the instrument (see Figure 4.15).*

4.8 Long-term stability of the instrumental output

In Figure 4.19, the raw data of the LOW calibration standard from December 2013 until May 2014 are shown. The red line indicates the instrumental drift. From GC measurements we know that the cylinder has not significantly drifted in CO_2 and CH_4 from August 2013 until May 2014. For the isotopic signatures we do not have such evidence. Within the evaluated 6 month, the output drifted by -0.07 ppm for CO_2, -0.2 ‰ for $\delta^{13}CO_2$, -0.1 ppb for CH_4, and -0.5 ‰ for $\delta^{13}CH_4$.

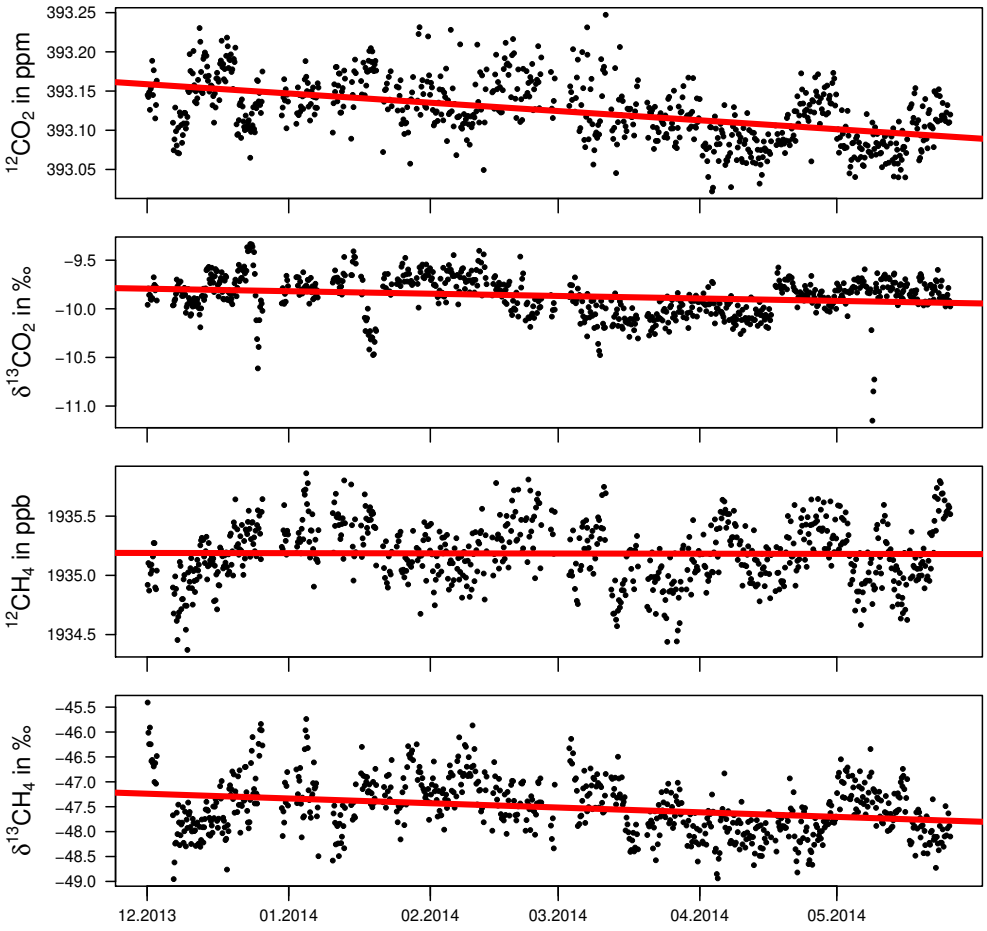

Figure 4.19: *Long-term stability of the instrument displayed by the raw data of LOW. The red lines indicate the instrumental long-term drift.*

5 Comparison with other instruments

5.1 WMO recommendations

In a measurement network it is mandatory that the contributing laboratories respectively instruments of the network measure compatible results. The World Meteorological Organization (WMO) has recommended, for all relevant greenhouse gases, inter laboratory compatibility targets (ILCT), which are required for merging the data of different laboratories to a global data set [*World Meteorological Organization*, 2011]. In 2014, these targets have often not been reached, especially for isotopic signatures.

Table 5.1: *WMO recommendations and reproducibility of CRDS. The reproducibility is the long term standard deviation of the TARGET cylinder, see Figure 4.17 and 4.18.*

Measured quantity	$[CO_2]$	$[CH_4]$	$\delta^{13}CO_2$	$\delta^{13}CH_4$
WMO recommendation	±0.10 ppm	± 2.0 ppb	±0.01 ‰	±0.02 ‰
Reproducibility of CRDS	±0.05 ppm	± 1.7 ppb	±0.10 ‰	±0.34 ‰

Besides a systematic inter-instrumental offset in absolute values, also an un-sufficient reproducibility may lead to a bad compatibility. Accordingly, from the reproducibility of our target cylinder (see Table 5.1) we expect that for $\delta^{13}CO_2$ and especially for $\delta^{13}CH_4$ the inter laboratory compatibility targets can not be reached by our instrument.

5.2 Integrated samples

CRDS is measuring virtually continuously with breaks only for calibration and quality control analysis. Other, especially non-optical, instruments are not able to measure continuously. In gas chromatography or mass spectrometry a single measurement may require between 5 and 60 min.

By using integrated samples this problem of only momentary values can be overcome. In Heidelberg, integrated ambient air samples are realised by a buffer volume, which is continuously flushed with ambient air from the South-East intake line. Similarly to the problematic of the flushing time (Section 4.3.1), the remains of an injected air parcel fade away exponentially in time where the life-time τ is given by the flushing flow divided by the buffer volume. The concentration of a just injected air parcel

is more contributing to the final concentration of the integrated sample than the concentration of an older air parcel. Theoretically, the temporal evolution of the supplying flow can be extracted from the integrated sample by regarding it as a sum of exponential decay functions, or rather as a convolution with a decay function [*Winderlich et al.*, 2010]. But this is only possible with simplifying approximations concerning the evolution of the ambient concentration like a linear increase between two measurements.

For comparison issues, it is easier and more accurate to do it inversely by using the continuous data from the CRDS to calculate theoretical values of integrated samples. This is given explicitly by the partition function:

$$c_{int}(t) = \frac{\sum_{n=0}^{\infty} \left[c(t - n \cdot \Delta t) \cdot e^{-n \cdot \Delta t/\tau}\right]}{\sum_{n=0}^{\infty} e^{-n \cdot \Delta t/\tau}} \tag{5.1}$$

with the (here used) measurement frequency $\Delta t = 1\,\mathrm{min}$ and the life-time τ associated to the buffer volume. More suitable for a big amount of data is the implicit function:

$$c_{int}(t + \Delta t) = [c_{int}(t) - c(t + \Delta t)] \cdot e^{-\Delta t/\tau} + c(t + \Delta t) \tag{5.2}$$

where at the starting time t_0 holds $c_{int}(t_0) \equiv c(t_0)$.

5.3 Comparison of CO_2 and CH_4 in ambient air measurements

5.3.1 Comparison with Fourier Transform-InfraRed Spectrometry

Since April 2011, in Heidelberg an in-situ Fourier Transform-InfraRed (FTIR) spectrometer is installed and in operation [*Konrad*, 2011], [*Hammer et al.*, 2013], [*Vardag*, 2012]. The instrument was developed by the University of Wollongong, Australia, [*Griffith*, 1996] and is able to measure simultaneously the trace gases $^{12}CO_2$, $^{13}CO_2$, $CO^{18}O$, CH_4, N_2O, and CO. The FTIR gives a data point every 3 min. Due to the internal cell volume of the FTIR and for increasing the precision of both instruments in general, we calculated and compared 30-min averages.

In Figure 5.1, the comparison in CO_2 concentration measurements is shown for March 2014. We observed only insignificant deviations in the measured concentrations of $\Delta[CO_2]_{CRDS-FTIR} = (0.06 \pm 1.33)$ ppm and $\Delta[CH_4]_{CRDS-FTIR} = (0.0 \pm 4.6)$ ppb. The large standard deviations are due to single spikes which are caused by rapid and extreme changes in the ambient concentration. To double-check whether these spikes also influenced the mean value of thhe difference, we also calculated the medians. For CO_2 the median was 0.10 ppm and for CH_4 −0.2 ppb. The mean values and standard deviations of the difference $\Delta[CO_2]_{CRDS-FTIR}$ of the months from January 2014 to May 2014 are listed in Table 5.2 (upper part), and the corresponding medians are listed in Table 5.3. The CH_4 concentrations measured by CRDS and FTIR match within the ILCT for all months. For the CO_2 concentration at least the mean difference over the 5 months matches the ILCT.

Table 5.2: *Difference in the data of the ambient air measurement between CRDS and FTIR or GC (CRDS-FTIR or CRDS-GC), given as mean values and standard deviations. Units: CO_2 ppm, CH_4 ppb, $\delta^{13}CO_2$ ‰*

	Jan 2014	Feb 2014	Mar 2014	Apr 2014	May 2014
FTIR CO_2	0.11 ± 1.19	0.11 ± 0.78	0.06 ± 1.33	0.15 ± 1.04	0.07 ± 0.59
FTIR CH_4	0.66 ± 4.06	0.23 ± 2.77	-0.03 ± 4.59	-0.19 ± 2.94	-0.50 ± 1.92
FTIR $\delta^{13}CO_2$	0.17 ± 0.14	0.19 ± 0.13	0.05 ± 0.14	0.07 ± 0.11	0.11 ± 0.11
GC/SE CO_2	-0.04 ± 0.57	0.02 ± 0.29	0.05 ± 1.10	0.10 ± 0.56	0.03 ± 0.52
GC/SE CH_4	0.52 ± 2.55	0.14 ± 2.00	0.09 ± 4.50	0.10 ± 2.39	0.02 ± 2.34
GC/SW CO_2	-0.12 ± 1.91	0.06 ± 1.18	0.20 ± 1.56	0.30 ± 1.41	0.15 ± 1.23
GC/SW CH_4	0.70 ± 5.88	0.48 ± 3.47	0.49 ± 4.77	0.41 ± 4.22	0.28 ± 3.39

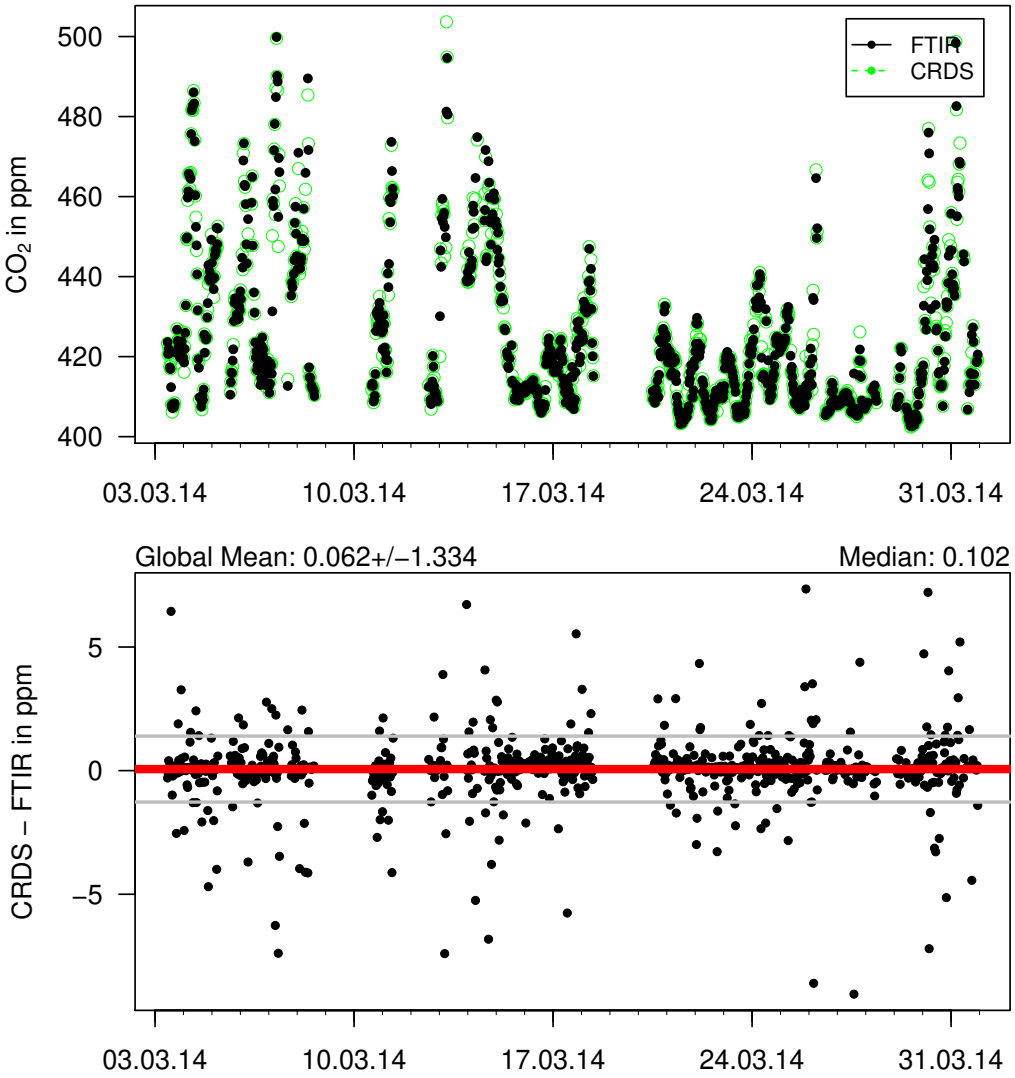

Figure 5.1: *Comparison of the ambient air CO_2 concentration in March 2014 measured by CRDS and FTIR. For the comparison in the lower panel, five outliers with an offset between 10 and 30 ppm were ignored.*

Table 5.3: *Difference in the data of the ambient air measurement between CRDS and FTIR or GC (CRDS-FTIR or CRDS-GC), given as medians. Units: CO_2 ppm, CH_4 ppb, $\delta^{13}CO_2$ ‰*

	Jan 2014	Feb 2014	Mar 2014	Apr 2014	May 2014
FTIR CO_2	0.06	0.07	0.10	0.15	0.10
FTIR CH_4	0.23	-0.04	-0.18	-0.32	-0.49
FTIR $\delta^{13}CO_2$	0.16	0.19	0.06	0.07	0.11
GC/SE CO_2	-0.02	0.01	0.02	0.08	0.01
GC/SE CH_4	0.36	0.15	0.20	0.09	-0.02
GC/SW CO_2	-0.10	-0.08	0.08	0.15	0.06
GC/SW CH_4	0.45	0.17	0.32	0.32	0.25

5.3.2 Comparison with Gas Chromatography

The current gas chromatograph was installed in 1995 [*Hammer et al.*, 2008]. It is able to measure the concentrations of the trace gases CO_2, CH_4, N_2O, SF_6, H_2, and CO, and is optimised for monitoring in the atmospheric range. Its temporal resolution is an injection every 5 min. When measuring ambient air it measures every 30 min air from the South-West intake line and every (30 ± 2) min an integrated sample from the South-East intake line. To compare the CRDS with the South-West line, we just compared the matching data. To compare with the South-East line, I manipulated the CRDS-data using Eq. 5.2 (and flagged unsuitable data) and varied the decay rate. As optimal value, I determined "by eye" $\tau = 20$ min. However, because the gas flow through the buffer volume is varying in time, this optimal estimation may not hold true in general. Finally, I compared the matching "integrated" 1-min CRDS values with the GC results.
In Figure 5.2, the comparison in CO_2 concentration between CRDS and the buffered South-East air GC data are shown for March 2014. Similar to the FTIR comparison, CO_2 and CH_4 concentration measured by CRDS and GC match within the ILCT. The mean values and medians of this comparison are listed as GC/SE in Table 5.2 and 5.3. When comparing CRDS with the continuous South-West air GC data, the results of CRDS and GC/SW match for most months within the ILCTs for CO_2 and CH_4 (see Table 5.2 and 5.3).

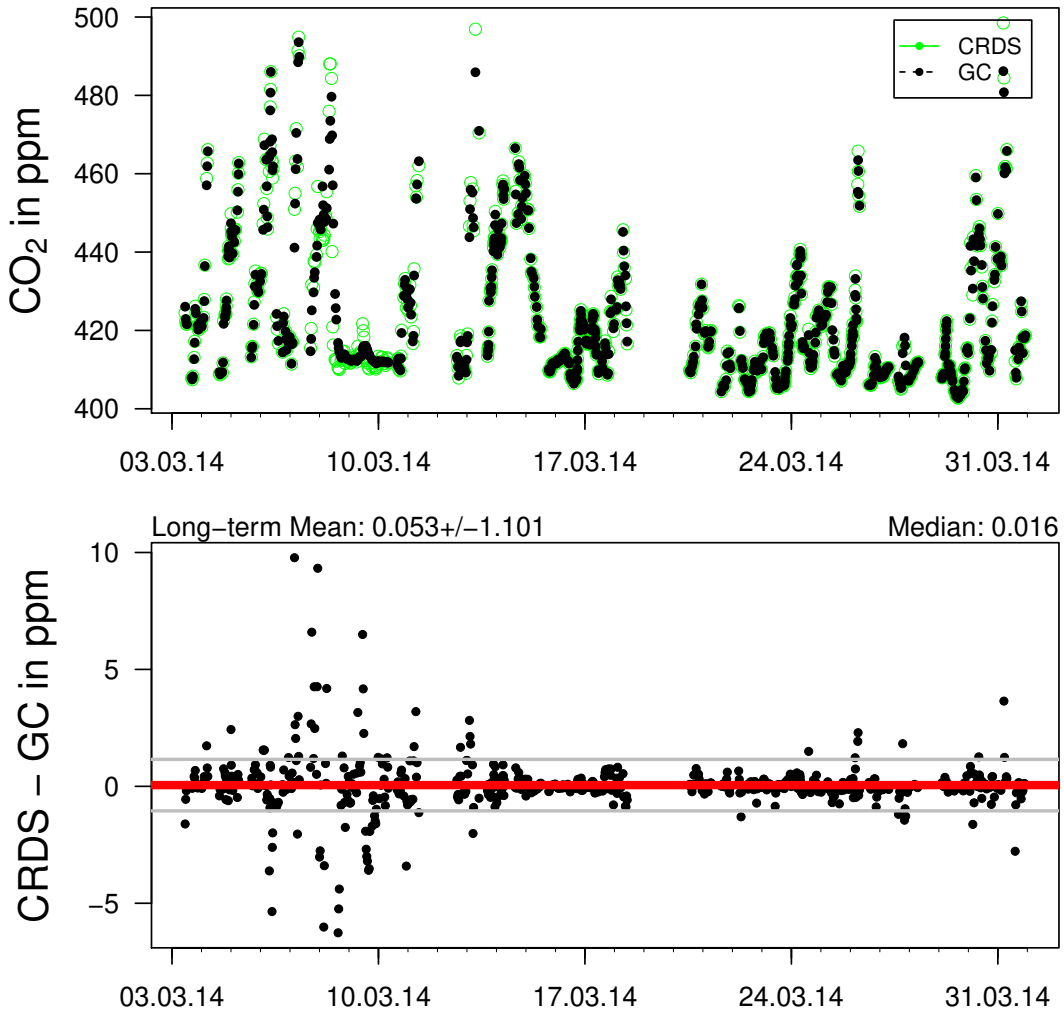

Figure 5.2: *Comparison of the ambient air data of CRDS and the buffered GC data. The upper panel shows the calibrated data of the instruments. The lower panel shows the difference of the measurement points of the instruments. Eight outliers with an offset between 10 and 20 ppm were ignored.*

5.4 Comparison of $\delta^{13}CO_2$ in ambient air samples

5.4.1 Comparison of $\delta^{13}CO_2$ in cylinder measurements

The FTIR and the mass spectrometer (MS) in Heidelberg are directly linked to the JRAS-scale by calibration cylinders which are specified by mass spectrometer measurements at the MPI for Biogeochemistry in Jena (later noted as JENA). The nominal $\delta^{13}CO_2$ values for the CRDS calibration are taken from MS measurements and is therefore linked to the Heidelberg MS-scale. And because the MS are linked to the JRAS-scale, also the CRDS results are linked to the JRAS-scale. In the upper panel of Figure 5.3, the results of flask measurements with the mass spectrometer in Heidelberg (MS) and in Jena (JENA) are compared. The results match, $\Delta(\delta^{13}CO_2)_{\mathrm{MS-JENA}} = (-0.012 \pm 0.011)\,‰$, and thus the MS is indeed linked to JRAS-scale. Furthermore, we observed mean differences of $\Delta(\delta^{13}CO_2)_{\mathrm{CRDS-MS}} = (0.017 \pm 0.023)\,‰$ and $\Delta(\delta^{13}CO_2)_{\mathrm{CRDS-FTIR}} = (0.036 \pm 0.023)\,‰$ (second and fourth panel of Figure 5.3). The offest between these differences of 0.019 ‰ matches the (un-significant) scale offset between MS and JENA and was expected because the FTIR is directly on JRAS-Scale.

All together, the CRDS is indeed linked to MS scale, the relatively large standard deviation is caused by two outliers which are possibly rather because of systematic errors, e.g. bad conditioned pressure reducers, than statistically significant. When comparing CRDS with FTIR and JENA we expect a scale offset of 0.012 ‰.

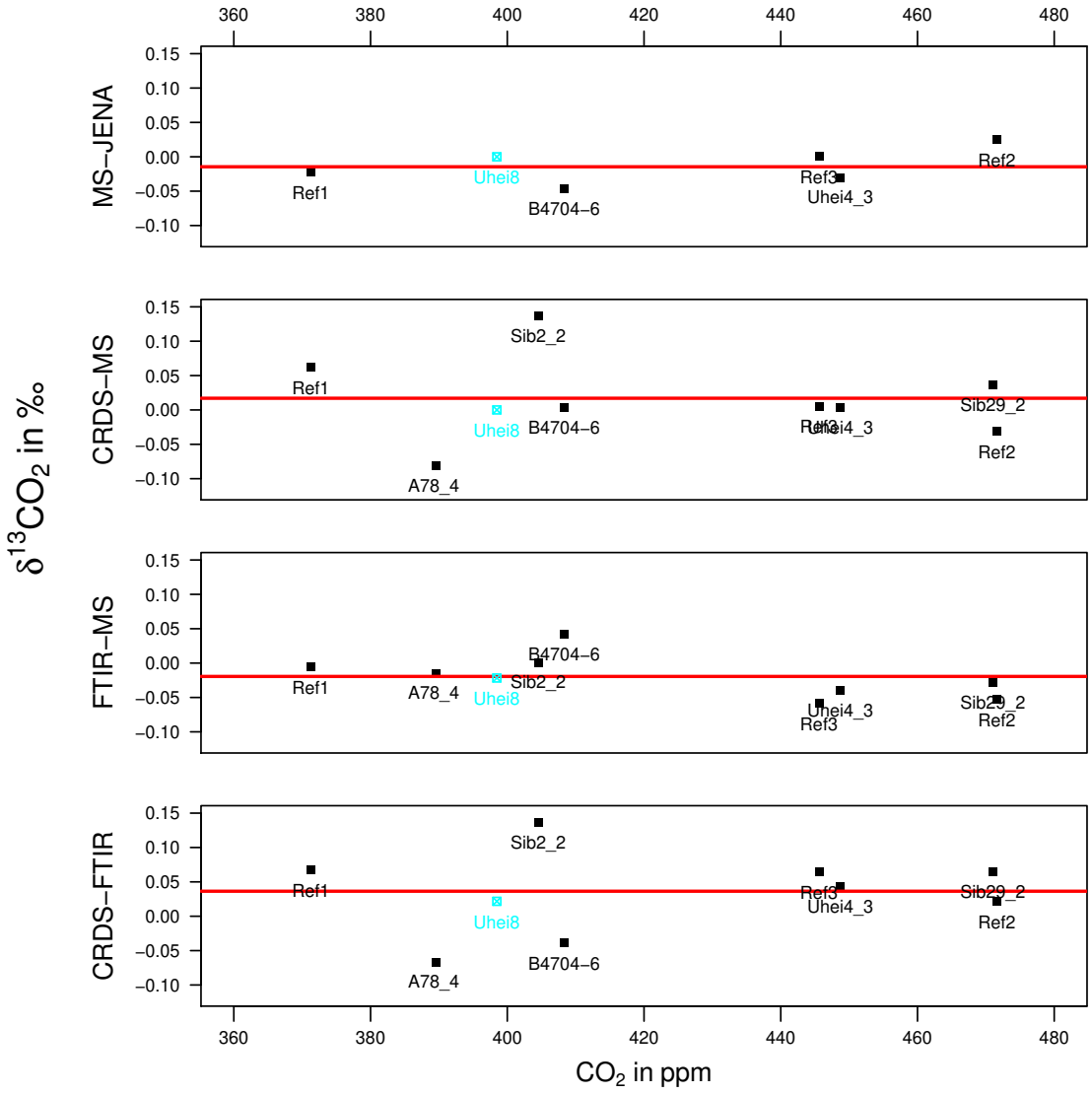

Figure 5.3: *Comparison of $\delta^{13}CO_2$ data from cylinder measurements of the CRDS (single-point calibration using UHEI8) and FTIR. The calibration standard UHEI8 of the CRDS is given in cyan and omitted from the quantitative comparison, i.e. mean values (red lines). We observed a slight negative offset between the HD MS-scale and the JRAS-scale of MS-JENA* $= (-0.012 \pm 0.011)$ ‰ *(upper panel) and a scale-offset of CRDS-MS* $= (0.017 \pm 0.023)$ ‰ *(second panel). Furthermore, we observed mean offset of CRDS-FTIR* $= (0.036 \pm 0.023)$ ‰ *(lower panel).*

5.4.2 Comparison of $\delta^{13}CO_2$ in continuous ambient air measurements

To compare the continuous data of $\delta^{13}CO_2$ in ambient air measured by CRDS and FTIR, we performed the same data averaging as for the comparison of concentrations (see Section 5.3.1). The comparison of the 30-min averages is shown in Figure 5.4. Already by eye, an offset between the data of the instruments can be seen (upper panel) and is quantified in the middle panel where $\Delta(\delta^{13}CO_2)_{\mathrm{CRDS-FTIR}} = (0.05 \pm 0.14)$ ‰. For every month of the evaluated period from January to May 2014, a significant positive offset was observed (see Table 5.2 and 5.3). In January and February 2014, the offset was up to 0.19 ‰ but for this period the FTIR data are not representative because the magnesium-perchlorate cartridge of the FTIR was potentially contaminated by an unknown substance from December 2013 until February 2014. All together, we observed a significant difference in ambient $\delta^{13}CO_2$ results of $\Delta(\delta^{13}CO_2)_{\mathrm{CRDS-FTIR}} = 0.06 - 0.11$ ‰ (monthly medians). This difference is about $+0.05$ ‰ larger than the scale-offset we have observed in cylinder measurements (see Section 5.4.1).

5.4.3 Comparison of $\delta^{13}CO_2$ with mass spectrometry by event flasks

While CRDS, FTIR, and GC are continuously monitoring the ambient air, a mass spectrometer usually measures cylinder and flask samples. On the other hand, mass spectrometry is currently the most accurate method of isotopic measurement and thus it is important to compare the isotopic data of any optical instrument with the results of the mass spectrometer. The ambient air samples for the mass spectrometer are taken with an event sampler [*Neubert et al.*, 2004] which takes semi-continuously every 2 hours an ambient air sample from the South-East ambient air intake line and has the possibility to collect 10 flasks. Thus, every 20 hours a filled flask is opened and refilled. When we detect an event, e.g. a peak in ambient $\delta^{13}CO_2$ or $\delta^{13}CH_4$ signature, with one of the in-situ instruments, we stop the event sampler. The event flasks are measured in Heidelberg at the GC for the gas concentrations and at the mass spectrometer for $\delta^{13}CO_2$. Additionally, for one event the flasks were measured at the mass spectrometers at the MPI in Jena for $\delta^{13}CO_2$ and $\delta^{13}CH_4$.

The event flasks are integrated samples. Each flask is continuously flushed at 1 bar until the event sampler closes its outlet. After the closing, the flask is filled to 2 bar, what requires approximately 5 min. To compare the continuous CRDS data with the event flasks, we calculated integrated CRDS data according to Eq. 5.2 until the closing and modelled the contribution of the extra 1 bar just by adding the concentration of the next minute. The FTIR has only 3-min values and for comparison just the average over the three 3-min average values before the closure time of the event flask is used. The time scale is afterwards adjusted as discussed below.

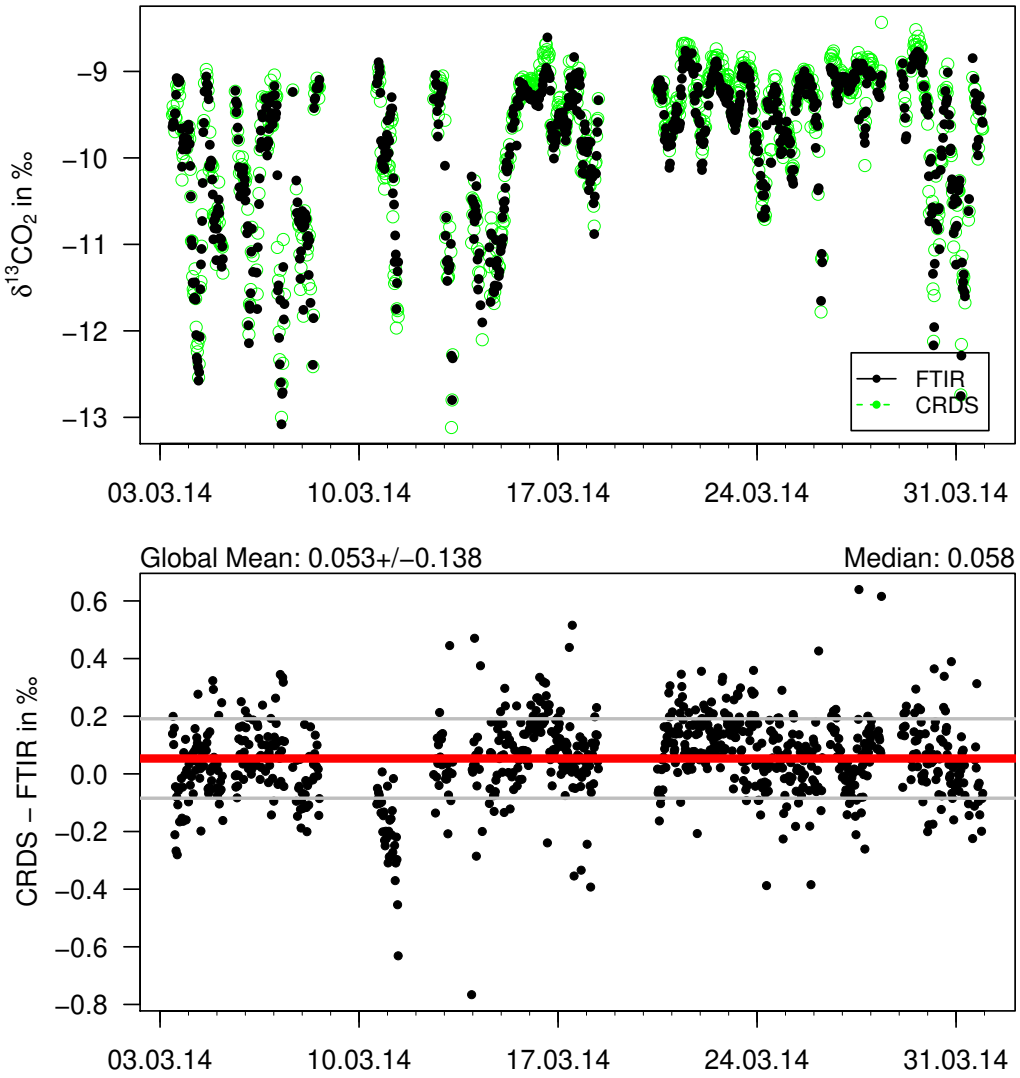

Figure 5.4: *Comparison of $\delta^{13}CO_2$ in ambient air measured with CRDS and FTIR*

We were able to catch the event from 03.03.2014 to 04.03.2014 where CO_2 increased by about 60 ppm and $\delta^{13}CO_2$ decreased by more than 3 ‰ and $\delta^{13}CH_4$ increased by 1 ‰ (see Figure 5.5). Unfortunately, the event sampler did not close the last flask, which would have monitored the decline of the concentration peak. Furthermore, the fourth and ninth flask have to be omitted from the comparison because its closure times collided with calibration or quality control intervals of the CRDS.
Despite the explained data treatment, we observed in the time series of the CO_2 and CH_4 concentrations that the flask data are delayed with respect to the integrated CRDS data. This might be caused by a wrong time stamp of the event sampler wherefore we treated the time stamp as a virtually free parameter. To adjust the time scales, we compared the time series of the CO_2 and CH_4 concentrations of CRDS and flasks, and looked for the best accordance by shifting the time stamp of the event flasks. As apparently optimal result, we shifted all flask data 16 min back in time. However, some data points match better for a shift of 2 more respectively less minutes. This uncertainty in time contributes strongly to the offset in the $\delta^{13}CO_2$ comparison.
The (integrated) $\delta^{13}CO_2$ data of CRDS, FTIR, and the mass spectrometer in Heidelberg (MS) and in Jena (JENA) are shown in Figure 5.6 in the middle and lower panels. The error bars indicate the variations within the enveloping 9-min interval, i.e. the maximum and minimum values, and give a hint of the impact of the uncertainty in time. Within these errors bars, the CRDS data match the JRAS-scale, i.e. JENA, within ± 0.1 ‰. For the second and fourth data point we observed a mean offset of $\Delta(\delta^{13}CO_2)_{\mathrm{CRDS-JENA}} = -0.3$ ‰. However, exactly for these data also the CO_2 and CH_4 did not match sufficiently after the time shift. Thus the mean offsets of these data points are dominated by a non-optimal comparison rather than a measurement offset.
For the applied time shift of 16 min, we observed no significant systematic offset between CRDS and the other instruments, the over-all mean offset and standard deviation are $\Delta(\delta^{13}CO_2)_{\mathrm{CRDS-JENA}} = (-0.11 \pm 0.18)$ ‰ and $\Delta(\delta^{13}CO_2)_{\mathrm{CRDS-FTIR}} = (-0.07 \pm 0.17)$ ‰, where the offsets are not significant and the standard deviation dominated by the uncertainty in time and the different temporal resolution of the instruments.
Furthermore, this is not that inconsistent with the comparison of continuous data in March 2014 (see Section 5.4.2) because at the 03.03.2014 and 03.04.2014 indeed no offset in CRDS and FTIR has been observed (see Figure 5.4).

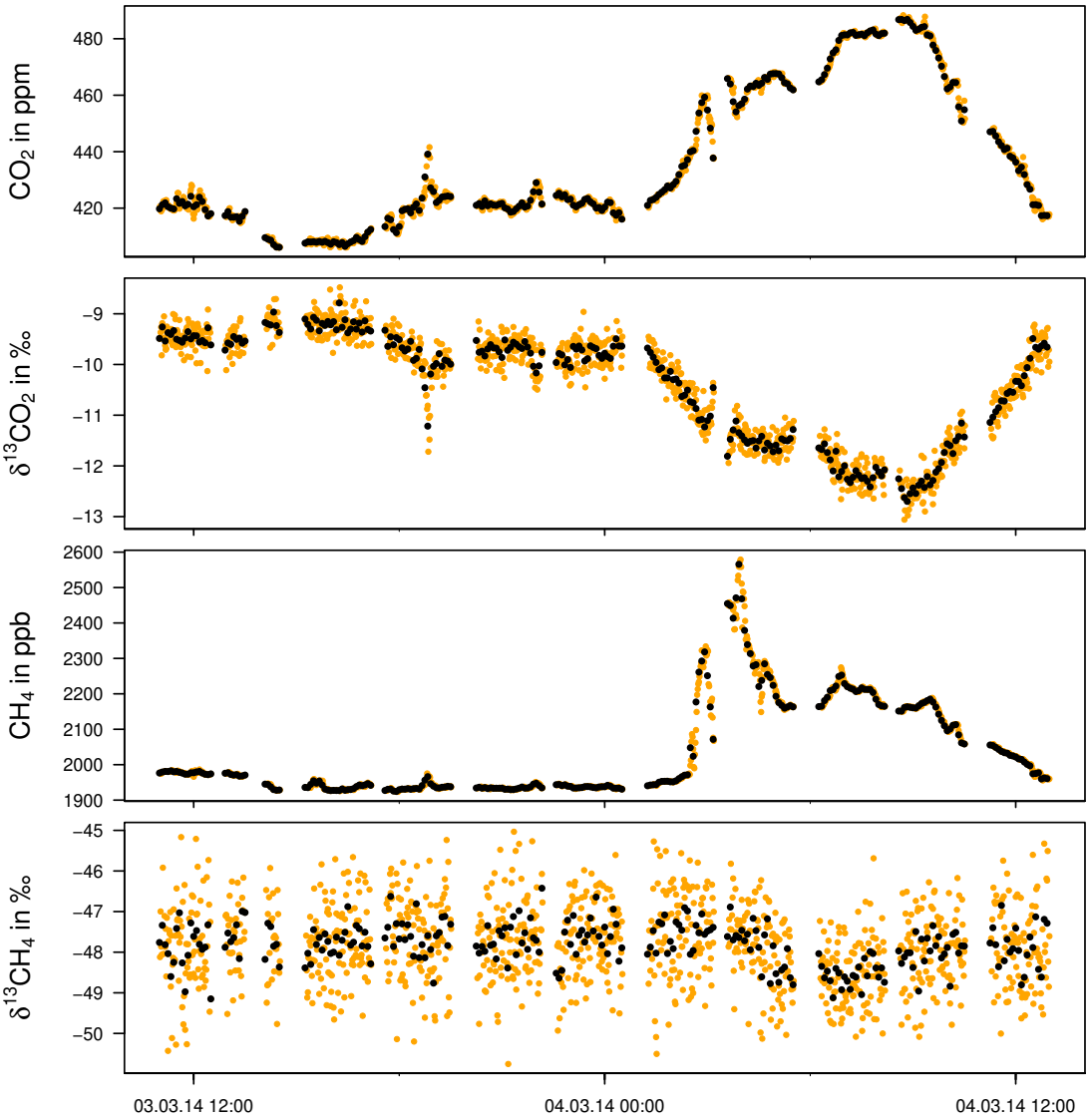

Figure 5.5: *The single point calibrated ambient air CRDS data (1-min data in yellow and 5-min averages in black) during the event from 03.03.2014 to 04.03.2014.*

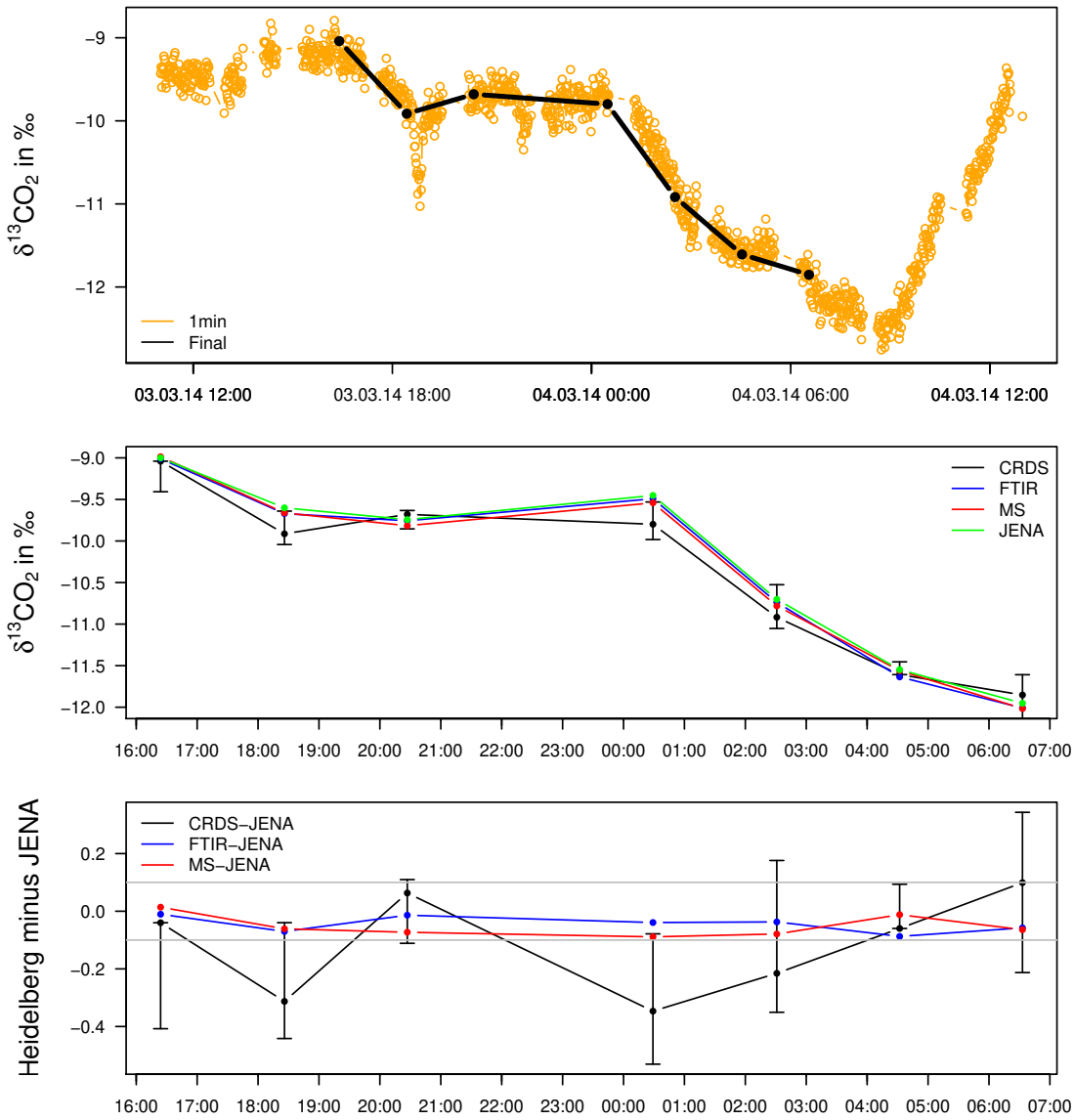

Figure 5.6: *Comparison of $\delta^{13}CO_2$ results of different instruments (CRDS, FTIR, MS in Heidelberg, and MS in JENA). Upper panel: The orange circles give the calculated integrated data measured by the CRDS with a resolution of 1 min. The black dots are the integrated CRDS data which are used for the comparison. Middle panel: Results of the four instruments. The error bars indicate the minimum and maximum CRDS-values within the enveloping 9-min interval. The errors of the other instruments are not shown. Lower panel: Deviation in $\delta^{13}CO_2$ measured by the mass spectrometer in Jena and the Heidelberg instruments.*

5.5 Comparison of $\delta^{13}CH_4$ with mass spectrometry

Besides the CRDS, only a mass spectrometer at the MPI in Jena is able to measure $\delta^{13}CH_4$. For the event flask comparison, we applied the similar data treatment as in the case of $\delta^{13}CO_2$ (see Figure 5.7). The actual event peak is sketched by 7-min averages calculated from the integrated CRDS data, the black points and error bars indicate the associated 1-min averages and the variations within the enveloping 7-min interval. The 7-min averages and JENA match perfectly for the fourth and seventh flasks but because of the large variations also theses differences are not significant. Thus, for 7-min averages CRDS and JENA are compatible within the standard deviation of about 0.5 ‰.
On the other hand, comparison with a higher temporal resolution is not possible. Namely the integration of the CRDS data did not worked sufficiently, first of all the peak at 06:30 on 04.03.2014 is not reproduced by the integrated 1-min data.

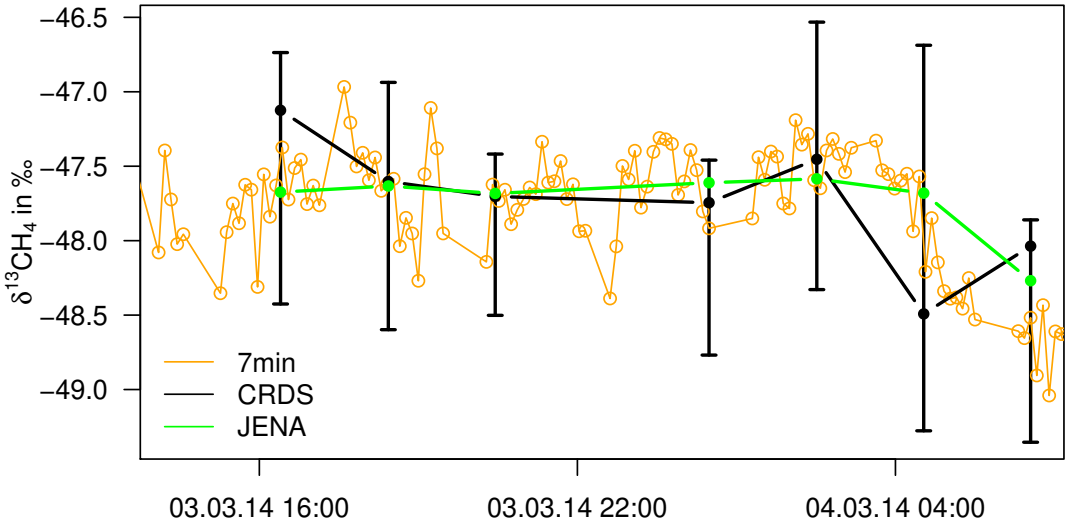

Figure 5.7: *Comparison in $\delta^{13}CH_4$ between CRDS and Jena MS. The actual event peak is sketched by 7-min averages calculated from the integrated CRDS data, the black points and error bars indicate the associated 1-min averages and the variations within the enveloping 7-min interval.*

6 Time series of $\delta^{13}CH_4$ in natural gas

The origin of the natural gas in the Heidelberg gas supply is either Russia or the North Sea. In the 1990s, in summer the supply consisted mostly of the cheaper Russian gas whereas in winter most of the gas came from the North Sea due to shortage of Russian gas. *Glatzel-Mattheier* [1997] observed this annual change by direct measurements of the natural gas provided by the Heidelberg gas supply. The measured isotopic signature showed significant seasonal variations. From 1991 to 1997, it varied roughly from $\delta^{13}CH_4 = -50\,‰$ in summer to $\delta^{13}CH_4 = -35\,‰$ in winter. These values match very well with the isotopic signature of North Sea gas and Russian gas, respectively. Knowledge about the annual variations in the $\delta^{13}CH_4$ signature of the domestic gas supply may lead to important applications. First of all, it allows an accurate estimation of the $\delta^{13}CO_2$ signature of (domestic) heating with natural gas and its seasonal variations.

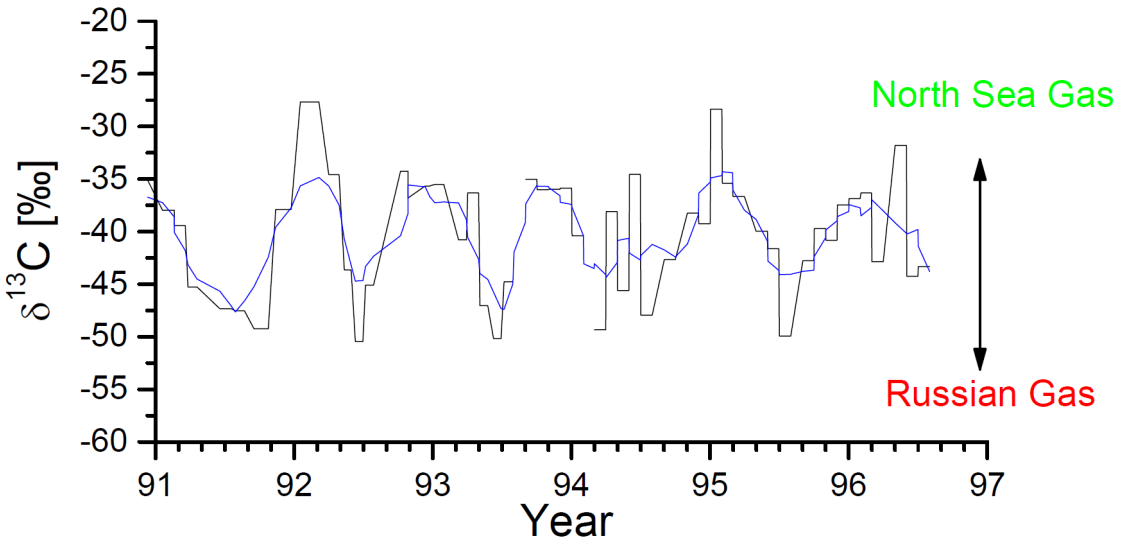

Figure 6.1: *Annual variation of the $\delta^{13}CH_4$ in the natural gas provided by Heidelberg Stadtwerke. The figure shows unpublished data from Levin et al., a similar figure can be found in [Glatzel-Mattheier, 1997].*

Between 1991 and 1997, only monthly integrated samples were analysed. This measurement program was stopped in the end of the last millenium, also due to the relatively high effort. Due to the possible application we want to continue this monitoring of the time series of $\delta^{13}CH_4$ in the natural gas using CRDS. Hereby,

pure natural gas samples can be measured every 30-60 min and with only moderate pretreatment.

6.1 Natural gas samples

From January 2012 to February 2014, every week once or twice two sample bags were filled with natural gas provided by the gas line in the ^{14}C-laboratory of our institute. To avoid a contribution from not-up-to-date gas, we flushed the gas line for 10-20 s before filling the bags. Unfortunately, for most of the time we were the only consumer in the whole seven-floored building. Thus, the main supply line of the overall building was not continuously flushed.
After we received the bad news in February 2014, we tested whether our flushing time was still long enough to flush also the main line or whether we always just obtained the gas which was standing in the main line since the last massive extraction. To test it, the main gas line was completely flushed by burning natural gas for hours and natural gas was sampled in bags before and after the flushing. We observed a highly significant change in the isotopic signature from $-37.5\,‰$ to $-42.1\,‰$ from before to after the flushing. Thus, we lost most temporal information about all bags archived until February 2014. These samples are therefore not further analysed.
As we did not want to completely flush the whole main line before filling an archive bag, we looked for a fluently flushed gas supply and found a temporary supply in the laboratory of the "Anorganic pracitical cource" in the Institute of Chemistry (Heidelberg University). Unfortunately, this course was ending in April 2014. However, we were able to archive several bags from February to April 2014 and are therefore able to give a typical isotopic signature for the end of the winter period. Due to the lack of a more suitable gas supply since April 2014, Martina Schmidt provided in June 2014 several samples taken from her domestic gas stove.

6.2 Measurement method

Measuring in the simultaneous mode, the guaranteed spectral concentration range for CH_4 is 1.8-12 ppm in HP-mode and 10-500 in HR-mode [*Picarro*, 2012]. Thus, highly concentrated samples like pure natural gas samples have to be diluted before measurement. The optimum precision of $0.2\,‰$ can be obtained with the highest possible concentration which are allowed in the HP-mode, at 10 ppm[1]. Consequently, we diluted our initial samples by a factor of 10^5 with zero air.[2]

[1] We will see later, that the HR-mode is already at 10 ppm more suited than the HP-mode.
[2] The dilution gas should be free of CH_4 and have the same gas matrix like ambient air.

6.2.1 Sample bags, syringes, and Luer-Lock-connectors

For all applications we used aluminium-coated polyethylene bags (from Tesseraux Spezialverpackungen GmbH, Bürstadt) as sample containers. Their maximum volume is about 1.4 L respectively they each can contain around 1.3 L without overpressure. Most of the bags are gas-tight in terms of days but significantly lose gas within months. However, several bags were still completely filled after 2 years. However, only a few are suited for a long-term archive.
For the extraction of gas from the archive bag we used syringes from Innovative Labor Systeme GmbH with a volume of 50 µL or 5 ml and a female Luer-Lock connector. The injection system was built of two Luer-Lock T-pieces which each have two male ports and one female port. Each T-piece has a switch to set which two ports are connected. The overall dead volume of the injection system is less than 1 ml.

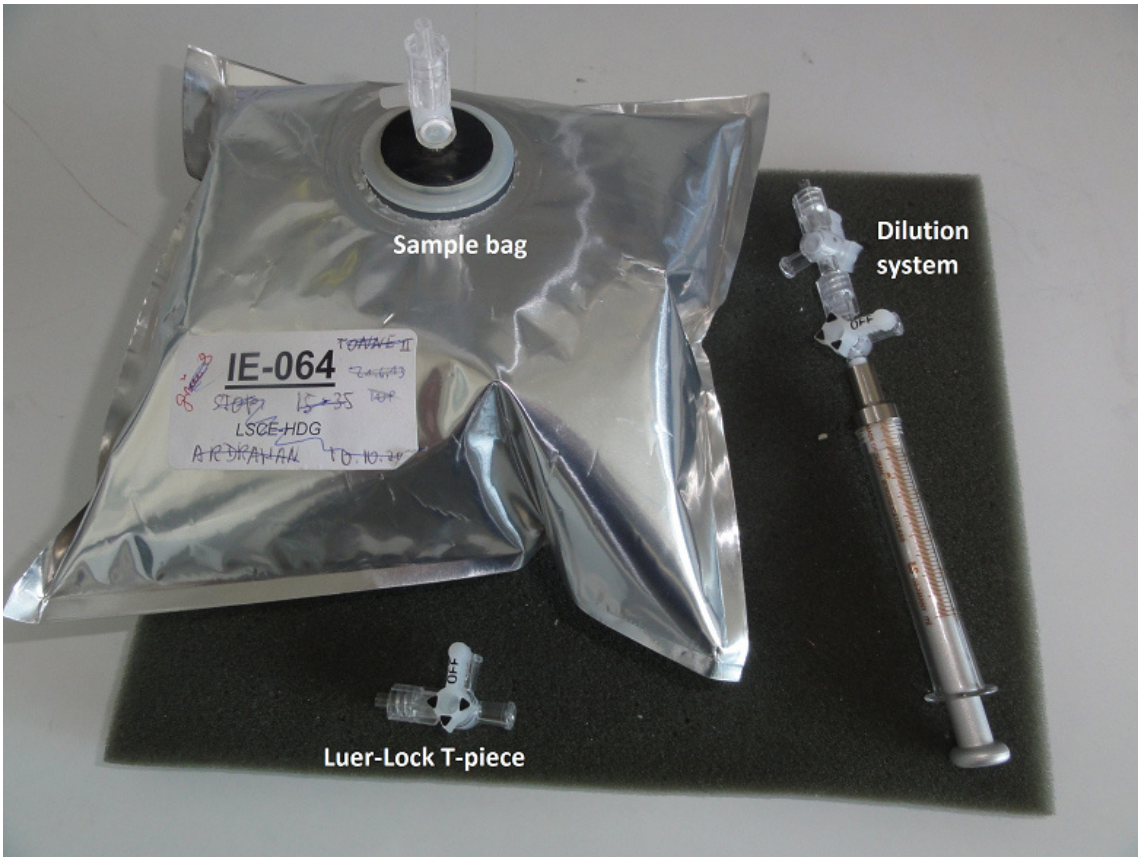

Figure 6.2: *Photography of a sample bag and a single Luer-Lock T-piece. The simple dilution system consists of a 5 ml syringe and 2 Luer-Lock T-pieces. For dilution, two bags are connected to the two free female ports at the Luer-Lock T-pieces.*

6.2.2 Dilution of the highly concentrated samples

The archive bags contain pure natural gas with more than 90 % CH_4. For accurate measurement, these samples have to be diluted by a factor of 10^5 with zero air to get a final CH_4 concentration of about 10 ppm. This dilution was realised in two steps with a 5 ml syringe. Therefore, we emptied two bags (later called intermediate respectively final bag) with a small pump and filled them afterwards with roughly 1.3 L of zero air. Then, we connected the syringe, the archive bag, and the intermediate bag via two Luer-Lock T-pieces in such a way that we are able to transfer archived gas via the syringe to the intermediate bag. Before connecting the intermediate bag, we flushed the injection system with archived gas to also flush all dead volumes. Afterwards, we injected 3.9 ml of the sample in the intermediate bag. Finally, we repeated the same procedure and injected 4.4 ml from the intermediate bag into the final bag.

When using a 50 µL-syringe instead, the dilution can be applied in one step. This would also lead to less contaminations because only one bag is required. However, our injection system has a systematic residual dead volume within the connector of the final bag which is in the order of the injected sample of 13 µL. Experiments have shown that bags diluted by this method lead to non-reproducible results.

6.2.3 Measurement strategy

The final bags, containing 10 ppm CH_4, were connected to the 16-port valve and treated like a cylinder. The crucial difference is that the bags have no overpressure, i.e. the supply flow from the bag to the CRDS has to be maintained by the Picarro pump only. For the best results, Picarro recommend a preload pressure of 0.2-0.5 bar, however, the measurement should also work without primary pressure (personal communication with Renato Winkler from Picarro, 2013).
The bags are sucked empty within 60 min. To avoid surface effects in a half-empty bag, we decided to measure a bag for 30 min. Assuming the quality of a bag measurement is comparable with a cylinder measurement, the expected measurement errors in $\delta^{13}CH_4$ are 0.2 ‰ respectively 0.1 ‰, depending on the measurement mode (see Table. 4.2).
For calibration, the 10 L high pressure cylinder MSTD (see Table. 4.7) which contains $CH_4 \approx 10$ ppm and $\delta^{13}CH_4 = -43.32$ ‰ was measured before and after each sequence of 3 or 4 sample bag measurements for 30 min. All measurements of highly enriched samples were separated by 10 min of ambient air measurement.

6.3 Reproducibility and accuracy

To test the repeatability of the bag measurements, we filled bags with air from the MSTD cylinder. By using the same sample for calibration and measurement, we are able to observe the effect of the dead volume or other bag specific effects. Furthermore, also no calibration errors occur because the single-point calibration should work well for a measured value very near to the assigned calibration value.

We run two tests. On 23.05.2014 we filled and measured four bags with air from the MSTD, the results are shown in the orange box in Figure 6.3 and 6.4. One bag contained more than 100 ppm and is therefore omitted from the evaluation. Before, this bag was used as intermediate bag and therefore was potentially contaminated with CH_4 from natural gas sampling. On 04.06.2014, we modified the test. We used three times the same bag (this bag was already used in the first test, at measurement number 3) and improved the filling. Within the 10 min of ambient air measurement we emptied the bag, filled it with 1.4 L of zero air, and emptied it again. By this, remains in the dead volume should be negligible due to dilution. Then we filled the bag with air from MSTD and reconnected it to the 16-port valve. The results of this test are shown in the green box of Figure 6.3 and 6.4.

We evaluated and compared the results of the HP-mode (Figure 6.3) and the HR-mode (Figure 6.4). For both modes no result matched with the nominal value of CH_4 in the cylinder (blue line). However, the relative deviation is only 1 % for the shown bags. For $\delta^{13}CH_4$, we observed in HP-mode a systematic offset of 0.3 ‰ from the nominal value. This might be caused by a saturation of the HR-$^{12}CH_4$-peak which would lead to an increased $\delta^{13}CH_4$ value. In HR-mode, the measured values match with the nominal value of the bags. On the other hand, the precision is indeed better in HP-mode. However, for CH_4 the relative measurement errors are negligible for both modes and for $\delta^{13}CH_4$ the precision is in HR-mode also already better than 0.3 ‰. Using the data of the multiply measured bag only (see red box in Figure 6.3 and 6.4), the reproducibility of $\delta^{13}CH_4$ is 0.1 ‰ in HP-mode and 0.3 ‰ in HR-mode).
All together, the HR-mode is more accurate and therefore more suitable than the HP-mode for the measurement of samples which contain at least 10 ppm CH_4.

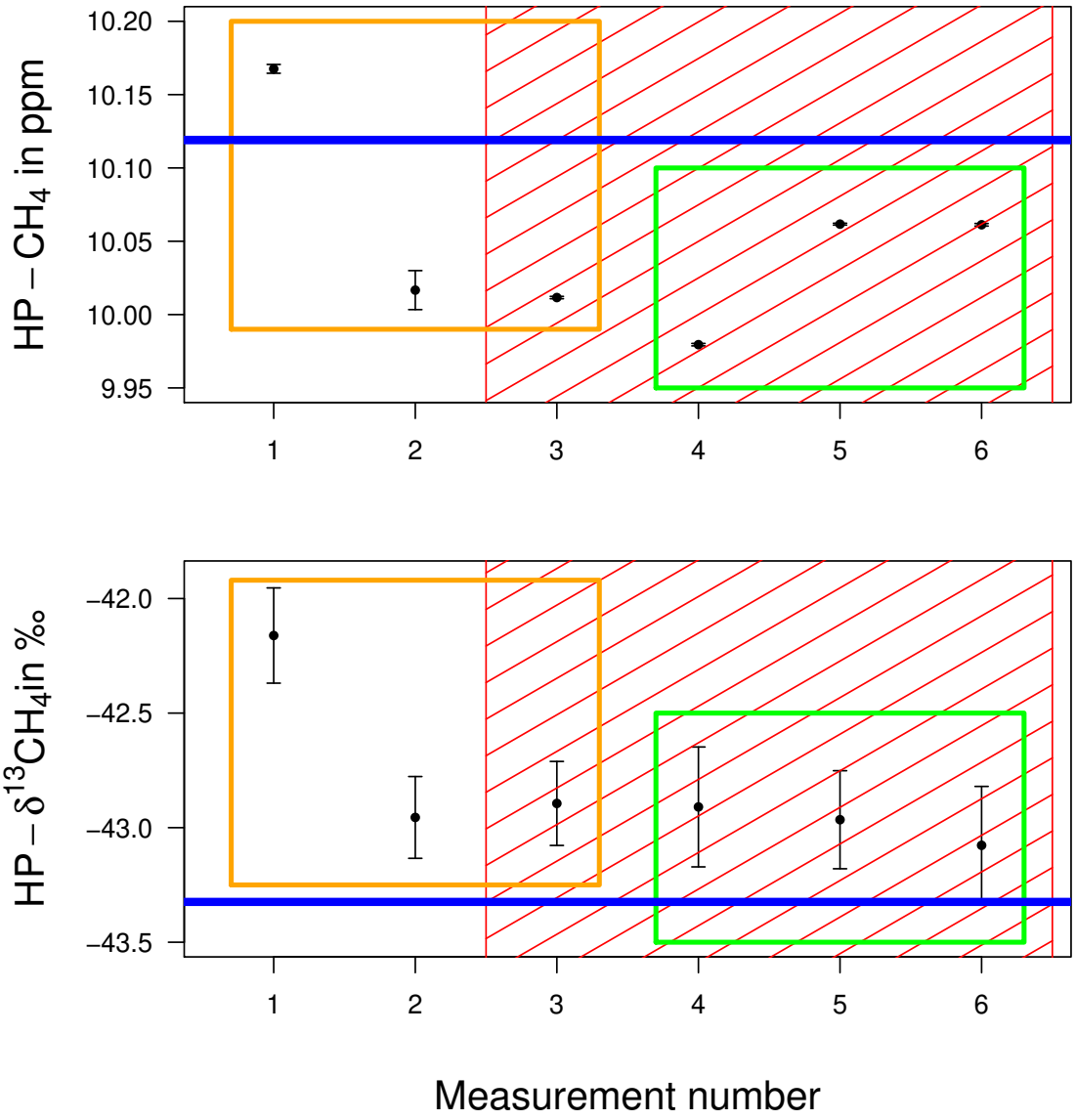

Figure 6.3: *Reproducibility of bag measurements in HP-mode:*
Calibrated HP-mode data of the sample bags which contained air from the MSTD cylinder. The blue lines give the nominal value of the MSTD cylinder and the bags. At different dates, two measurement series were performed. The measurement number gives the chronological order of the sample measurements. In the first series (orange box) three different bags were used, in the second series (green box) only one bag was used for all samples. This bag was already used at the measurement number 3 (red box).

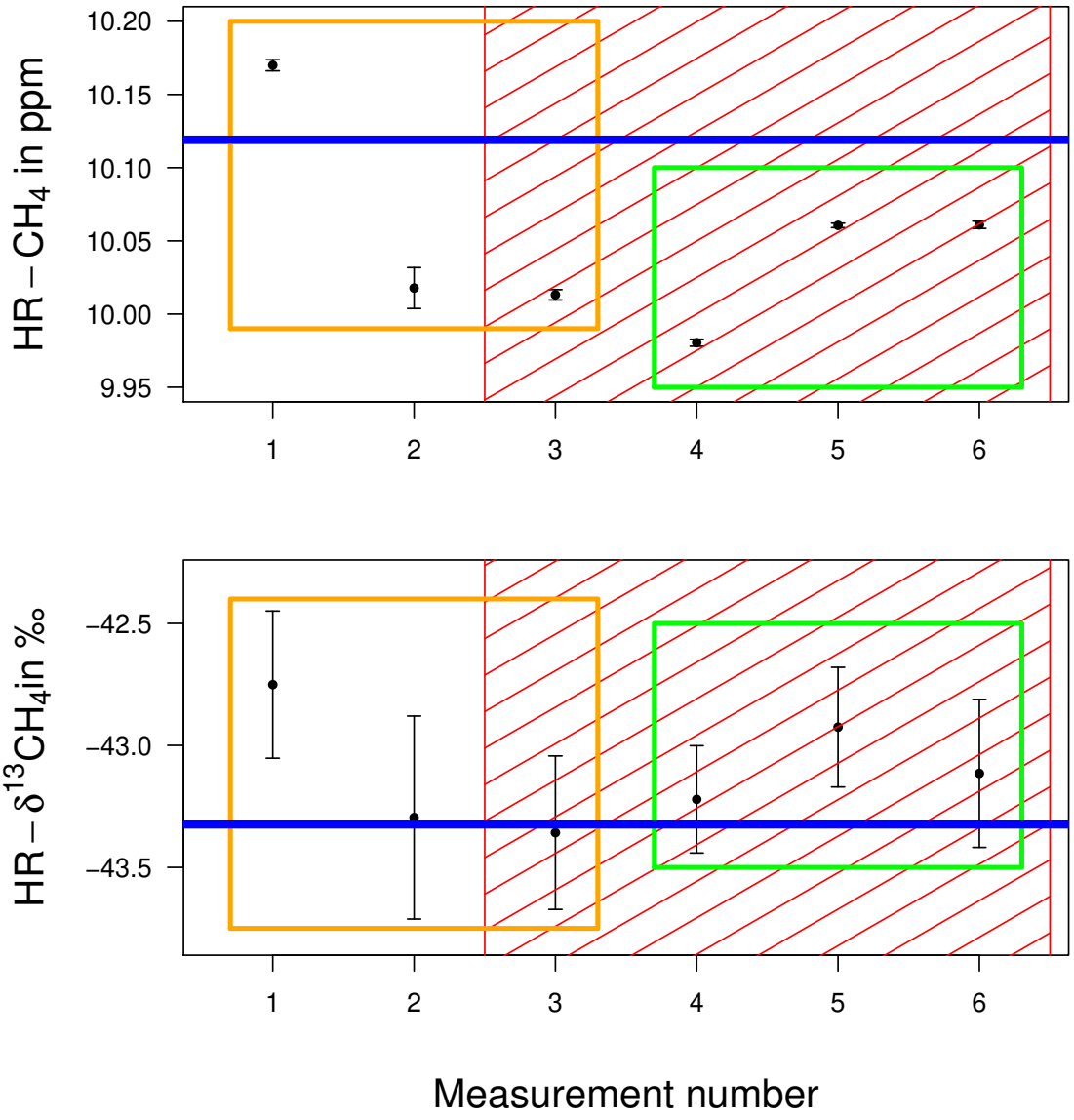

Figure 6.4: *Reproducibility of bag measurements in HR-mode:*
Calibrated HR-mode data of the sample bags which contained air from the MSTD cylinder. The blue lines give the nominal value of the MSTD cylinder and the bags. At different dates, two measurement series were performed. The measurement number gives the chronological order of the sample measurements. In the first series (orange box) three different bags were used, in the second series (green box) only one bag was used for all samples. This bag was already used at the measurement number 3 (red box).

6.4 Results

We measured natural gas samples from February, March, and June 2014. The results are shown in Figure 6.5 where the error bars indicate the standard deviation of the sample measurement, which means 2 or 3 measurements per sample. Although we have only 6 data points, we can carefully observe the following accordance with the data shown in Figure 6.1:

- There is a maximum in $\delta^{13}CH_4$ around -35 ‰ and a minimum around -44 ‰.
- The value matches perfectly for June. The peak is shifted from January to March, at least for 2014. Following [*Glatzel-Mattheier*, 1997], this could be interpreted as follows: Because the winter 2013/2014 was relatively warm, the German/regional gas storage, which was filled with Russian gas in summer, lasted until February 2014. Or in general, the stored range of Russian gas might have increased since the 1990s such that in winter less North Sea gas has to be purchased.

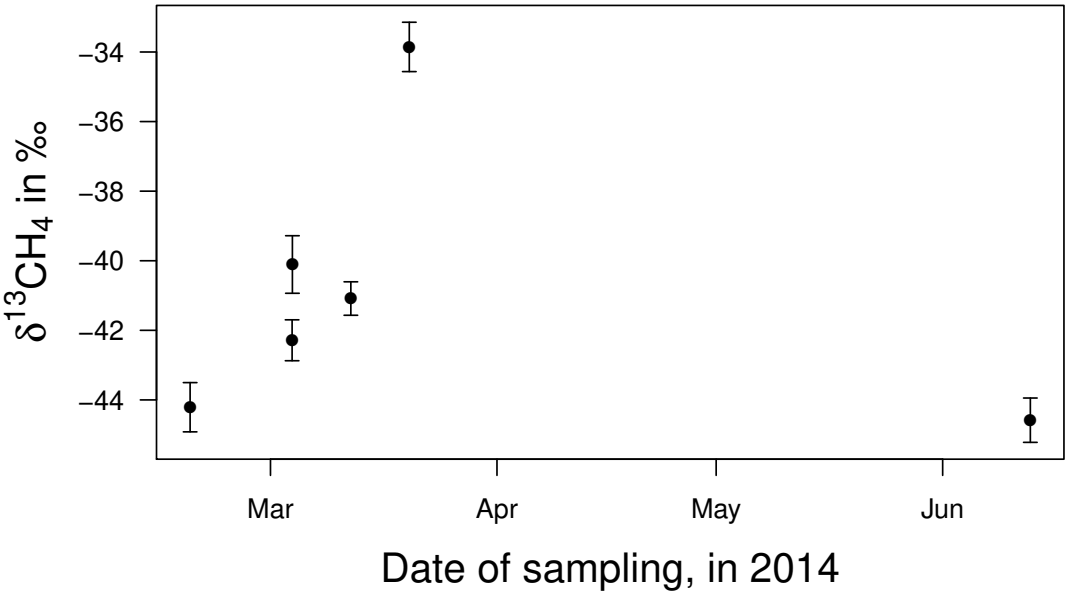

Figure 6.5: *Results of the analysis of the natural gas, provided by the municipal utilities in Heidelberg, analysis. We observed the winter, or here: late winter, peak in $\delta^{13}CH_4$ which is probably caused by a shortage in Russian gas in March 2014.*

6.5 Possible improvements of bag sample analysis

- Because every bag seems to have an individual behaviour in leakage and memory, a worse reproducibility is expected when using different sample bags. Furthermore, only few bags are as gas-dense as required for a storage container of the long-term archive. Aiming for high accuracy and precision in both, archive and measurement, glass or steel flasks should be used as containers.

- Syringes with a small volume like 50 µL lead to inaccuracy due to the relative large dead volume in the Luer-Lock injection set-up. But when using syringes with a larger volume of 5 ml two dilution steps are required. To keep both, the dead volume and contamination, as low as possible a new injection system has to be constructed which does the dilution automatically and without unevacuating steps.

- The best precision can be reached in $\delta^{13}CH_4$-only mode. But the switch back to the simultaneous mode has to be manually, i.e. is not automatable.

7 Summary and outlook

The instrument measures the CO_2 and CH_4 concentrations in ambient air with high precision: The Allan deviation of 1-min averages is 0.04 ppm for CO_2 and 0.1 ppb for CH_4. The virtually optimal precision is reached by 15-min averages with 0.01 ppm and 0.08 ppb, respectively. Measuring in simultaneous mode, the precision of the $\delta^{13}CO_2$ and $\delta^{13}CH_4$ data is unsatisfactory for 1-min averages (0.2 ‰ and 0.9 ‰, respectively) and optimal for 60-min averages (0.03 ‰ and 0.14 ‰, respectively). When measuring in the $\delta^{13}CH_4$-only mode, the precision of $\delta^{13}CH_4$ data increases to, e.g., 0.10 ‰ for 60-min averages.

The data show no significant CO_2 cross-sensitivity and, since the repair by Picarro in October 2013, no reproducible correlation with the barometric pressure. I observed a significant H_2O cross-sensitivity of the internally water vapour corrected data within a water vapour range from 0 to 1.5 %. Thus, the internal water vapour correction appears to be insufficient for highly accurate measurements of the concentrations and $\delta^{13}C$ signatures of ambient CO_2 and CH_4.

Furthermore, the instrument has a slight non-linearity in CO_2 and CH_4 concentration measurement. Thus, for most accurate results either at least a two-point calibration is required or the single-point calibrated data has to be corrected for this non-linearity. Unfortunately, most of the time of this thesis, I was efficiently only able to calibrate with one calibration standard. Since May 2014, three calibration standards are measured continuously every 5 hours, spanning a CO_2 range from 398 ppm to 485 ppm and a CH_4 range from 1935 ppb to 2350 ppb. For the future I recommend to apply a suitable two-point calibration for this instrument to improve the instrumental accuracy. Moreover, it has to be double-checked which calibration method gives the better $\delta^{13}C$ results when applying a two-point calibration, the preceding ^{13}C calibration or the subsequent $\delta^{13}C$ calibration.

I compared the single-point calibrated data, which I did not further corrected for the non-linearity, with the data from the Fourier Transform InfraRed (FTIR) spectrometer, the gas chromatograph (GC), and the mass spectrometers in Heidelberg (MS) and at the MPI for Biogeochemistry. For the CO_2 and CH_4 concentrations, the data of CRDS, FTIR, and GC match within the WMO recommendation of 0.1 ppm and 2 ppb, respectively. For $\delta^{13}CO_2$, I observed offsets of $\Delta(\delta^{13}CO_2)_{\mathrm{CRDS-MS}} = (0.017 \pm 0.023)$ ‰ and $\Delta(\delta^{13}CO_2)_{\mathrm{CRDS-FTIR}} = (0.036 \pm 0.023)$ ‰ in cylinder measurement, and $\Delta(\delta^{13}CO_2)_{\mathrm{CRDS-FTIR}} \approx 0.08$ ‰ in ambient air measurement. For $\delta^{13}CH_4$, I had only few data to compare because, besides the CRDS, only a mass

spectrometer in Jena measured some of our samples for $\delta^{13}CH_4$. Within the standard deviation of 0.5 ‰, the 7-min averaged CRDS-data was compatible with Jena.

I developed a measurement strategy for measuring the $\delta^{13}CH_4$ signature of highly concentrated CH_4 samples. For samples with 10 ppm CH_4 and $\delta^{13}CH_4 \approx -43$ ‰, the accuracy of the HR-mode is better than the HP-mode which measures a systematic offset of 0.3 ‰. At 10 ppm CH_4 and 25-min averages, the precision of HR-mode and HP-mode is 0.3 ‰ and 0.2 ‰, respectively. The reproducibility is 0.3 ‰ and 0.1 ‰, respectively. I recommend to measure in HR-mode because of the better accuracy. By this measurement strategy, I wanted to measure the time series of $\delta^{13}CH_4$ in the natural gas provided by the municipal utilities in Heidelberg. In the 1990s, significant annual variations from -50 ‰ to -35 ‰ were observed, depending on the momentary ratio in natural gas from the North Sea or from Russia. Although we had to omit most of our archived samples, I measured a range of $\delta^{13}CH_4 \approx$ -44 ‰ to -34 ‰ from February to June 2014. This matched approximately with the expected seasonal variation, however, the annual maximum appeared to be shifted from January to March. Further monitoring will help to quantify the seasonal cycle of the source signature of natural gas consumed in Heidelberg.

At our institute this CRDS analyser is the only instrument which measures $\delta^{13}CH_4$ signatures. This capability, and the small size of the overall measurement system which fits in a normal-sized car, provides several interesting field experiments. As a further application, this analyser might measure as a mobile instrument the source signals of landfill sites or cowhouses can be measured directly at the location. Furthermore, it has to be shown (http://www.picarrosurveyor.com), that the analyser can also operate while driving. By this, horizontal profiles of $\delta^{13}CH_4$ (but also of CO_2, CH_4, and $\delta^{13}CO_2$) can be measured what means a better local resolution. Additionally, the measurement of the time series of $\delta^{13}CH_4$ in natural gas seems to be more promising than the monitoring of $\delta^{13}CH_4$ ambient air because the precision of $\delta^{13}CH_4$ measurements is better for highly concentrated CH_4 samples.

A Appendix

A.1 List of Figures

A.2 List of Tables

A.3 Ambient air data

Half-annual variations The data of 6 month of ambient air monitoring is shown in Figure A.1 and A.2. Neither for CO_2 nor CH_4 a significant trend could be determined within this short time range. Rather the monthly means are dominated by particular events like the operating construction site which most probably cause the elevated concentrations in the beginning of March 2014. We observed a highly significant correlation in the CO_2 concentration and the isotopic $\delta^{13}CO_2$ signature (Figure A.1 and A.5). For CH_4 we did not observed such correlations.

Weekly and diurnal variations In Figure A.3 and A.4 the weekly variations in CO_2 and CH_4 during a week in March 2014 are shown (for orientation: 24.03.2014 was a Sunday). In Figure A.5 the integrated diurnal course during March 2014 is shown. For CH_4 no correlated courses were observed.

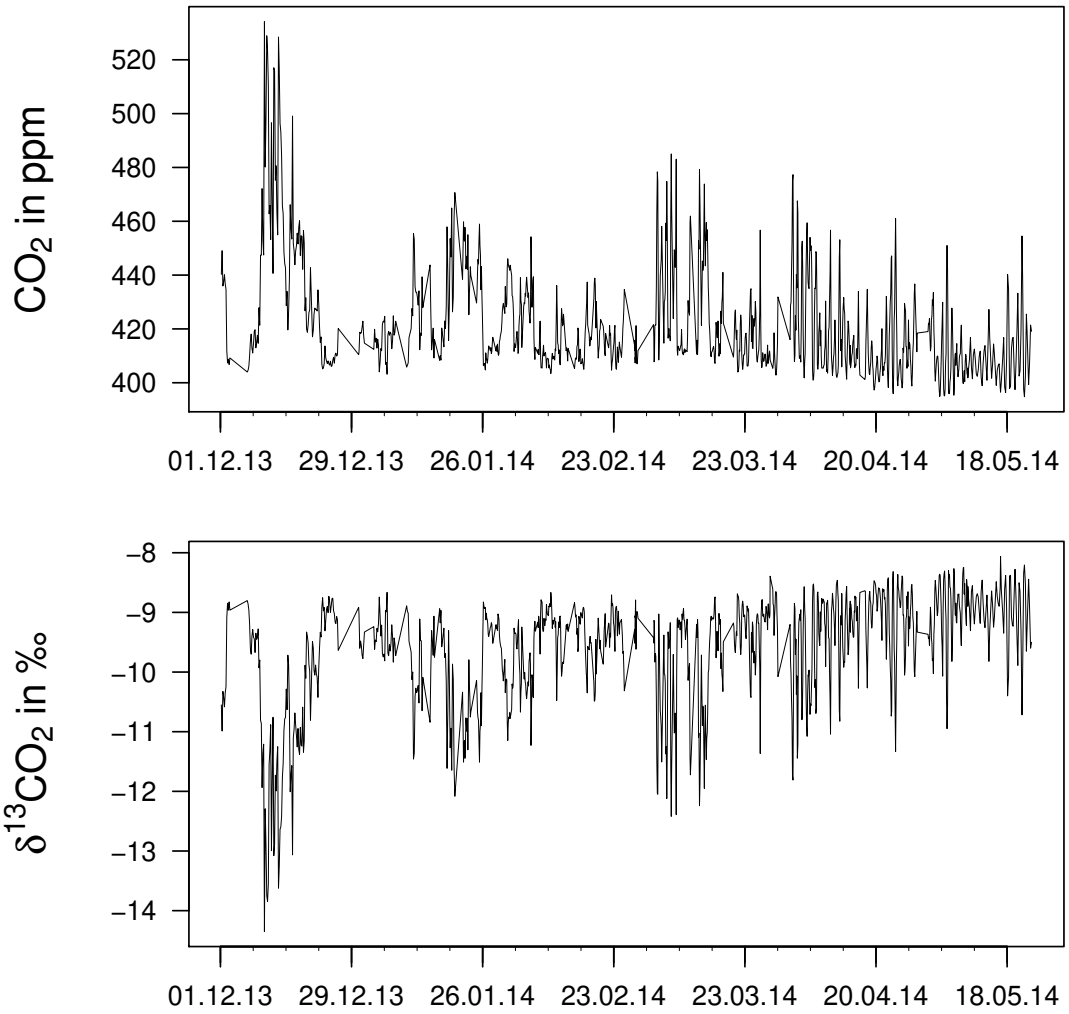

Figure A.1: *Monitored concentration and isotopic signature of CO_2 in the ambient air from December 2013 until May 2014. The variations are governed by particular events like an operating construction site which most probably cause the elevated concentrations in the beginning of March 2014. Since April 2014 the base level off CO_2 concentration is slightly decreasing and increasing for $\delta^{13}CO_2$.*

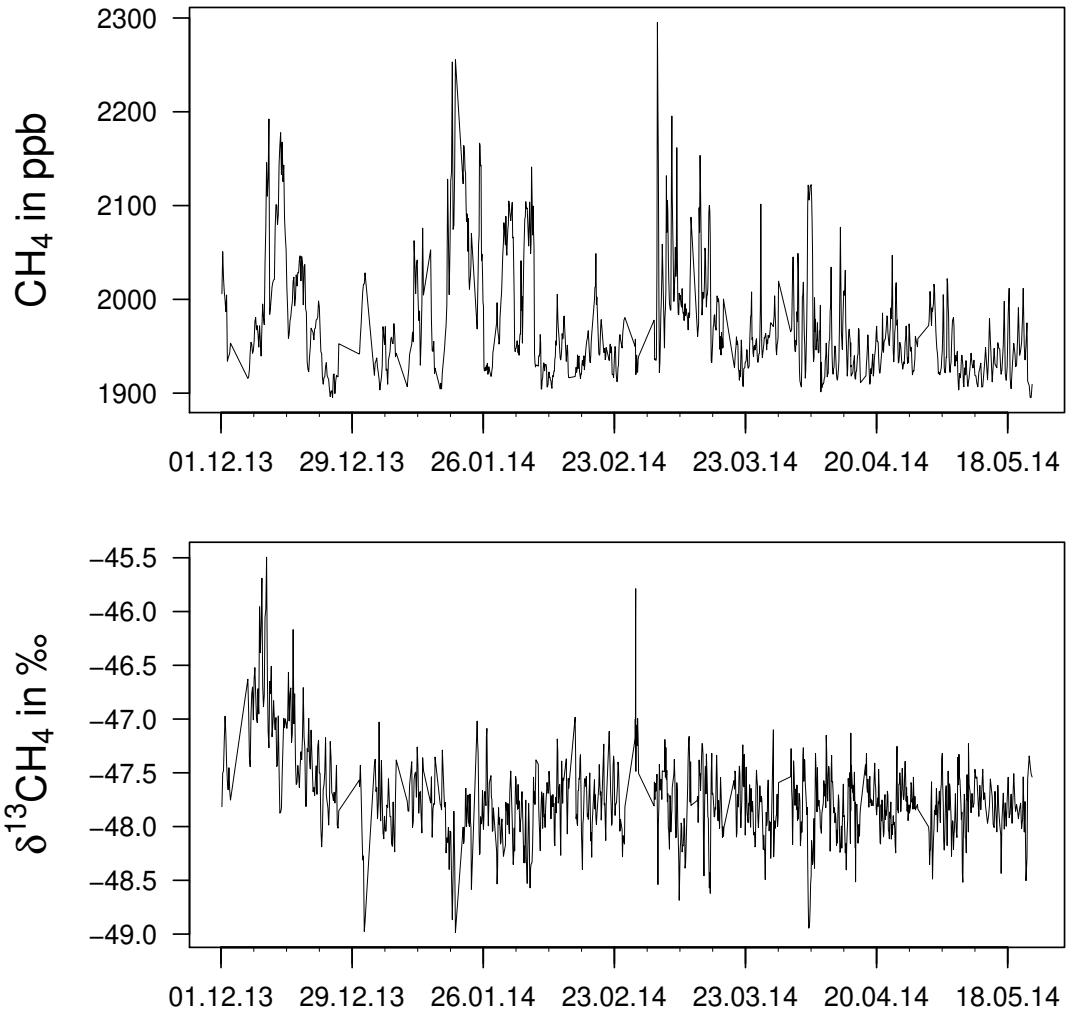

Figure A.2: *Monitored concentration and isotopic signature of CH_4 in the ambient air from December 2013 until May 2014. Neither in CH_4 concentration nor in $\delta^{13}CH_4$ a trend could observed.*

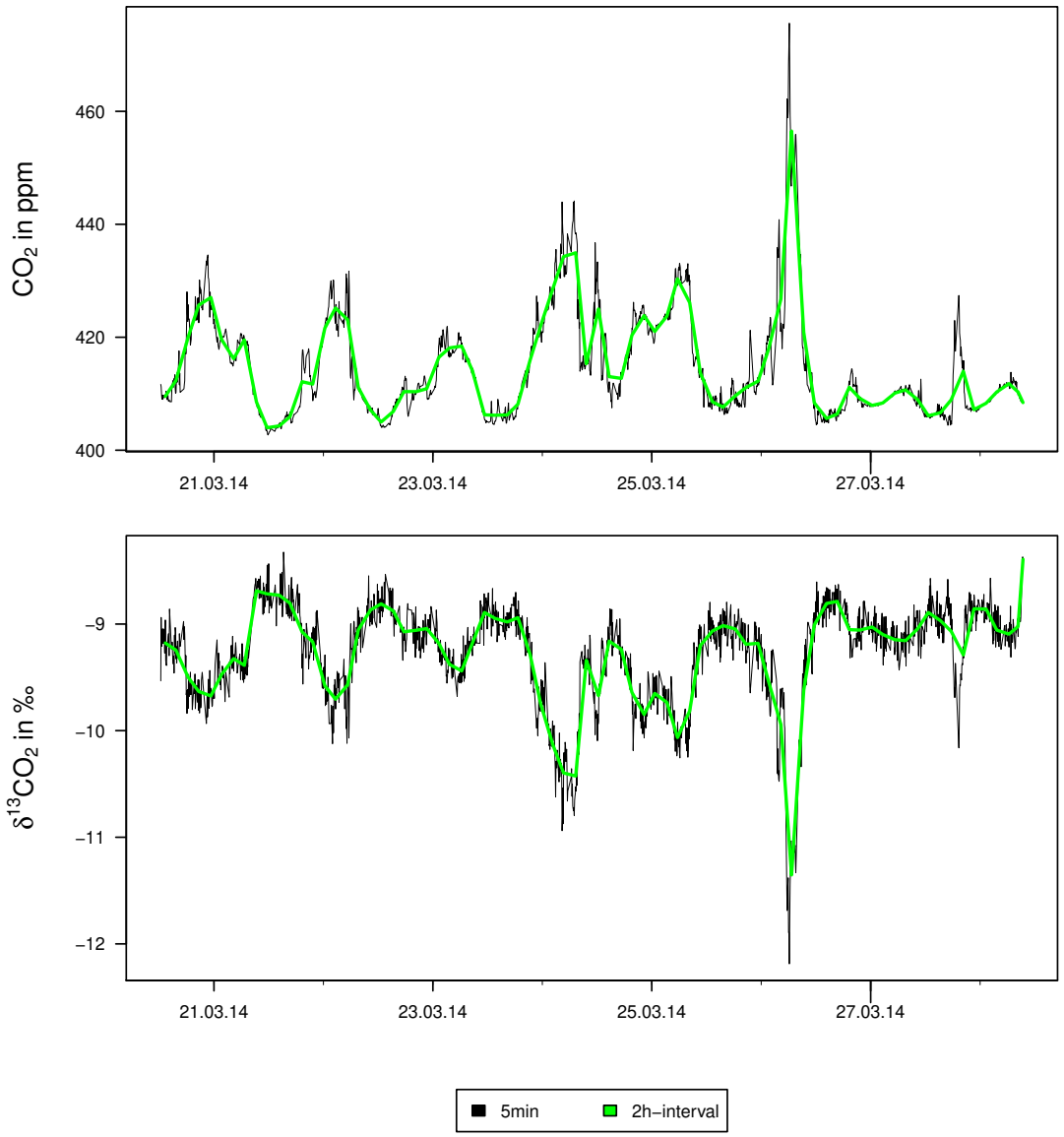

Figure A.3: *Weekly variations in CO_2 in March 2014*

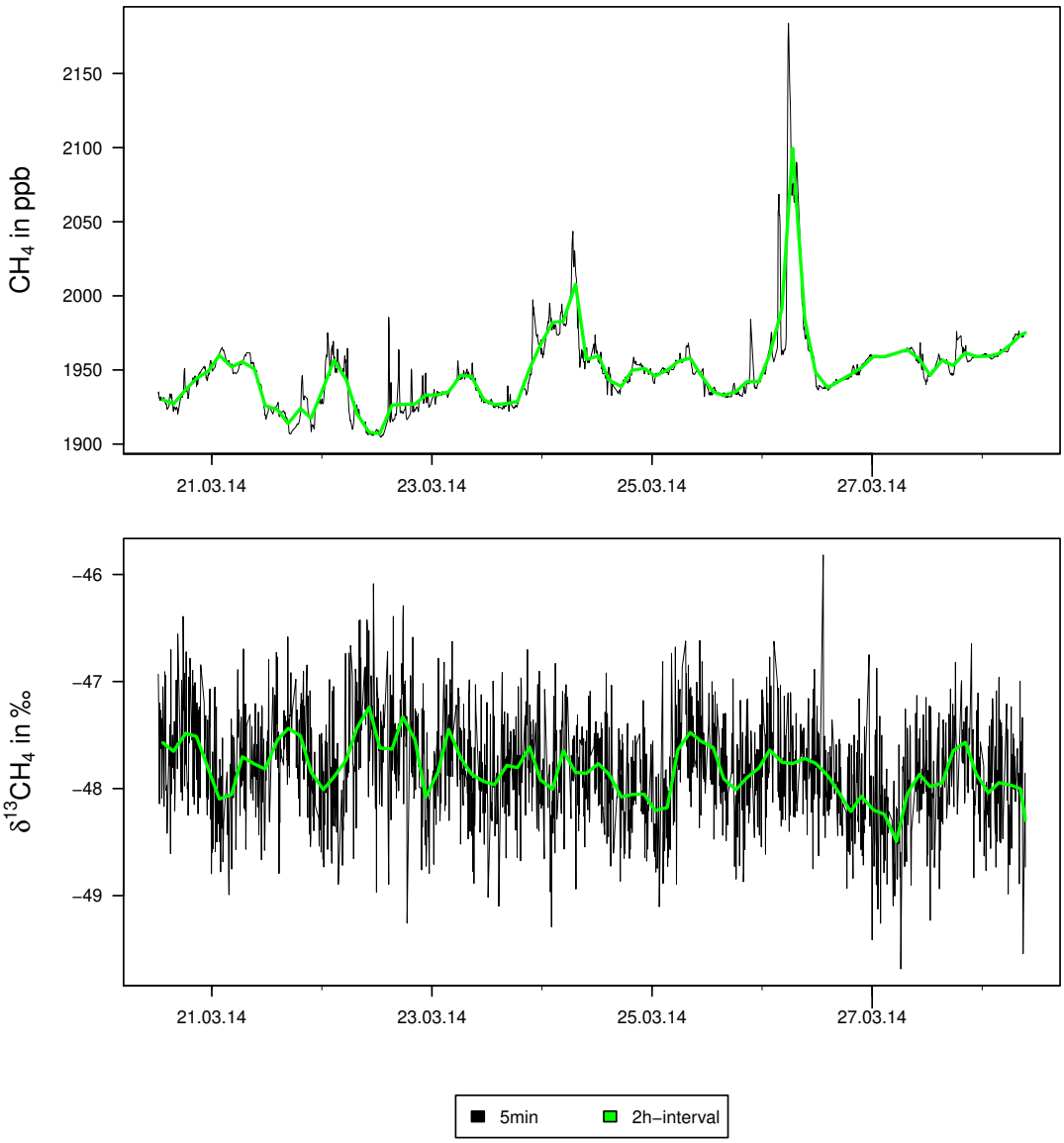

Figure A.4: *Weekly variations in CH_4 in March 2014*

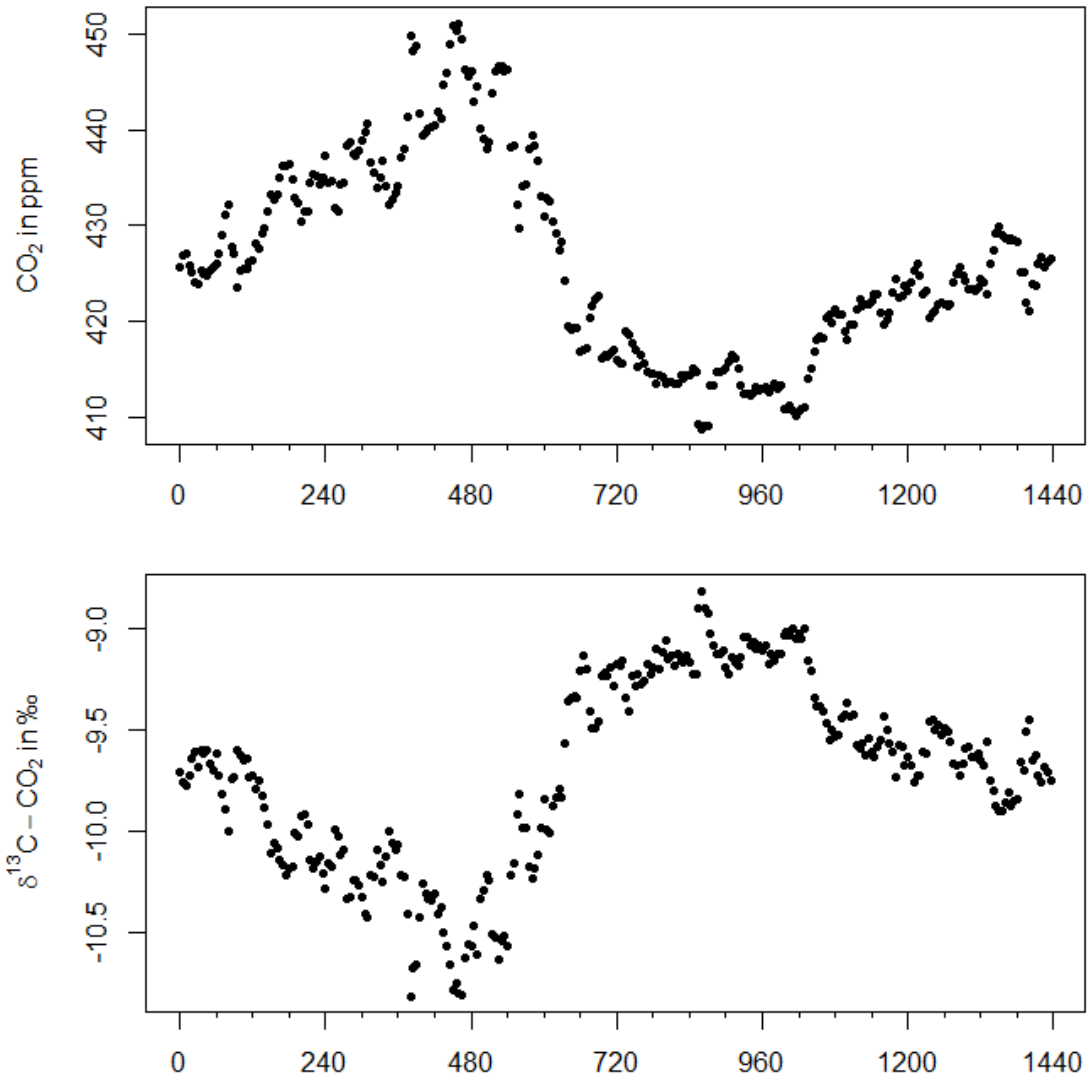

Figure A.5: *Diurnal variations in CO_2 and $\delta^{13}CO_2$ integrated over the complete March 2014 which was a quite warm and sunny March in Heidelberg. The time axis is given in minutes since midnight (UTC). There is a strong correlation in the signals of CO_2 and $\delta^{13}CO_2$. Since minute 480, which corresponds to 9:00 local time, the biosphere began to absorb CO_2 from the atmosphere. Coincidentally, the $\delta^{13}CO_2$ increased because of the fractionation by the biosphere.*

A.4 Small Sample Isotopic Module (SSIM)

Picarro offers a periphery device, the *Small Sample Isotope Module* (SSIM), for the isotopic measurement of small samples (less than 100 ml). If required, it provides an automatic dilution of the highly concentrated samples. We tested whether the SSIM offers a good alternative for the direct measurement explained in Section 6.

Dilution In operation, three gas sources are connected to the SSIM: The actual gas sample, a zero air cylinder for flushing the SSIM and the cavity between two sample measurements, and a calibration cylinder for automatic single-point calibration. Furthermore the SSIM requires an additional vacuum pump. Depending on the preload pressure at the zero air cylinder, the SSIM provides (if desired) a dilution of a factor of up to 4.8. Accordingly, also with the SSIM at least one manual dilution step is required. To reach a final CH_4 concentration of 10 ppm we filled an emptied sample bag with a total volume of 4-5 L with zero air. Afterwards, we transferred by a 5 ml-syringe roughly 0.2 ml of the actual sample to the zero air bag. By our manual dilution we reached a CH_4 concentration of roughly $\frac{0.2\,\mathrm{ml}}{4\,\mathrm{L}} \cdot 99\,\% = 50\,\mathrm{ppm}$. With the subsequent internal dilution a final concentration of 10 ppm was reached.

Automatic measurement For a SSIM-measurement, the outlet of the SSIM was connected to the 16-port valve and was measured like a cylinder gas sample. The (possibly diluted) sample and the calibration standard are measured in turns, where the number of sample measurements between two calibration measurements can be user modified. Between every measurement interval the cavity is flushed for several minutes by the zero air.

We decided to measure a sample five times between two calibration points, where we later ignored the first measurement interval due to remains of the former sample in the tubing within the SSIM. Furthermore we measured every bag twice due to better statistics. Nevertheless, we were not able to generate reproducible results. First of all, the final CH_4 concentration depended on the preload pressure from the zero air cylinder which was also used for filling the bags between the measurements. Thus an important possible source of cross-sensitivity was either not constant or would have required additional manpower. Finally, we had no idea what the device is doing and how the calibration was applied. Furthermore, the set-up allows a single point calibration only.

All in all, the device let more open questions as it helped. The dilution and measurement method explained in Chapter 6 appears to be better suited than a SSIM measurement. This result was supported by the fact, that the SSIM broke in February 2014 for unknown reasons.

A.5 Supplemental figures

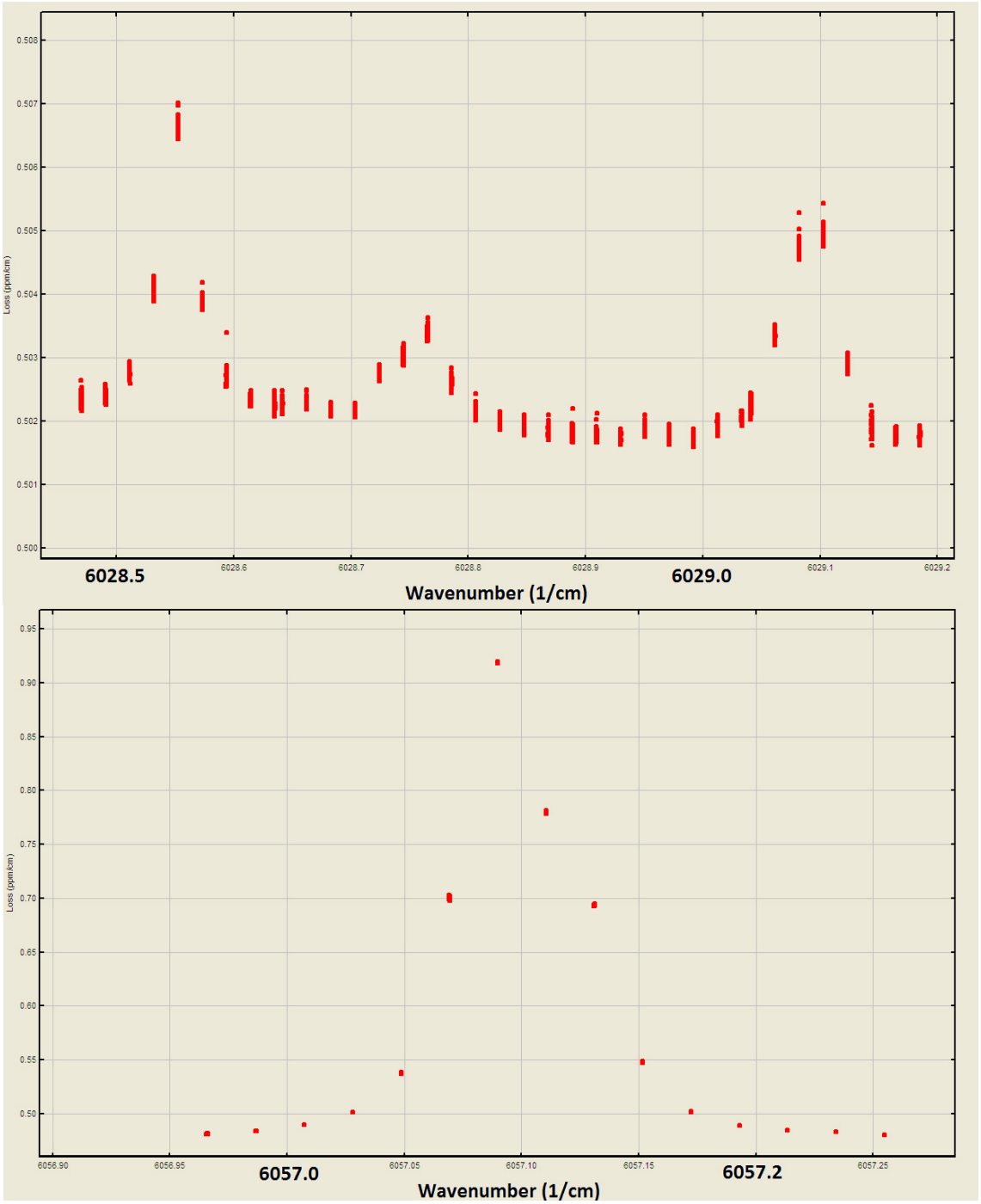

Figure A.6: *Absorption lines scanned by the lasers, centred at 1651 nm and 1659 nm, during an ambient air measurement. Compare with the theoretical absorption lines in Figure 3.3.*

Methan-Emissionen in Baden-Württemberg seit 1990 nach Sektoren

Jahr	CH_4-Emissionen insgesamt			Davon durch ...				
				Verkehr[1]	Feuerungen[2]	Abfallwirtschaft/Abwasserbeseitigung[3]	Landwirtschaft[4]	Gewinnung und Verteilung von Brennstoffen[5]
	1.000 t	kg/EW[6]	1990=100	1.000 t				
1990	411,2	42,3	100,0	5,1	3,6	233,6	142,8	26,0
1991	402,1	40,6	97,8	4,6	5,3	231,0	135,7	25,4
1992	396,8	39,4	96,5	4,4	4,9	230,8	131,8	24,9
1993	389,3	38,2	94,7	4,0	4,9	224,9	130,9	24,6
1994	378,6	36,9	92,1	3,7	5,0	214,4	132,2	23,3
1995	365,9	35,5	89,0	4,2	4,7	203,2	131,3	22,5
1996	350,0	33,8	85,1	3,9	4,8	189,4	129,9	21,9
1997	322,9	31,1	78,5	3,7	5,4	167,9	124,8	21,2
1998	302,8	29,1	73,6	3,4	5,0	152,0	122,3	20,2
1999	283,4	27,1	68,9	3,1	5,0	134,4	121,1	19,8
2000	270,9	25,8	65,9	2,8	5,5	125,0	118,2	19,4
2001	261,4	24,8	63,6	2,7	5,6	116,3	117,3	19,5
2002	251,0	23,6	61,0	2,4	5,9	108,7	114,4	19,6
2003	241,3	22,6	58,7	2,2	6,1	101,1	112,2	19,8
2004	229,0	21,4	55,7	2,0	5,2	93,5	108,0	20,3
2005	222,4	20,7	54,1	1,6	5,2	87,1	108,0	20,5
2006	216,8	20,2	52,7	1,6	5,4	83,5	105,5	20,8
2007	205,6	19,1	50,0	1,5	5,0	74,7	103,2	21,2
2008	199,6	18,6	48,5	1,4	5,2	67,9	104,0	21,1
2009	193,8	18,0	47,1	1,3	5,0	63,6	103,3	20,6
2010	188,6	17,5	45,9	1,2	6,2	58,6	101,7	20,9
2011[7]	180,6	16,8	43,9	1,2	5,5	54,0	98,9	21,0

1) Straßenverkehr und Sonstiger Verkehr einschließlich Off-Road-Verkehr.
2) Öffentliche Wärmekraftwerke und Fernheizwerke, Industrie, Haushalte und Kleinverbraucher.
3) Hausmülldeponien, Kompostierunsanlagen, Sickergruben.
4) Viehwirtschaft.
5) Bergbau - ohne stillgelegte Kohlegruben, Gewinnung von Erdöl und Erdgas einschl. Prozesse, Gasverteilung.
6) Einwohner zum Jahresmittel.
7) Voräufige Werte.
Berechnungsstand: Dezember 2013.

Figure A.7: *CH_4 emissions in Baden-Württemberg, see [Statistisches Landesamt Baden-Württemberg, 2014b].*

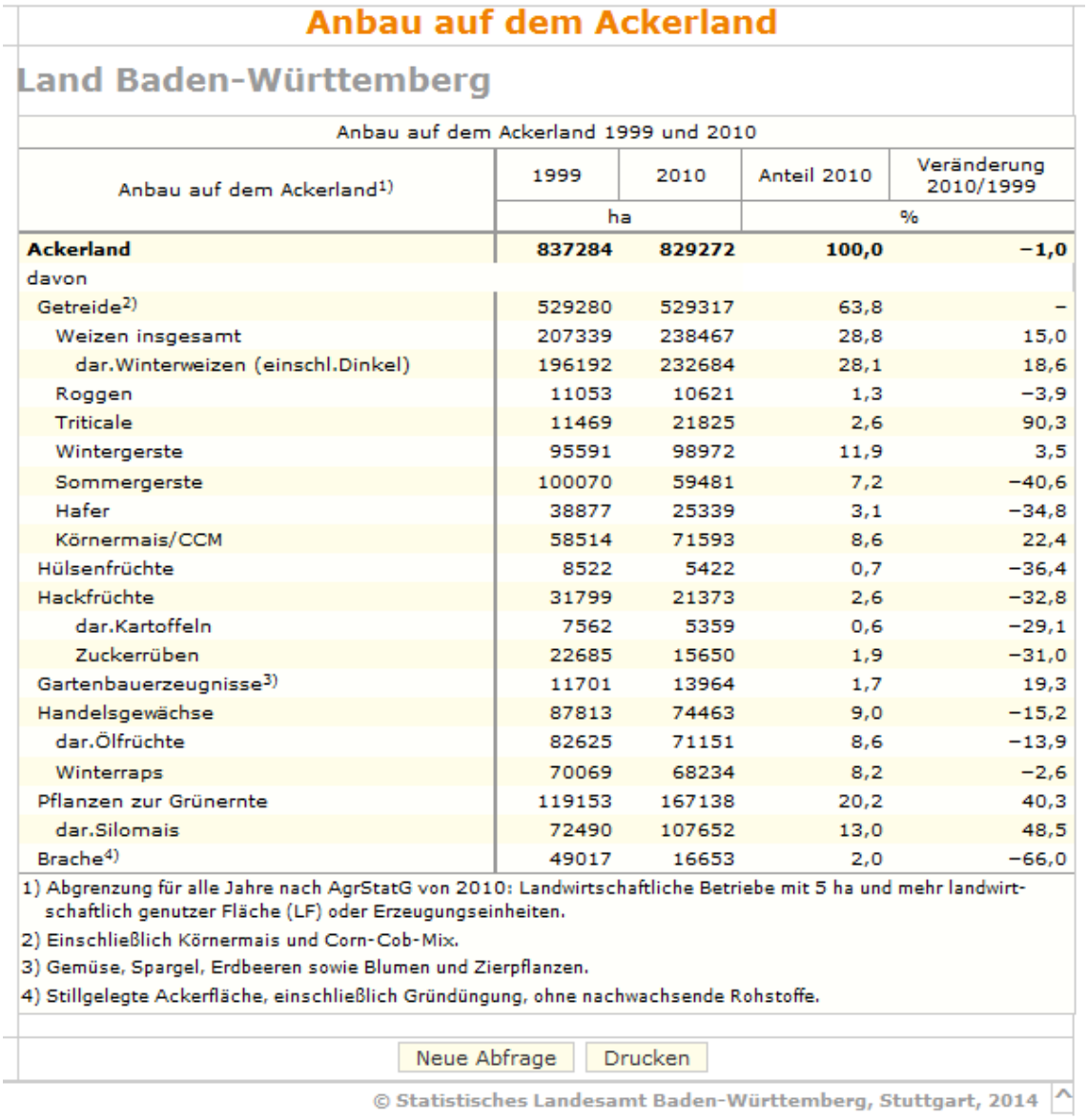

Anbau auf dem Ackerland

Land Baden-Württemberg

Anbau auf dem Ackerland 1999 und 2010

Anbau auf dem Ackerland[1]	1999	2010	Anteil 2010	Veränderung 2010/1999
	ha		%	
Ackerland	**837284**	**829272**	**100,0**	**−1,0**
davon				
Getreide[2]	529280	529317	63,8	–
Weizen insgesamt	207339	238467	28,8	15,0
dar.Winterweizen (einschl.Dinkel)	196192	232684	28,1	18,6
Roggen	11053	10621	1,3	−3,9
Triticale	11469	21825	2,6	90,3
Wintergerste	95591	98972	11,9	3,5
Sommergerste	100070	59481	7,2	−40,6
Hafer	38877	25339	3,1	−34,8
Körnermais/CCM	58514	71593	8,6	22,4
Hülsenfrüchte	8522	5422	0,7	−36,4
Hackfrüchte	31799	21373	2,6	−32,8
dar.Kartoffeln	7562	5359	0,6	−29,1
Zuckerrüben	22685	15650	1,9	−31,0
Gartenbauerzeugnisse[3]	11701	13964	1,7	19,3
Handelsgewächse	87813	74463	9,0	−15,2
dar.Ölfrüchte	82625	71151	8,6	−13,9
Winterraps	70069	68234	8,2	−2,6
Pflanzen zur Grünernte	119153	167138	20,2	40,3
dar.Silomais	72490	107652	13,0	48,5
Brache[4]	49017	16653	2,0	−66,0

1) Abgrenzung für alle Jahre nach AgrStatG von 2010: Landwirtschaftliche Betriebe mit 5 ha und mehr landwirtschaftlich genutzter Fläche (LF) oder Erzeugungseinheiten.

2) Einschließlich Körnermais und Corn-Cob-Mix.

3) Gemüse, Spargel, Erdbeeren sowie Blumen und Zierpflanzen.

4) Stillgelegte Ackerfläche, einschließlich Gründüngung, ohne nachwachsende Rohstoffe.

Neue Abfrage | Drucken

Figure A.8: *Cultivation of cropland in Baden-Württemberg, listed by the different plants, see [Statistisches Landesamt Baden-Württemberg, 2014a].*

B Bibliography

Arrhenius, S. (1896), On the Influce of Carbonic Acid in the Air upon the Temperature of the Ground, *Philosophical Magazineand Journal of Science*.

Bergamaschi, P., C. Lubina, R. Königstedt, H. Fischer, A. C. Veltkamp, and O. Zwaagstra (1998), Stable isotopic signatures (δ13C, δD) of methane from European landfill sites, *Journal of Geophysical Research: Atmospheres*, *103*(D7), 8251–8265, doi:10.1029/98JD00105.

Bönisch, H. (1997), Aufbau einer teilautomatischen Aufbereitungsapparatur für Methan aus Luftproben zur massnespektrometrischen Isotopiebestimmung, Master's thesis, Heidelberg University.

Demtröder, W. (2010), *Experimentalphysik 3*, Springer-Verlag.

Glatzel-Mattheier, H. (1997), Bilanzierung von CH_4-Emissionen in Deutschland anhand atmosphaerischer Messungen in Heidelberg, Ph.D. thesis.

Griffith, D. W. T. (1996), Synthetic Calibration and Quantitative Analysis of Gas-Phase FT-IR Spectra, *Applied Spectroscopy*, *50*(1), 59–70, doi:doi:10.1366/0003702963906627.

Hammer, S., et al. (2008), A gas chromatographic system for high-precision quasi-continuous atmospheric measurements of CO_2, CH_4, N_2O, SF_6, CO and H_2, *www.iup.uni-heidelberg.de/institut/forschung/groups/kk/GC_Hammer_25_SEP_2008.pdf*.

Hammer, S., D. W. T. Griffith, G. Konrad, S. Vardag, C. Caldow, and I. Levin (2013), Assessment of a multi-species in situ FTIR for precise atmospheric greenhouse gas observations, *Atmospheric Measurement Techniques*, *6*(5), 1153–1170, doi:10.5194/amt-6-1153-2013.

Huntington, E. (1917), Climatic Change and Agricultural Exhaustion as Elements in the Fall of Rome, *The quaterly journal of economics*.

IAEA (1993), Reference and intercomparison materials for stable isotopes of light elements, in *Proceedings of a consultants meeting held in Vienna, 1-3 December 1993*.

Internal presentation of Picarro provided by Chris Rella (2014), Calibration of $\delta^{13}CH_4$ and $\delta^{13}CO_2$.

IPCC (2013), Fifth Assessment Report WG1, *Tech. rep.*, IPCC.

Keeling, C. D. (1960), The Concentration and Isotopic Abundances of Carbon Dioxide in the Atmosphere, *Tellus*, *12*(2), 200–203, doi:10.1111/j.2153-3490.1960.tb01300.x.

Konrad, G. (2011), Charakterisierung eines Fourier Transform Infrarot Spektrometers zur Messung atmosphärischer Spurengase und Vergleich mit etablierten Messmethoden, Master's thesis.

Levin, I., B. Kromer, M. Schmidt, and H. Sartorius (2003), A novel approach for independent budgeting of fossil fuel CO_2 over Europe by $^{14}CO_2$ observations, *Geophysical Research Letters*, *30*(23), n/a–n/a, doi:10.1029/2003GL018477.

Levin, I., S. Hammer, E. Eichelmann, and F. R. Vogel (2011), Verification of greenhouse gas emission reductions: the prospect of atmospheric monitoring in polluted areas, *Phil Trans R Soc A 2011 369: 1906-1924.*

Mook, W. (2000), *Environmental isotopes in the hydrological cycle- Principles and applications, Technical Documents in Hydrology, I.*

Neubert, R., L. L. Spijkervet, J. K. Schut, H. Been, and H. A. J. Meijer (2004), A computer-controlled continuous air drying and flask sampling system., *J. Atmos. Oceanic Technol. 21, 651–659.*

NOAA (2014), Mace Head data, *http://www.esrl.noaa.gov/gmd/dv/data/?site=MHD (Last visited: 24.06.2014).*

Paldus, B., and A. Kachanov (2005), An historical overview of cavity–enhanced methods, *Canadian Journal of Physics.*

Park, R., and S. Epstein (1961), Metabolic fractionation of ^{13}C & ^{12}C in plants, *Plant Physiol. Mar 1961; 36(2): 133–138.*

Picarro (2012), PICARRO G2201-i, CRDS Analyzer for Isotopic Carbon in CO_2 and CH_4, *http://www.picarro.com/products_solutions/isotope_analyzers/13c_for_ch4_co2 (Last visit: 2014-06-24).*

Picarro (2014), PICARRO G2201-i CRDS Analyzer for Isotopic Carbon in CO_2 and CH_4, *https://picarro.app.box.com/s/2gol3ahbi6xc8idoql34 (Last visit: 2014-06-24).*

Rödel, W., and T. Wagner (2011), *Physik unserer Umwelt: Die Atmosphäre*, Springer-Verlag.

Rella, C. (2010), Accurate Greenhouse Gas Measurements in Humid Gas Streams Using the Picarro G1301 Carbon Dioxide / Methane / Water Vapor Gas Analyzer, *Tech. rep.*, Picarro.

Schmidt, K. (2014), Revision der regionalen CO_2-Bilanzen für Baden-Württemberg, *Statistisches Monatsheft Baden-Württemberg 4/2014*.

Statistisches Landesamt Baden-Württemberg (2014a), Regional cultivation of cropland, *http://www.statistik.baden-wuerttemberg.de/SRDB/Tabelle.asp?H=7&U=02&T=0502503?&E=KR&R=KR221*.

Statistisches Landesamt Baden-Württemberg (2014b), Regional CH_4-Emissionen, *http://www.statistik-bw.de/UmweltVerkehr/Landesdaten/l1b07.asp*.

Valentin, J. R., G. C. Carle, and J. B. Phillips (1985), Determination of methane in ambient air by multiplex gas chromatography, *Analytical Chemistry*, *57*(6), 1035–1039, doi:10.1021/ac00283a017, pMID: 11536559.

Van Pelt, A. (2008), Real-Time Atmospheric Monitoring of Stable Isotopes and Trace Greenhouse Gases, *www.picarro.com*.

Vardag, S. (2012), CO_2 source apportionment in the Heidelberg region using continuous $^{13}CO_2$ measurements, Master's thesis.

Vogel, F. R., S. Hammer, A. Steinhof, B. Kromer, and I. Levin (2010), Implication of weekly and diurnal 14C calibration on hourly estimates of CO-based fossil fuel CO2 at a moderately polluted site in southwestern Germany, *Tellus B*, *62*(5), 512–520, doi:10.1111/j.1600-0889.2010.00477.x.

Vogel, F. R., L. Huang, D. Ernst, L. Giroux, S. Racki, and D. E. J. Worthy (2013), Evaluation of a cavity ring-down spectrometer for in situ observations of $^{13}CO_2$, *Armospheric Measurement Techniques*.

Wen, X.-F., Y. Meng, X.-Y. Zhang, X.-M. Sun, and X. Lee (2013), Evaluating calibration strategies for isotope ratio infrared spectroscopy for atmospheric $^{13}CO_2/^{12}CO_2$ measurement.

Werle, P., R. Muecke, and F. Slemr (1993), The limits of signal averaging in atmospheric trace-gas monitoring by tunable diode-laser absorption spectroscopy (TDLAS), *Applied Physics B*, *57*(2), 131–139, doi:10.1007/BF00425997.

Winderlich, J., H. Chen, C. Gerbig, T. Seifert, O. Kolle, J. V. Lavrič, C. Kaiser, A. Höfer, and M. Heimann (2010), Continuous low-maintenance $CO_2/CH_4/H_2O$ measurements at the Zotino Tall Tower Observatory (ZOTTO) in Central Siberia, *Atmospheric Measurement Techniques, 3(4), 1113-1128*.

World Meteorological Organization (2011), GAW Report No. 206, 16th WMO/IAEA Meeting on Carbon Dioxide, Other Greenhouse Gases, and Related Measurement Techniques (GGMT-2011), *Tech. rep.*, World Meteorological Organization.

Giving thanks

I am greatful for having had the opportunity to fulfill at least some of the curiosity which rules my life. I want to thank the many pleasant people who shared their curiosity and knowledge with me for the last six years.

Many thanks to Ingeborg Levin who made it possible for me to work in the exciting research field of climate change. She taught me not only in scientific terminology, spoken and written, but also to question what is called "common knowledge".

A special thanks goes to Martina Schmidt who was an understanding and communicative supervisor. Amongst many other things, she showed me how to set up a measurement system and her profound knowledge about the topic and the research community helped a lot in understanding the instrument and its results.

Thanks you, Sanam Vardag, for having been such a pleasant and motivating colleague and office mate!

Thanks to Michael Sabasch for measuring my cylinder samples and for all the other technical support.

I want to thank the Carbon group for the nice working atmosphere. Several problems became clearer after the discussion in the group meeting.

Last but not least, I want to thank my parents for their support during my studies and for arousing my curiosity for sciences from the early beginning on. I want to thank Lisa for managing a life together with me, and finally, I want to thank Hanna and Julian for having granted me at least a couple of hours of sleep each night.

Selbstständigkeitserklärung

Ich versichere, dass ich diese Arbeit selbstständig verfasst habe und keine anderen als die angegebenen Quellen und Hilfsmittel benutzt habe.

Heidelberg, den 27.06.2014 .....